University of North Dakota
UND Scholarly Commons

Theses and Dissertations

Theses, Dissertations, and Senior Projects

January 2014

Design And Optimization Of Organic Rankine Cycle For Low Temperature Geothermal Power Plant

Kirtipal Barse

How does access to this work benefit you? Let us know!

Follow this and additional works at: https://commons.und.edu/theses

Recommended Citation

Barse, Kirtipal, "Design And Optimization Of Organic Rankine Cycle For Low Temperature Geothermal Power Plant" (2014). *Theses and Dissertations*. 1503.
https://commons.und.edu/theses/1503

This Dissertation is brought to you for free and open access by the Theses, Dissertations, and Senior Projects at UND Scholarly Commons. It has been accepted for inclusion in Theses and Dissertations by an authorized administrator of UND Scholarly Commons. For more information, please contact und.commons@library.und.edu.

DESIGN AND OPTIMIZATION OF ORGANIC RANKINE CYCLE FOR LOW TEMPERATURE GEOTHERMAL POWER PLANT

by

Kirtipal A. Barse
Master of Science, University of North Dakota, 2009

A Dissertation
Submitted to the Graduate Faculty

of the

University of North Dakota

in partial fulfillment of the requirements

for the degree of

Doctor of Philosophy

Grand Forks, North Dakota
May
2014

This dissertation, submitted by Kirtipal A. Barse in partial fulfillment of the requirements for the Degree of Doctor of Philosophy from the University of North Dakota, has been read by the Faculty Advisory Committee under whom the work has been done and is hereby approved.

Michael Mann

William Gosnold

Hossein Salehfar

Nanak Grewal

Santhosh Seelan

This dissertation meets the standards for appearance, conforms to the style and format requirements of the Graduate School of the University of North Dakota, and is hereby approved.

Wayne Swisher
Dean of the Graduate School

Date

PERMISSION

Title	Design and Optimization of Organic Rankine Cycle for Low Temperature Geothermal Power Plant
Department	Chemical Engineering
Degree	Doctor of Philosophy

In presenting this dissertation in partial fulfillment of the requirements for a graduate degree from the University of North Dakota, I agree that the library of this University shall make it freely available for inspection. I further agree that permission for extensive copying for scholarly purposes may be granted by the professor who supervised my dissertation work or, in his absence, by the chairperson of the department or the dean of the Graduate School. It is understood that any copying or publication or other use of this dissertation or part thereof for financial gain shall not be allowed without my written permission. It is also understood that due recognition shall be given to me and to the University of North Dakota in any scholarly use which may be made of any material in my dissertation.

Signature	KIRTIPAL BARSE
Date	3/6/2014

TABLE OF CONTENTS

CHAPTER

LIST OF FIGURES

LIST OF TABLES

Table Page

ACKNOWLEDGEMENTS

I would like to express my immense gratitude to my advisor Dr. Michael Mann, who has supervised me with enormous support and encouragement. No word are sufficient to express how profoundly grateful I am for his guidance in moving me forward to finish my research. I am also grateful to my research committee members, Dr. William Gosnold, Dr. Hossein Salehfar, Dr. Nanak Grewal and Dr. Santhosh Seelan for their valuable input for my research and reviewing the dissertation.

I would like to thank the United States Department of Energy (DOE) and Petroleum Research, Education, and Entrepreneurship Center (PREEC) for funding the project and helping me to carry out the research.

I am greatly indebted to the Department of Chemical Engineering and Department of Geology and Geological Engineering of UND for giving me the opportunity to work on my research. Finally, I would like to thank all other people who have contributed directly or indirectly to my research that I am unable to thank individually.

Dedicated to my Parents

ABSTRACT

Rising oil prices and environmental concerns have increased attention to renewable energy. Geothermal energy is a very attractive source of renewable energy. Although low temperature resources (90°C to 150°C) are the most common and most abundant source of geothermal energy, they were not considered economical and technologically feasible for commercial power generation. Organic Rankine Cycle (ORC) technology makes it feasible to use low temperature resources to generate power by using low boiling temperature organic liquids. The first hypothesis for this research is that using ORC is technologically and economically feasible to generate electricity from low temperature geothermal resources. The second hypothesis for this research is redesigning the ORC system for the given resource condition will improve efficiency along with improving economics.

ORC model was developed using process simulator and validated with the data obtained from Chena Hot Springs, Alaska. A correlation was observed between the critical temperature of the working fluid and the efficiency for the cycle. Exergy analysis of the cycle revealed that the highest exergy destruction occurs in evaporator followed by condenser, turbine and working fluid pump for the base case scenarios.

Performance of ORC was studied using twelve working fluids in base, Internal Heat Exchanger and turbine bleeding constrained and non-constrained configurations. R601a, R245ca, R600 showed highest first and second law efficiency in the non-constrained IHX configuration. The highest net power was observed for R245ca, R601a and R601 working fluids in the non-constrained base configuration. Combined heat exchanger area and size parameter of the turbine showed an increasing trend as the critical temperature of the working fluid decreased. The lowest levelized cost of electricity was observed for R245ca followed by R601a, R236ea in non-constrained base configuration. The next best candidates in terms of LCOE were R601a, R245ca and R600 in non-constrained IHX configuration. LCOE is dependent on net power and higher net power favors to lower the cost of electricity.

Overall R245ca, R601, R601a, R600 and R236ea show better performance among the fluids studied. Non constrained configurations display better performance compared to the constrained configurations. Base non-constrained offered the highest net power and lowest LCOE.

.

CHAPTER I

BACKGROUND

1.1 Motivation for the study

Currently fossil fuels are the primary sources of energy used to generate electricity. Fossil fuels are a non-renewable energy source and their availability is limited. Rising fuel prices and environmental concerns have increased attention to renewable energy. Solar, wind, hydro, geothermal, biomass and biofuels are some of the primarily renewable energy sources widely used.

Geothermal energy is defined as the energy obtained from the earth. Geothermal energy provides an attractive source of renewable energy as a potential replacement to conventional fossil fuels. Geothermal energy is considered renewable energy and has much lower emissions compared to fossil fuels. It makes a very good candidate for supplying base-load power since geothermal resources do not have variance. Geothermal energy has been used to generate electricity and heat for combined heat and power applications, space heating and cooling, etc. White et al. classified geothermal energy in three broad categories; high temperature resources having temperature higher than 150°C, intermediate temperature resources having temperature between 90°C and 150°C, and low temperature resources having temperature below 90°C (White, D. Williams, 1975). Geothermal energy applications can be broadly classified into power generation and direct use categories. Binary cycle, dry steam, and flash steam are the types of existing geothermal power plants used for power generation using high and low medium temperature resources. Dry steam and flash steam systems are used to produce electricity from high temperature resources (Hettiarachchi, Golubovic, Worek, Ikegami, & Madhawa Hettiarachchi, 2007). The medium temperature geothermal resources are used in single and double flash and, binary power plants to generate electricity (Kanoglu & Bolatturk, 2008). Low temperature geothermal resources are commonly utilized for direct applications such as space heating, greenhouses, etc. (Yari, 2010).

Using low temperature resources for power generation has technical challenges and hence their uses are limited to direct use applications. The availability of low temperature geothermal resources is abundant all across the United States. Figure 1 shows the temperature profile of the state of North Dakota at 1km depth (Gosnold, 2006). It can be observed that western side of the state have temperatures above 90°C and has a vast potential of low temperature geothermal resources.

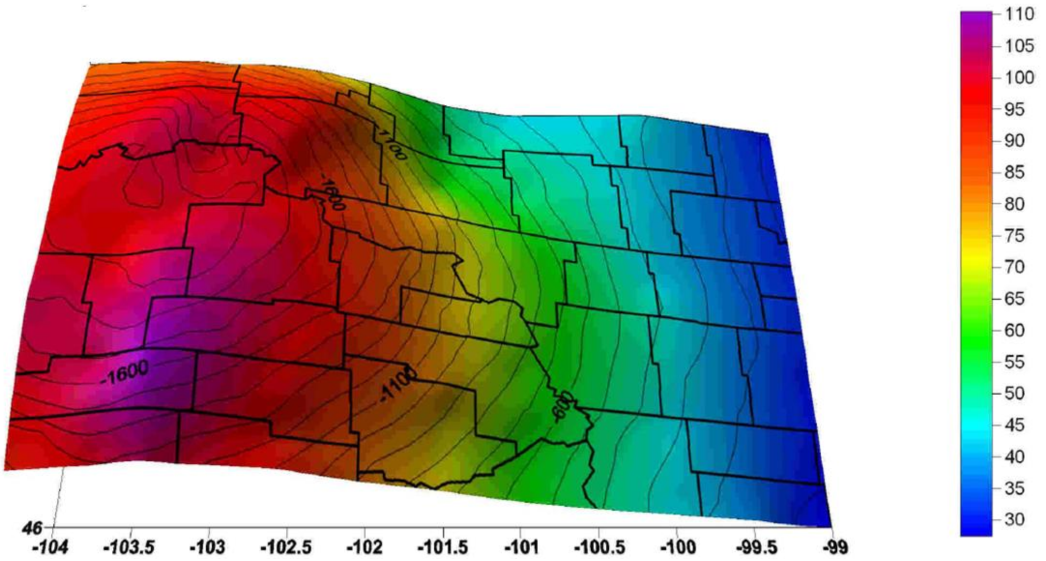

Figure 1 North Dakota potential for low temperature geothermal energy

As previously mentioned, most of the power generation technologies use steam as their working fluid. The temperature of low temperature geothermal resources is not high enough to generate steam which is essential to operate steam based power plants. With the advent of new technologies like the Organic Rankine Cycle (ORC) and Kalina Cycle, power generation from low temperatures is technologically possible. Low temperature geothermal resources below 150°C employ binary type energy conversion systems (DiPippo, 2004).

An ORC power plant has several advantages over other types of geothermal power plants. Lower temperatures are needed to vaporize the working fluid compared to water allowing electricity generation from low temperature geothermal resources. The working fluid and geothermal water flows through closed loop system eliminating any emissions to the atmosphere (Manolakos, Kosmadakis, Kyritsis, & Papadakis, 2009). Other ORC advantages include long service life, low maintenance costs, automated operation, etc., over conventional rankine cycle (Obernberger, Thonhofer, & Reisenhofer, 2002).

1.2 Rankine Cycle

The Rankine cycle has been traditionally used to produce power using steam. The Rankine cycle is a proven form of technology and offers efficiencies on the order of 33 to 38%. However, the traditional Rankine cycle uses steam as the working fluid to produce power and can be used only for resources with temperatures greater than boiling point of water. Therefore, Rankine cycle cannot be used for low temperature applications below 100°C.

Figure 2 shows the typical temperature entropy (T-s) diagram for a Rankine cycle. Paths 1-2 and 3-4 represent evaporation and condensation curves in the cycle (adapted from Cengel & Boles, 2006). The expansion curve 2-3 intersects the saturation curve resulting in condensation of steam. The turbine exhaust in Rankine cycle typically has moisture content less than 10%. The moisture forms water droplets and causes erosion of the turbine blades. In order to avoid the condensation of steam in the turbine, superheating of steam is required (Calise, Capuozzo, & Vanoli, 2013). However, superheating of steam has two main challenges associated with it. First, superheating is achieved by increasing the enthalpy of the steam and hence requires higher operating temperatures of the steam. This prohibits use of low temperature sources as they may not be able to provide the required superheat. Second, the heat transfer coefficients are lower in the vapor phase which increases the required heat exchanger area (Desai & Bandyopadhyay, 2009), (Schuster, Karellas, Kakaras, & Spliethoff, 2009). This results in higher cost of the superheater and may result in unfeasible economics for the power plant. Therefore, a steam based Rankine cycle is not feasible for low temperature applications.

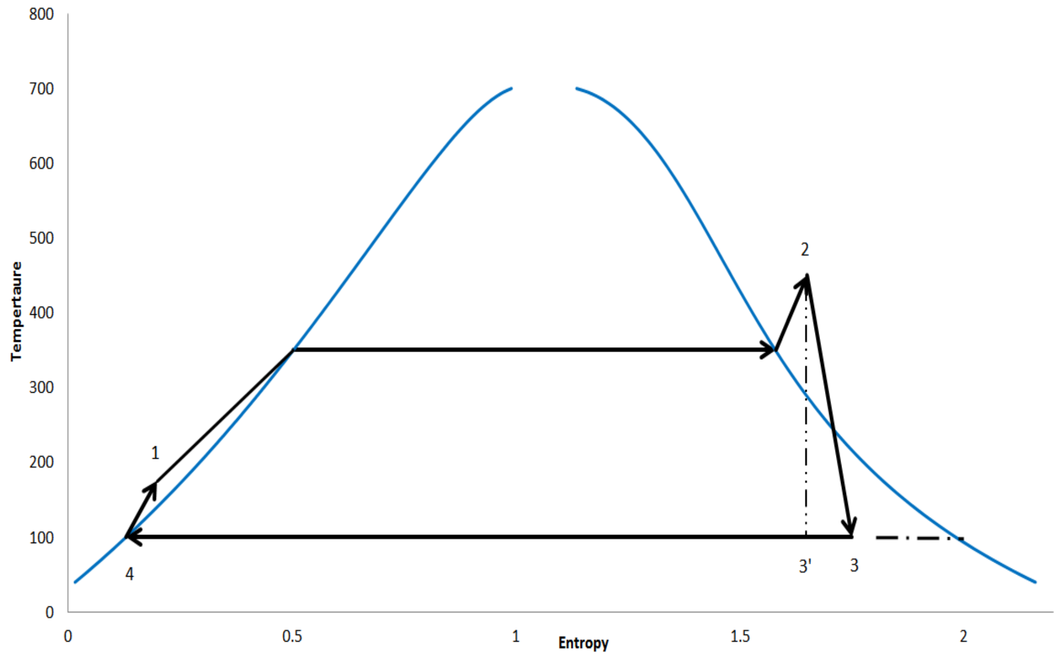

Figure 2 Typical temperature entropy diagram for Rankine Cycle

1.3 Organic Rankine Cycle

The Organic Rankine Cycle (ORC) is a Rankine cycle that uses organic fluids such as 1,1,1,3,3-pentafluoropropane (R245fa), 1,1,1,2-tetrafluoroethane (R134a), isopentane etc., as working medium instead of steam (Desai & Bandyopadhyay, 2009), (Yamamoto, Furuhata, Arai, & Mori, 2001). The traditional steam rankine cycle does not perform adequately in case of low grade waste energy due to its low thermal efficiency and large volume flows (Y. Chen, Lundqvist, Johansson, & Platell, 2006), (Angelino, Colonna, & Paliano, 1998). ORC is a promising technology for converting low grade energy including waste heat and low temperature geothermal resources to electricity (T. C. Hung, Shai, Wang, & Polytechnic, 1997), (Schuster et al., 2009). The benefit of using organic liquids as working fluids is that they require lower temperature to vaporize compared to steam. The organic liquid vaporizes at much lower temperature compared to water and makes feasible the use of low temperature resources. For example, R134a and R245fa are commonly used working fluids and have boiling point of 15.14°C and -26°C respectively. Other examples of commonly used working fluids include pentane, isopentane, ammonia, etc.

ORC has been used to generate power from various low temperature heat sources such as waste heat, solar, biomass, geothermal, etc. (Bruno, López-Villada, Letelier, Romera, & Coronas, 2008) (Cayer, Galanis, Desilets, Nesreddine, & Roy, 2009), (Manolakos et al., 2009), (Drescher & Brüggemann, 2007), (DiPippo, 2004). The Neustadt – Glewe geothermal power plant in Germany produces 210 kW electricity from a 98°C water resourse using ORC techonology (Lund, 2005). A study based on electric power generation from solar energy power ORC suggests that optimal evaporation temperatures for ORC is around 120°C (Jing, Gang, & Jie, 2010). ORC offers advantages such as long service life, low maintenance costs, automated operation, etc., over conventional Rankine cycle (Obernberger et al., 2002).

An ORC has the same working principle and components as a typical Rankine cycle. Figure 3 shows the schematic of an ORC and its components. Working fluid enters the evaporator as high pressure liquid. The evaporator generates slightly superheated vapors at high pressure. These vapors expand in the turbine and exit as vapors at low pressure. The turbine drives the electrical generator producing power. The low pressure vapors are completely condensed in the condenser and delivered to the working fluid pump to raise the pressure. This process is repeated in cycle. The geothermal brine, working fluid and the cooling water used in the condenser remain in separate closed loops.

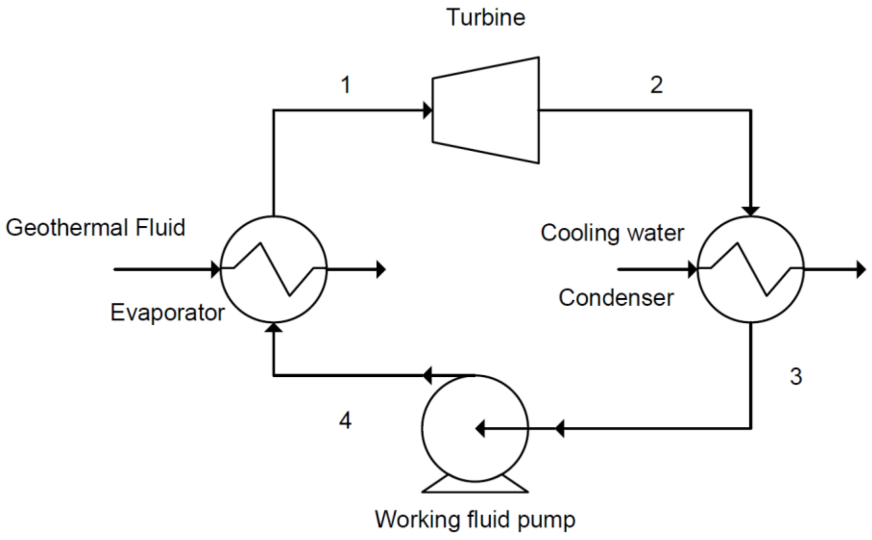

Figure 3 Schematic of simple Organic Rankine Cycle

Binary cycle power plants using ORC have several advantages over the steam power plants including efficient utilization of energy resources, smaller systems and outstanding economic performance (Shengjun, Huaixin, & Tao, 2011). Table 1 lists some of the manufactures of ORC around the world (Quoilin, Broek, Declaye, Dewallef, & Lemort, 2013). Lower temperatures are needed to vaporize the working fluid compared to steam allowing electricity generation from low temperature geothermal resources. The working fluid and geothermal water flow through closed loop systems eliminating any emissions to the atmosphere (Manolakos et al., 2009).

Table 1 List of some of the Current ORC Manufactures

Manufacturer	Heat Source Temperature, (°C)
ORMAT, US	150-300
Turboden, Italy	100-300
Adoratec/Maxxtec, Germany	300
Opcon, Sweden	<120
GMK, Germany	120-350
Bosch KWK, Germany	120-150
Turboden Purecycle, US	91-149
GE, Cleancycle	>121
Cryostar, France	100-400
Tri-o-gen, Netherlands	>350
Electratherm, US	>93
Turbine Air System, US	90

ORC can be operated in a subcritical or supercritical (transcritical) cycle. In a subcritical cycle, the working fluid always remains below its critcal temperature. In a supercritical cycle, the evaporation of the working fluid ends in supercritical region and the heat rejection occurs in the subcritical region. Tao et al. compared the performance of subcritical ORC using R245fa to a CO_2 transcritical rankine cycle (T. Guo, Wang, & Zhang, 2010). It was observed that subcritical cycle has 18 to 27% higher thermal efficiency and 3 to 7% lower net power compared to transcritical cycle. However, transcritical cycle requires larger heat exchanger area. Also, the transcritical cycle has very high operating pressure, 10.5 to 13.5 MPa as compared to 0.345 to 0.643 MPa for subcritical cycles. The higher pressures require use of higher strength heat exchanger material. Higher operating pressures, higher heat exchanger area and high strength material leads to very high capital costs. Based on this discussion, subcritical cycle was chosen as the focus for this study.

1.4 Modeling and Simulation of Organic Rankine Cycle

The first step involved in this study was developing a computer model of the ORC using a process simulator. Aspen HYSYS® was used to develop a model of the ORC power plant. Aspen HYSYS® is a commercial software package provided by Aspentech and was chosen for this study due to its accurate results, wide use in industries and ease of programming. Aspen HYSYS® has in built models of unit operations that were used for the development of the model. The inbuilt models offer options to vary the input conditions of the unit operations to replicate the real world process. Results obtained from the process simulator included the thermodynamic conditions at each state in the cycle, the mass flow rates, work and power in the cycle.

The results obtained from Aspen HYSYS® were compared to the REFPROP database provided by NIST. REFPROP developed by the National Institute of Standards and Technology (NIST), is an abbreviation for Reference Fluid Properties and contains the physical and thermodynamic data for common refrigerants and hydrocarbons. REFPROP was the thermodynamic property package used for modeling for this study. The simulation results obtained from the model were compared to the real data for validation. This model was subsequently used to study the performance of the power plant at various operating conditions such as flow rate and temperature of both geothermal resource and cooling medium, and working fluids.

Based on the resource conditions for the geothermal resource of interest and the size of the equipment, the performance of ORC was studied for 12 working fluids for 250kW generator output. The first law of thermodynamics was used to determine the thermal efficiency of ORC. Several authors have used the first law analysis for working fluids screening studies (Saleh, Koglbauer, Wendland, & Fischer, 2007), (Kanoglu & Bolatturk, 2008). Exergy efficiency was calculated to identify process deficiencies. Exergy destruction factor (EDF) was determined to understand the irreversibility distribution across the ORC system.

1.5 Selection of working fluids

Working fluid is the most important factor that determines the performance of the ORC. There are two major criteria to consider while selecting the working fluid for ORC. The first criterion is the type of working fluid which is determined by the slope of their saturation curves. The second criterion is the environmental impact of the working fluid which is determined by the ozone depletion potential, global warming potential and atmospheric life time.

The working fluids can be classified into three different categories based on the slopes of their saturation curves that influences the efficiency and arrangement of equipment in the ORC (T. Hung, 2001). The categories are wet fluids having negative slope, dry fluids having positive and isentropic fluids having nearly vertical saturated vapor curves. Figure 4 shows the three types of working fluids. The wet fluid after expansion in turbine contains lot of saturated liquid and can cause condensation of the working fluid. The condensate can cause damage to the turbine blades and reduce the isentropic efficiency of the turbine. In order to avoid the condensation of the working fluid on the turbine blades, the working fluid must be superheated. For a Rankine cycle using low temperature source, the driving force to superheat the working fluid at the turbine inlet may not be present. Also, the heat transfer area required is increased due to decrease in heat transfer coefficient in vapor phase thereby significantly increasing the overall cost of superheater. Aljundi and Liu et al. reports that presence of hydrogen bonds in certain molecules results in wet fluids due to larger vaporizing enthalpy (Aljundi, 2011), (Liu, Chien, & Wang, 2004). Hydrogen bond rarely exists in organic fluids due to their symmetry. Some of the wet fluids such as water and ammonia are known to have hydrogen bond. Due to the nonexistence of the hydrogen bond, most organic fluids are dry or isentropic in nature (Gu, Weng, Wang, & Zheng, 2009). Dry and isentropic working fluids do not encounter this problem as the turbine exit stream is saturated or superheated vapor. The expansion process in the turbine terminates in the superheated region. Therefore, dry and isentropic fluids show better efficiencies (P J; Mago, Chamra, Srinivasan, & Somayaji, 2008), (T. C. Hung, Wang, Kuo, Pei, & Tsai, 2010) and are considered here for this study and listed in Table 2 along with their thermodynamic properties. As observed from Table 2, 8 dry fluids, 3 isentropic fluids and 1 wet fluid were chosen for this study. The working fluids are arranged in decreasing order of their critical temperature. R134a is an isentropic fluid with almost infinite slope and R245ca is a dry fluid with positive slope. R152a is a wet fluid with negative slope and is used in this study for performance comparison with dry and isentropic fluids.

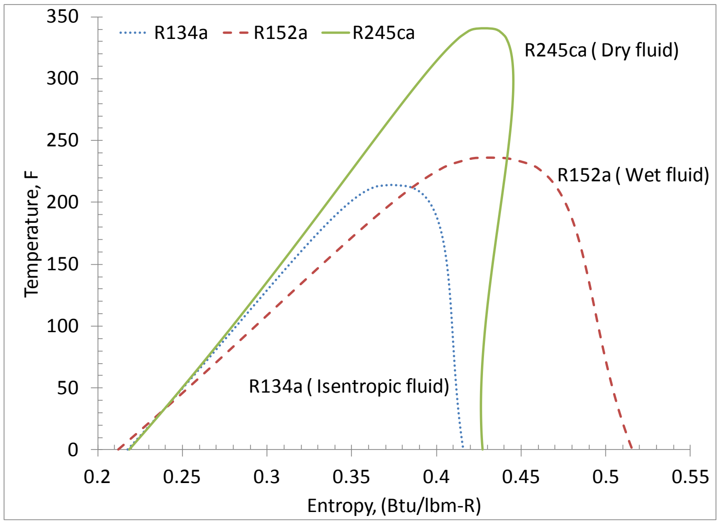

Figure 4 Types of working fluids

Table 2 Thermodynamic Data for the Working Fluids

Working fluid	T_c (°F)	P_c (psia)	NBP (°F)	Type	GWP (100 yr)	ODP	ALT (yr)
R601	385.79	488.78	96.908	Dry	0	0	0
R601a	368.96	489.94	82.094	Dry	0	0	0
R123	362.63	531.1	82.081	Isentropic	77	0	1.3
R245ca	345.96	569.27	77.234	Dry	693	0	62
R245fa	309.22	529.53	59.252	Isentropic	1030	0	7.6
R600	305.56	550.56	31.118	Dry	20	0	0.02
R236ea	282.72	507.92	43.142	Dry	710	0	8
R600a	274.39	526.34	10.852	Dry	20	0	0.02
R236fa	256.86	464.12	29.408	Dry	9810	0	240
R152a	235.87	655.1	-11.241	Wet	124	0	1.4
R227ea	215.15	424.24	2.588	Dry	3220	0	42
R134a	213.91	588.75	-14.933	Isentropic	1430	0	14

Dry fluids have a positive slope and are the most preferred working fluid for the ORC system using low grade heat sources (Desai & Bandyopadhyay, 2009). Only the subcritical region of the working fluids is considered for the study and therefore all the fluids selected here have critical temperature above the new geothermal resource temperature. Superheating dry fluids is not preferred as it decreases the ORC efficiency due to the limited temperature difference between the hot and cold sides (Kang, 2012),(Pan, Wang, & Shi, 2012), (T. C. Hung et al., 1997). The irreversibility in the system increases and the second law efficiency decreases with superheating a dry working fluid (P J Mago, Chamra, & Somayaji, 2007).

A lot of research has been conducted by various authors in selection of working fluids for ORC. Hung et al. showed that the slopes and the shapes of the saturated vapor curves of the working fluid affects the ORC efficiency (T. C. Hung et al., 1997, 2010). They studied the effect of working fluids such as benzene, ammonia, R11, R12 and R134a on the ORC efficiency. Hettiarachchi et al. compared the optimum cycle performance for ammonia, HCFC123, R601, and PF5050 (Hettiarachchi et al., 2007). Wei et al. studied the analysis and optimization of ORC system using R245fa as the working fluid (Wei, Lu, Lu, & Gu, 2007). Kang, 2012 conducted experiments using R245fa working fluid for low temprature resources (Kang, 2012). Bamgbopa et al., used R245fa to study the performance of ORC under steady and variable heat input (Bamgbopa & Uzgoren, 2013). Sauret, 2011 analyzed the performance of HFC134a, HFC143a, HFC236ea, HFC245fa and n-pentane (R601) as working fluids for 150°C geothermal resource. Torres et al. used R245ca as one the working fluids to perform optimization of low temperature solar ORC (Delgado-Torres & García-Rodríguez, 2010). Datla & Brasz found that R601, R245fa and R123 have better performance in terms thermal efficiency, turbine size and speed among the 11 working fluids studied (Datla & Brasz, 2012). Liu et al. used water, ethanaol, HFE7100, n-pentane (R601), iso-pentane (R601a), R11, R123, benzene as working fluids to analyze their effect on subcritical ORC (Liu et al., 2004). Heberle et al. performed the optimization of ORC to maximize the output power and concluded that R227ea and isopentane are preffered working fluid

(Heberle & Brüggemann, 2010). Nguyen et al. designed and developed small scale ORC system to generate electrcity from low temperature heat using n-pentane as the working fluid (Nguyen, Doherty, & Ri, 2001). Aleksandra et al. suggested R236fa as optimal working fluid for ORC utilizing 80°C-120°C geothermal water (Borsukiewicz-gozdur & Nowak, 2007). Gu et al. 2009 used 75°C - 100°C hot water and recommended as R600a as a suitable ORC working fluid. Hung et al. studied refrigerants and benzene series fluids for ORC applications (T. C. Hung et al., 2010). Rayegan et al. performed screening studies of 115 fuilds suitable for solar ORC (Rayegan & Tao, 2011). Hung et al. showed that the irreversibility of the system depends on the type of working fluid and heat sources (T. Hung, 2001). (H. Chen, Goswami, & Stefanakos, 2010) conducted a screening study for 35 working fluids for ORC. (Saleh et al., 2007) screened 31 pure components working fluids for ORC . Mago et. al. used second law analysis to convert low grade heat to power and observed R123 has the best performance for heat source temperatures between 380 and 430K (P J Mago et al., 2007). Several other studies concluded that R123 has better performance compared to other working fluids (T. Hung, 2001), (H. Chen et al., 2010), (Roy, Mishra, & Misra, 2011), (J. Wang, Dai, Gao, & Ma, 2009). Maizza et al. evaluated the thermodynamic performance of 20 unconventional fluids used in ORC (Maizza & Maizza, 2001). For small scale low power turbine applications, the ORC working fluids with high molecular weight are preferred due to reduced rotational speed or number of turbine stages and allowing reasonable mass flow rates and turbine nozzle areas (X. D. Wang et al., 2010). Based on the above literature review, the 12 working fluids listed in Table 2 were chosen for this study.

The second important criterion for choosing the working fluid is its effect on the environment. Ozone depletion potential (ODP), global warming potential (GWP) and the atmospheric lifetime (ALT) are the three important factors to measure the effect on the environment. ODP of a chemical compound is the ability of the compound to degrade ozone layer compared to CFC-11 which has an ODP value of 1. GWP is the potential of the compound to contribute towards global warming and is usually measured over a 100 year period. Carbon dioxide has a GWP of 1 by convention. ALT is the amount of time required for the greenhouse gases to leave the atmosphere. The working fluids selected for this study were based on previous literature and studies (Quoilin et al., 2013), (T. Hung, 2001), (P J; Mago et al., 2008). Non-corrosive, non-flammable, non-toxic and affordable are other important characteristics desired when choosing working fluid (Arvay, Muller, & Ramdeen, 2011), (Hettiarachchi et al., 2007), (Papadopoulos, Stijepovic, & Linke, 2010), (B. F. Tchanche, Papadakis, Lambrinos, & Frangoudakis, 2009). For each working fluid selected for the study, the thermodynamic conditions for the ORC were determined along with the mass flow rate of working fluid and cooling water, and working fluid pump power. First and second law efficiency and EDF were calculated for the performance comparison. Figure 5 shows the temperature entropy diagrams for the selected working fluids. As observed, each working fluid differs in shape and size of the T-s curve and governs the performance of the working fluid.

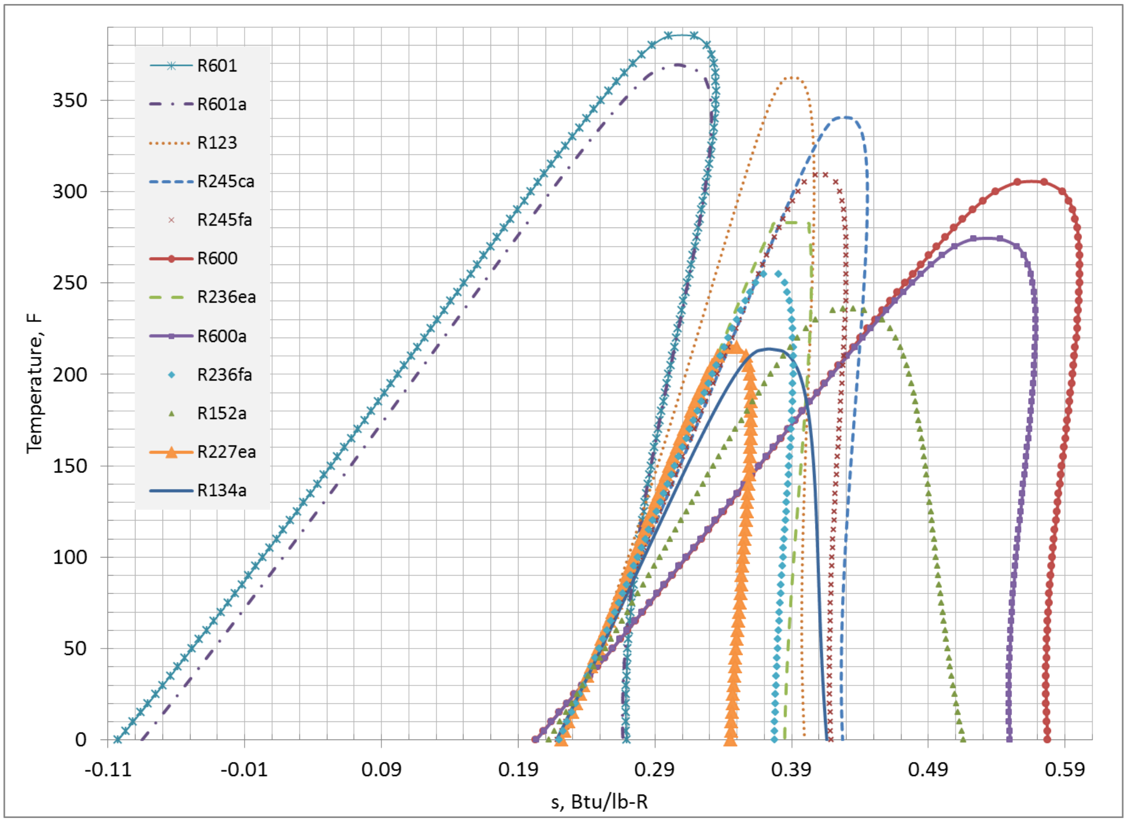

Figure 5 Temperature entropy diagrams for the selected working fluids

1.6 Thermodynamic Analysis

The thermodynamic analysis is critical to study the performance of the ORC under various operating conditions and working fluids. Several authors used first law efficiency in their investigations (T. C. Hung et al., 2010), (Quoilin, Lemort, & Lebrun, 2010), (Schuster, Karellas, & Aumann, 2010). The energy analysis is based on first law of thermodynamics. The first law of thermodynamics takes into account the actual heat transferred to system and determines the efficiency of the system. The first law efficiency is the ratio of net work produced to heat input to the system.

Thermal efficiency is defined as

$$\eta_I = \frac{(W_t - W_p)}{Q_e}$$ Equation 1

The maximum value of first law efficiency is given by the Carnot efficiency.

$$\text{Carnot efficiency} = \left[1 - \frac{T_L}{T_H}\right]$$ Equation 2

Where, T_L and T_H is the temperature of heat sink and heat source respectively.

The second law efficiency is the ratio of thermal efficiency to the maximum possible efficiency (Shengjun et al., 2011). The second law efficiency serves as an approximation of the system's behavior under reversible operation. When the second law efficiency value approaches zero, complete exergy of the resource is destroyed. As the efficiency approaches unity, the system behaves ideally and no exergy is destroyed. Second law efficiency as defined by (B. F. Tchanche et al., 2009) and (Aljundi, 2011) is defined as:

$$\eta_{II} = {}^{\eta_I}\Big/\left(1 - {}^{T_0}/_{T_H}\right)$$ Equation 3

Several studies used second law analysis to study the performance of ORC (Heberle & Brüggemann, 2010), (Dai, Wang, & Gao, 2009), (B. F. F. Tchanche, Lambrinos, Frangoudakis, & Papadakis, 2010),(Kanoglu & Bolatturk, 2008) , (Kanoglu, 2002), (DiPippo, 2004), (Yari, 2010), (B. F. Tchanche et al., 2009), (B. F. F. Tchanche et al., 2010), (P J Mago et al., 2007). Exergy is the maximum work potential theoretically obtained from a source with respect to the surrounding (DiPippo, 2004). It can also be defined as the maximum possible work when a system undergoes reversible process from the specified initial state to dead state. A dead state of a fluid occurs when the fluid is in equilibrium with the surrounding and there is no potential for doing work. Exergy of a stream defined by (DiPippo, 2004) is given as:

$$Exergy_{stream} = (h - h_0) - T_0(s - s_0)$$

Equation 4

Irreversibility is the difference between reversible work and useful work and is equivalent to exergy destroyed. Fluid friction and heat loss to the surrounding are the two common sources of irreversibility. Irreversibility in the system is generated primarily by pressure drop due to the friction in the pipes, unrestrained expansions in the turbine, and internal energy transfer over a finite temperature difference in the components (Roy et al., 2011). Exergy is destroyed in the plant by the fluid lost in the condenser, exergy of brine that is reinjected, the turbine pump losses, and the preheater vaporizer losses (Yari, 2010).

The equations used for thermodynamic analysis for each component are listed below. The following assumptions were made for the modeling of the system.

- Each component is considered as a steady state flow system.
- Specific heat of the source and sink are constant
- The turbine and pump efficiencies remains constant for all working fluids

Evaporator

$$I_e = T_0 \dot{m}_{ORC} \left[(s_4 - s_1) - \left(\frac{h_4 - h_1}{T_H} \right) \right]$$

Equation 5

$$\dot{Q}_e = \dot{m}_{ORC} (h_4 - h_1)$$

Equation 6

Turbine

$$I_t = T_0\dot{m}_{ORC}(s_2 - s_1)$$

Equation 7

$$W_t = \dot{m}_{ORC}(h_2 - h_1)$$

Equation 8

Refrigerant pump

$$I_p = T_0\dot{m}_{ORC}(s_4 - s_3)$$

Equation 9

$$W_p = \dot{m}_{ORC}(h_4 - h_3)$$

Equation 10

Condenser

$$I_c = T_0\dot{m}_{ORC}\left[(s_3 - s_2) - \left(\frac{\mathrm{h}_3 - \mathrm{h}_2}{\mathrm{T}_\mathrm{L}}\right)\right]$$

Equation 11

$$\dot{Q}_h = \dot{m}_{ORC}(h_3 - h_2)$$

Equation 12

Total irreversibility in the system

$$I_{tot} = I_p + I_e + I_t + I_c = T_0\dot{m}\left[-\left(\frac{h_4 - h_1}{T_H}\right) - \left(\frac{\mathrm{h}_3 - \mathrm{h}_2}{\mathrm{T}_\mathrm{L}}\right)\right]$$

Equation 13

Net-work obtained from the system

$$W_{net} = W_t - W_p$$

Equation 14

Exergy destruction factor (EDF)

$$EDF_{component} = {}^{I_{component}}\!/_{W_{net}}$$

Equation 15

1.7 Configuration of ORC

The ORC consists of evaporator, turbine, condenser and a working fluid pump as the major components in the basic configuration. The schematic of the basic configuration is given in Figure 3. The ORC can be used in various configurations to increase the efficiency. Desai & Bandyopadhyay suggested that the choice of cycle configuration for appropriate integration with the background process depends on the heat rejection profile of the background processes (Desai & Bandyopadhyay, 2009). The thermal efficiency of the ORC slightly decreases with superheating in configuration of dry fluids. Larjola concluded that for low to medium heat source, the best efficiency and power is obtained when the temperature profile of the working fluid matches the heat source temperature profile (Larjola, 1995). Gu et al. suggested that the system performance can be improved by improving the heat/exergy input and by enhancing the heat work conversion ability of the system (J. Guo, Xu, & Cheng, 2010).

An internal heat exchanger can be added to preheat the working fluid entering by the turbine exhaust. This configuration is referred as Internal Heat Exchanger (IHX) or regeneration and the schematic is given in Figure 6. The temperature of the superheated vapor at the turbine outlet is higher than that of the liquid entering the evaporator. Therefore, adding an IHX can be beneficial to improve the thermal efficiency of the system. Efficiency of the ORC can be increased by increasing the temperature at which the heat is added to the system and by lowering the temperature at which the heat is rejected by the system. Adding an internal heat exchanger to the ORC increases the efficiency in two ways. First, it increases the average temperature of heat transfer to the cycle by increasing the temperature of working fluid entering the evaporator. Second, the temperature of the vapors entering the condenser is decreased in the internal heat exchanger by heating the working fluid entering the evaporator thereby lowering the average heat rejection temperature (Aljundi, 2011). Cayer studied the effect of internal heat exchanger on transcritical ORC cycle (Cayer et al., 2009). Yari et al. studied the regenerative ORC using isobutene, isopentane, R113, R123 as working fluids (Yari, 2010). Mago et al. found that regenerative ORC show higher efficiency compared to the basic ORC using first and second law analysis (Pedro J. Mago et al., 2008). Desai et al. observed a 16.5% increase in efficiency for the 16 working fluids studied by employing regenerative ORC (Desai & Bandyopadhyay, 2009). Li et al. performed experimental study using R123 as working fluid (M. Li et al., 2013). They observed efficiency of regenerative ORC is 1.83% higher than the basic ORC. Saleh et al. reported that the highest thermal efficiencies are obtained with dry fluids in subcritical ORC with a regenerator (Saleh et al., 2007). Xi et al. reported higher exergy efficiencies by employing a regenerative ORC configuration (Xi, Li, Xu, & He, 2013).

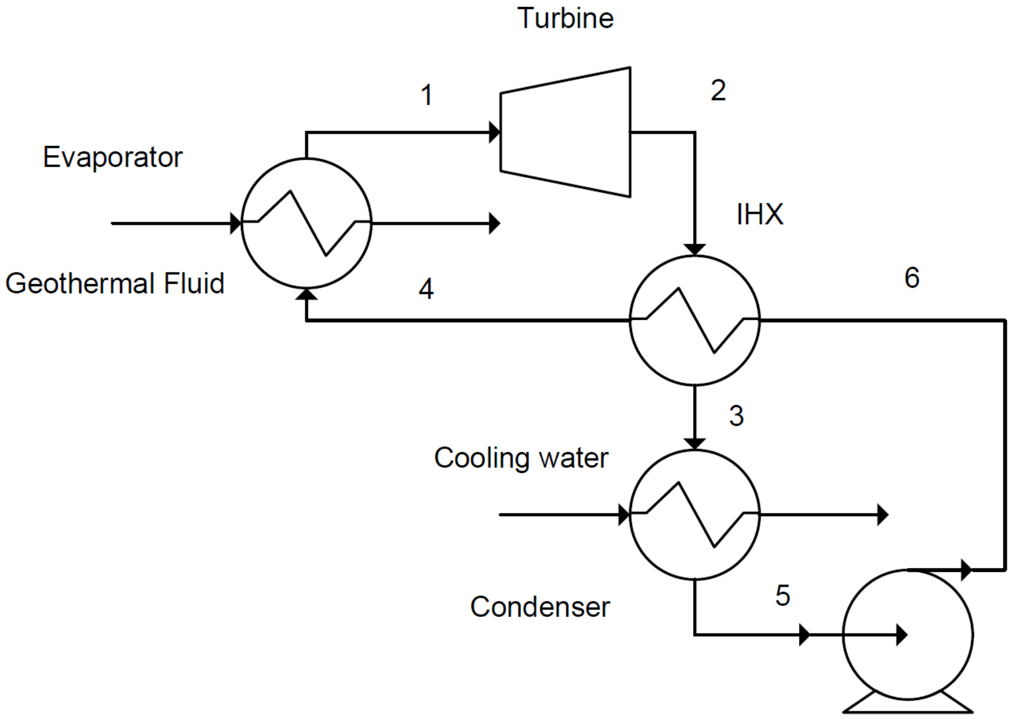

Figure 6 ORC with Internal Heat Exchanger Configuration

Turbine bleeding is a process when a small fraction of working fluid is extracted from the turbine and is mixed with the working fluid before it enters the evaporator. Turbine bleeding increases the mean temperature of heat addition to increase the thermodynamic efficiency of the overall power cycle. The temperature of vapors entering the turbine is significantly higher compared to the stream exiting from the pump. Mixing vapors from the turbine with the pump exit stream increases the average temperature of heat addition to the ORC system leading to increase in efficiency. However, the net shaft work is reduced due to the extraction of the working fluid for the turbine (P J Mago, Srinivasan, Chamra, & Somayaji, 2008).

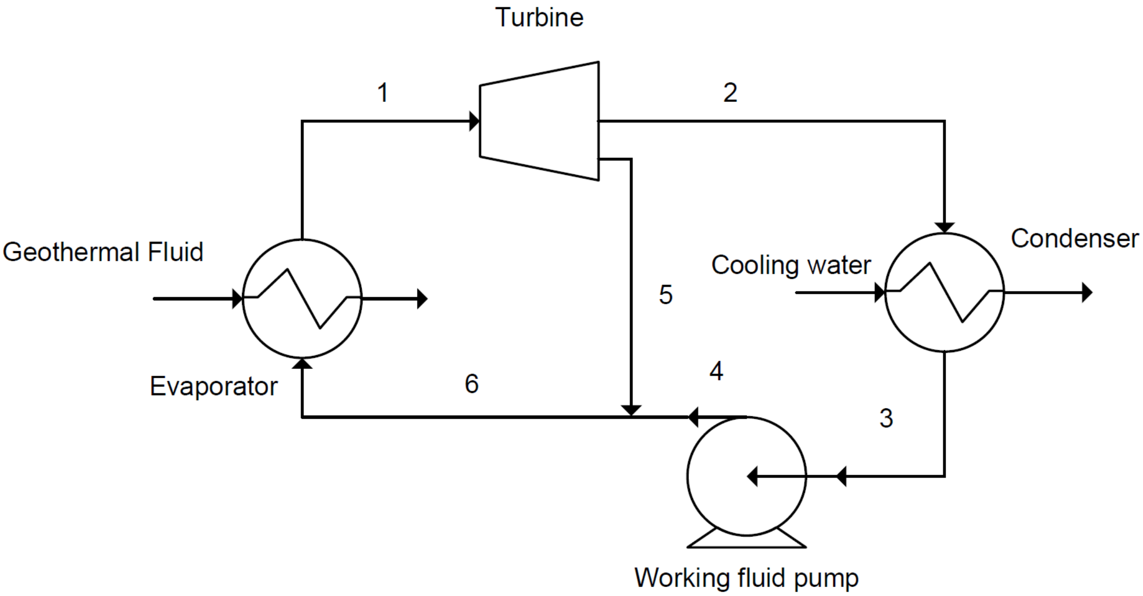

Figure 7 ORC with Turbine Bleeding configuration

1.8 Economic considerations

The investment cost of geothermal plants can be categorized into surface equipment and the subsurface investment. Economics of the ORC system must be taken into account during optimization. An ORC system designed to deliver maximum efficiency may not be the most economical design. There is no precise information available for the capital cost of ORC power plant. Also, the capital cost differs for various manufactures and various sizes of equipment. The capital cost of low temperature ORC systems is strongly dependent on the cost of the components such as heat exchangers, turbine and pumps. The cost of these ORC components is directly related to their sizes (Lakew & Bolland, 2010). The typical drilling cost of a low temperature developments lies between 10% to 20% of the total development cost (Stefánsson, 2002). This study is focused on the capital cost of the ORC system for the economic consideration.

The maximum working pressure, the total heat transfer area and the expander size are the important parameters that influence the economics of the ORC system (He, et al., 2012). The maximum working pressure is set by the corresponding saturation temperature of the working fluid in the evaporator. The saturation temperature is restricted by the resource temperature and the pinch point temperature in the evaporator. The total heat exchanger consists of the evporator and condenser area, and IHX area in case of IHX configuration. The heat exchanger areas for each indivual heat exchangers are obtained from the simulation results. The turbine size parameter is an indicator of turbine size (He et al., 2012) , (Lakew & Bolland, 2010), (Khennich & Galanis, 2012). The size parameter to calculate the expander size is given below

$$SP = \frac{\sqrt{V}}{\sqrt[4]{\Delta H}} \qquad \text{Equation 16}$$

Where, V(m^3/s) is the volumetric flow rate of the working fluid and ΔH (J/kg) is the specfic enthalpy drop across the turbine.

The study presented here consists of constrained and non constrained desgins. It is reasonable to assume the cost of the heat exchangers (evaporator, condenser, internal heat exchanger) to be representative of the capital cost of the ORC power plant (Hettiarachchi et al., 2007).

Many economic indicators have been suggested by several authors. Shengjun et. al 2011 used area per unit power output and levelized energy cost as two economic indicators. Levelized Cost of Electricity (LCOE) is defined as the cost of electricity generation over the life of the power plant. The typical installed costs for an ORC range from $1,800 to $3,000 per kilowatt. The installed costs can be as low as $1,300 per kilowatt for HVAC derived units (Arvay et al., 2011).

The LCOE was for this study was calculated using NREL’s simple LCOE calculator (NREL, 2013). The calculator is a simple model to calculate the LCOE for both utility-scale and distributed generation renewable energy technologies. The LCOE is based on the combination of captial costs, operations and maintenance, performance, and fuel costs. The calculator does not include financing issues, discount issues, future replacement, or degradation costs.

1.9 Optimization of ORC

The definition of first law efficiency can be misleading when comparing different working fluids. A cycle may have smaller input and produce small power and can have high efficiency. One way to compare the performance of the working fluids would be compare the output power. (Dai et al., 2009) used exergy efficiency as the objective function for optimization of basic and IHX configuration.

In a study conducted by Khennich & Galanis, it was found that two optimum evaporation temperatures exist for a given working fluid and source condition (Khennich & Galanis, 2012). The first optimum evaporation temperature minimizes the total thermal conductance of the evaporator and condenser together. The second optimum evaporation temperature maximizes the net power output. The continuation of this study was performed to evaluate the effect of varying the evaporation temperature on thermal efficiency, total exergy losses, thermal conductance and turbine size SP (Khennich & Galanis, 2012). They observed that the conditions for a given working fluid maximizing the thermal efficiency are essentially the same as those minimize the total exergy loss. The conditions minimizing total thermal conductance require a turbine size similar to the size corresponding to the minimum value of SP obtained by minimizing SP. The total thermal conductance corresponding to the minimum turbine size required a very large total thermal conductance. Based on the above discussion, maximizing the thermal efficiency was chosen to be the optimization criterion.

Hettiarachchi et al. performed optimization of ORC using total heat transfer to total new power produced as the objective function (Hettiarachchi et al., 2007). Invernizzi et al. conducted optimization of evaporation temperature of the ORC using overall recovery efficiency as the objective function (Invernizzi, Iora, & Silva, 2007). Bamgbopa et al. concluded that adjusting the flow rate working fluid helps in improving the thermal efficiency and maintaining the steady stead operation (Bamgbopa & Uzgoren, 2013).

Madhawa et al. used evaporation and condensation temperatures, geothermal and cooling water velocities are the variables for optimization (Hettiarachchi et al., 2007). Ammonia, HCFC123, n-pentane and PF5050 were evaluated for optimum cycle performance. The objective function which is a ratio of total heat transfer area to total net power was used as optimization criterion. It was found out that ammonia has minimum objective function and maximum geothermal water utilization but not necessarily maximum cycle efficiency (Hettiarachchi et al., 2007). Cayer chose six indicators for optimization of transcritical ORC (Cayer, Galanis, & Nesreddine, 2010). These indicators include thermal efficiency, specific net output, exergy efficiency, total conductance of the heat exchangers, and surface of the heat exchangers and the relative cost of the system. Shengjun et al. used thermal efficiency, exergy efficiency, recovery efficiency, area per unit power, and levelized cost of electricity as five indicators to evaluate the working fluids for ORC (Shengjun et al., 2011). For the study presented here, thermal efficiency, exergy efficiency, net power, \$/kW and Levelized Cost of Electricity (LCOE) as performance indicators for the evaluation of the working fluids.

CHAPTER II

METHODOLOGY

2.1 Model development

The first step involved in this study was developing a computer model of the Organic Rankine Cycle (ORC) using a process simulator. Aspen HYSYS$^{®}$ was used to develop a model of the ORC power plant. Aspen HYSYS$^{®}$ is a commercial software package provided by Aspentech and was chosen for this study due to its ease of programming and accurate results. The results obtained from Aspen HYSYS$^{®}$ were compared to the database provided by NIST.

Mago et al. concluded that organic fluids must be operated at saturation conditions to reduce the total irreversibility of the system. He further added that superheating of dry organic fluids lowers the efficiency of the ORC by increasing the irreversibility. Therefore, superheating is not required for organic fluids compared to water where efficiency is proportional to the superheat of the steam.

REFPROP is the property package developed by the National Institute of Standards and Technology (NIST). REFPROP is an abbreviation for Reference Fluid Properties and was the property package used for all the simulations for this study. The simulation results obtained from the model were compared to the real plant data for validation. This model was next used to study the performance of the power plant at various operating conditions such as flow rate and temperature of both geothermal resource and cooling medium. Based on the resource conditions for the new geothermal resource and the size of the equipment, the performance of ORC was studied for 12 working fluids for 250kW generator output. The first law of thermodynamics was used to determine the thermal efficiency of ORC. Exergy efficiency was calculated to identify process deficiencies. Exergy destruction factor (EDF) was determined to understand the irreversibility distribution across the ORC system. In this approach, the size of equipment and the maximum output power from the system was constrained. Base, internal heat exchanger and turbine bleeding configurations were studied using this approach.

A non-constrained design approach was also studied where the resource and cooling media conditions were kept constant and other parameters such as working fluid flow rate, size of equipment and maximum power output from the system were variables. The rationale behind using this approach is to optimize the ORC system for a given resource and cooling media without any constraints. Base, internal heat exchanger and turbine bleeding configurations were studied using this approach.

The results obtained from thermodynamic modeling using HYSYS were compared to the NIST Reference Fluid Thermodynamic and Transport Properties Database (REFPROP): Version 9.1 for validation.

2.2 Optimization of ORC

The optimization of the ORC was performed to maximize the thermal efficiency. By the definition, exergy efficiency is dependent and directly proportional to the thermal efficiency. The optimization of the ORC was conducted using the “optimizer” tool of Aspen Hysys. The optimizer tool used thermal efficiency as the objective function and was set to maximize. The maximum working fluid pressure and mass flow rate were the two parameters varied to maximize the thermal efficiency. For constrained cases, the turbine power was set to 250kW and the pressure and the mass flow were varied to maximize thermal efficiency. The maximum values of thermal conductance for the heat exchangers are restricted to the value obtained from the model validation with the Chena Geothermal Power Plant. The maximum pressure possible for the working fluid is set by the saturation temperature and is restricted by the source temperature.

For non-constrained cases, thermal efficiency was maximized by varying the maximum pressure and mass flow rate of the working fluid. The turbine power was no longer restricted and was calculated by the optimized conditions. The thermal conductance for the heat exchangers is calculated by optimized conditions. Table 3 shows the design differences between the constrained and non-constrained cases.

Table 3 Design for the constrained and non-constrained cases

	Constrained	Non-Constrained
Geothermal Resource Temperature (°F)	210	210
Geothermal Resource Flow Rate, GPM	875	875
Cooling Water Temperature (°F)	70	70
Maximum Gross Turbine Output, kW	250	Variable
Maximum Evaporator UA Value (Btu/F-hr)	2.20×10^5	Variable
Maximum Condenser UA Value (Btu/F-hr)	5.85×10^5	Variable
Maximum Turbine Size, m	0.15	Variable
Ambient Temperature, T_0 (°F)	77	77
ΔT at Pinch Points in Heat Exchangers , (°F)	10	10
ΔT of the Cooling Water, (°F)	10	10
Turbine Efficiency	0.8	0.8
Maximum Pressure in the Cycle, psia	Variable	Variable
Maximum Flow Rate of Working Fluid, lb/hr	Variable	Variable
Configurations	Base, IHX, TB	Base, IHX, TB

2.3 Cost analysis of ORC

The cost analysis was performed using capital cost expressed as installed equipment cost and levelized cost of electricity. The installed equipment cost was obtained using Aspen Hysys for each individual working fluid for all the six configurations. The equipment cost was divided by the net power produced for each case to express the equipment cost into $/kWh. The cost analysis performed in this study does not include any drilling or exploration cost for the geothermal resource. The Levelized Cost Of Electricity (LCOE) was calculated using National Renewable Energy Laboratory's simple calculator (NREL, 2013). The values of the parameters used for LCOE calculation are summarized in Table 4.

Table 4 Parameters for Levelized Cost of Electricity Calculation

Parameter	Value
Periods (year)	20
Discount Rate (%)	3
Capital Cost ($/kW)	Equipment cost/Net Power
Capacity Factor (%)	90
Fixed O&M Cost ($/kW-yr)	180
Variable O&M Cost ($/kWh)	0
Heat Rate (Btu/kWh)	0
Fuel Cost ($/MMBtu)	0
Electricity Price (cents/kWh)	7
Cost Escalation Rate (%)	1.6%

The useful project life was assumed to be 20 years. The Discount rate was adapted from Federal Energy Management Program (Rushing, Kneifel, & Lippiatt, 2013). Geothermal plants fall under base-load power plants and generally have higher capacity factor. The capacity factor value was chosen to be 90% based on the report published by NREL (Tidball, Bluestein, Rodriguez, & Knoke, 2010). The fixed and variable operation and maintenance costs, heat rate and fuel cost were also selected based on the NREL report (Tidball et al., 2010). For renewable energy systems, the heat rate and fuel cost assumed by the model is 0. The electricity price and its commercial cost escalation rate was chosen as 7 cents per kWh and 1.6% for Midwest region respectively (NREL, 2013). The net power output, total heat exchanger area, size parameter and LCOE were used as economic indicators.

Chapter III

RESULTS & DISCUSSIONS

3.1 Model validation against the Chena Geothermal Power Plant

The Chena geothermal power plant was built at the Chena Hot Springs, Alaska in 2006. The plant uses United Technology's Pure-cycle ORC unit which produces 250kW gross power. The ORC model developed for this study was compared to the data obtained from Chena Geothermal Power Plant for validation of the model. The ORC model developed using the Aspen HYSYS$^{®}$ process simulator. Figure 3 shows the schematic of an ORC. The design conditions for the modeling were adapted from the published literature and are given in

Table 5 (Holdmann, 2007), (Aneke, Agnew, & Underwood, 2011). REFPROP property method was used for the simulation of the ORC power plant. REFPROP is based on the most accurate pure fluid and mixture models currently available. Table 6 compares the results obtained from the simulation to the actual plant data for validation. It can be observed that the simulation results are comparable to the plant data.

Table 5 Design Conditions for the ORC Model

Geothermal fluid temperature (°F)	164
Geothermal fluid mass flow rate (gpm)	530
Cooling water source temperature (°F)	40
Cooing water source flow rate (gpm)	1614
Working Fluid	R134a
Turbine efficiency	0.8
Turbine inlet pressure (psia)	232
Gross generator power (kW)	250

Table 6 Comparison of the Simulation Results

	Plant data	Simulation result	Relative error $\lvert\Delta X\rvert \times 100/X$
Turbine outlet pressure (psia)	63.67	63.26	0.64
Pump power (kW)	40	39.55	1.13
Geothermal exit temperature(°F)	130	132.1	1.62
Cooling water exit temperature (°F)	50	49.54	0.92
Working fluid mass flow rate (kg/s)	12.17	11.52	5.34
Net plant power (kW)	210	210.45	0.21
Thermal efficiency	0.08	0.085	6.29
Evaporator heat transfer rate (kWth)	2580	2475	4.07
Condenser heat transfer rate (kWth)	2360	2264	4.07
Evaporator UA value (Btu/F-hr)		2.20×10^5	
Condenser UA value (Btu/F-hr)		5.85×10^5	

Figure 8 and Figure 9 show the heat flow diagrams obtained by the simulation for the evaporator and the condenser respectively. The x and y axis represents the stream heat flow and temperatures across the heat exchanger respectively. It is assumed here that the both the heat exchangers operate in counter-flow fashion. Heat flow diagrams are useful to detect the pinch points in the heat exchanger. A pinch point is the point where the temperature difference between hot and cold curve is minimum. The heat flow in a heat exchanger is proportional to the temperature difference between the two streams and is governed by simple equation below.

$$Q = U\,A\,\Delta T \qquad \text{Equation 17}$$

Where Q is the heat flow, A is the heat exchanger area and ΔT is the temperature difference between the heat exchanging streams at any given point in the exchanger. As the temperature difference between the streams exchanging heat decreases, the heat flow across the streams decreases. In a situation where the heat curves intersect, the temperature difference is reduced to zero and there is no heat flow at the pinch point.

Pinch point temperature difference and heat exchanger area are inversely proportional to each other (Lakew & Bolland, 2010) (Y.-R. Li, Wang & Du 2012). The heat exchanger area must be increased to compensate for the decreased temperature difference in order to maintain the same heat flow. More heat is absorbed when the pinch is decreased. However, the heat exchanger area required will increase. Therefore, it is important to make a tradeoff between heat exchanger area and heat flow which dictates the performance of the cycle. Pinch point temperature difference plays an important role in the cost efficiency tradeoff (Y.-R. Li et al., 2012). The pinch point temperature difference affects the evaporation temperature and the condensation temperature (Y.-R. Li et al., 2012). The pinch point constrains the temperature boundaries for the working fluid which sets the pressure range for the ORC cycle. The saturation pressures are limited by their corresponding temperatures. As well, the exergy efficiency of the ORC decreases as the temperature difference at pinch point decreases (Xi et al., 2013).

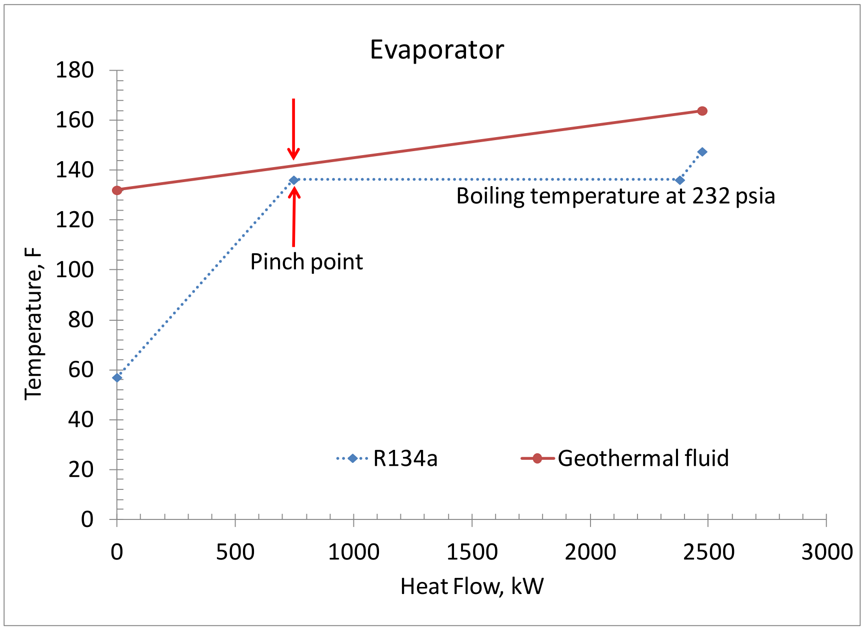

Figure 8 Heat flow diagram for the evaporator

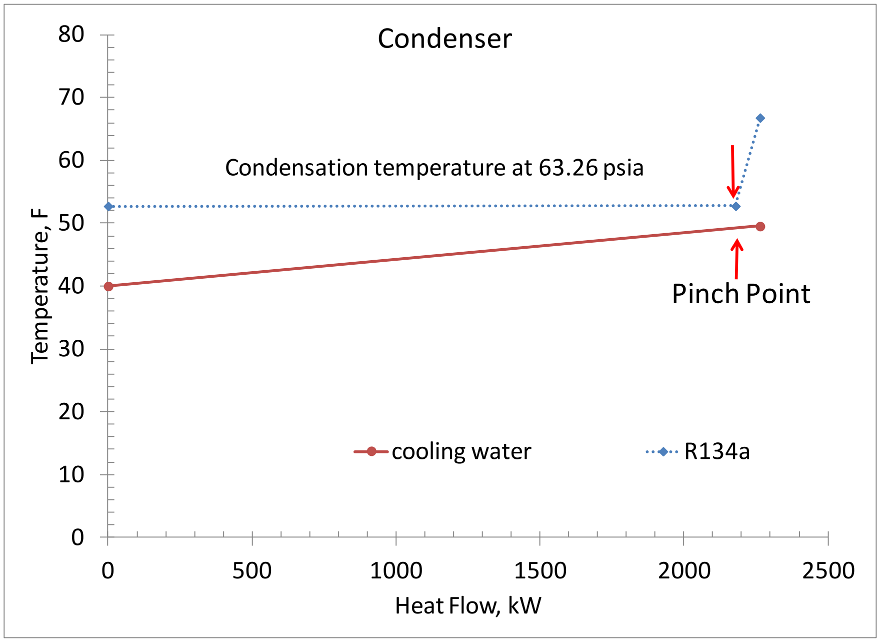

Figure 9 Heat flow diagram for the condenser

Heat curves in Figure 8 and Figure 9 also shows the temperature profile and match degree between the thermal fluids in the heat exchangers. The match degree can be referred as how parallel the heat curves are to each other. Match degree can be best described using Figure 10 which compares the profile actually obtained in the evaporator to the ideal case profile. The dashed line shows the profile which could have been obtained if there were no phase change of the working fluid. If the pinch point did not exist, then the working fluid temperature would have been much higher than it is in real case. The difference between the dashed line and translates into lost potential in the evaporator. Therefore, it is essential to have a good profile match in the heat exchanger to minimize this lost potential.

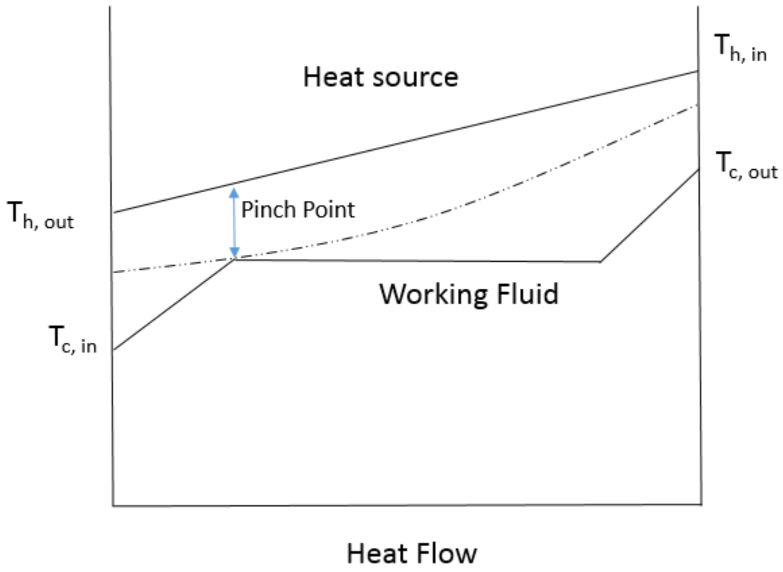

Figure 10 Heat flow diagram with working fluid exhibiting ideal match degree

3.2 Performance of the ORC Model

The ORC model was developed using Aspen HYSYS and is explained in the previous sections. The ORC model was validated using the Chena geothermal power plant. This section studies the effect of varying some of the conditions on the performance of Chena power plant. For turbine systems, turbine inlet temperature and pressure ratio in the turbine are the important factors governing the efficiency of the system (Yamamoto et al., 2001). The pressure ratio in the turbine dictates the power produced by the turbine. For the Chena geothermal power plant, the evaporator input power was varied at each pressure ratio across the turbine and the corresponding power output was observed. The higher and lower boundaries of pressures are set by the resource and heat sink temperatures. The maximum value of pressure is the saturation pressure corresponding to the maximum temperature in the system. The maximum temperature in the system is the difference between the source temperature and the pinch point temperature. As per the second law, both the higher evaporation temperature and the lower condensation temperature increase the system thermal efficiency (Quoilin, Declaye, Tchanche, & Lemort, 2011).

As observed in Figure 11, the output power of turbine increases as the heat input to the evaporator is increased. As the evaporator input increases, the working fluid gains more heat which in turn increases the output power of the turbine. A linear correlation is observed between the heat input to the evaporator and the turbine output power. The pressure ratio also has a significant effect on the output power of the turbine. As the pressure ratio is increased, the turbine output power increases substantially. The output power increased from 170 kW to 250 kW when the pressure ratio is increased from 2.4 to 3.6. The power produced by the turbine is directly proportional to the enthalpy difference between the inlet and outlet streams. The enthalpy of the stream is governed by the pressure of the stream in addition to its temperature. Therefore, with a higher pressure ratio more power is extracted from the stream across the turbine which leads to increased output power.

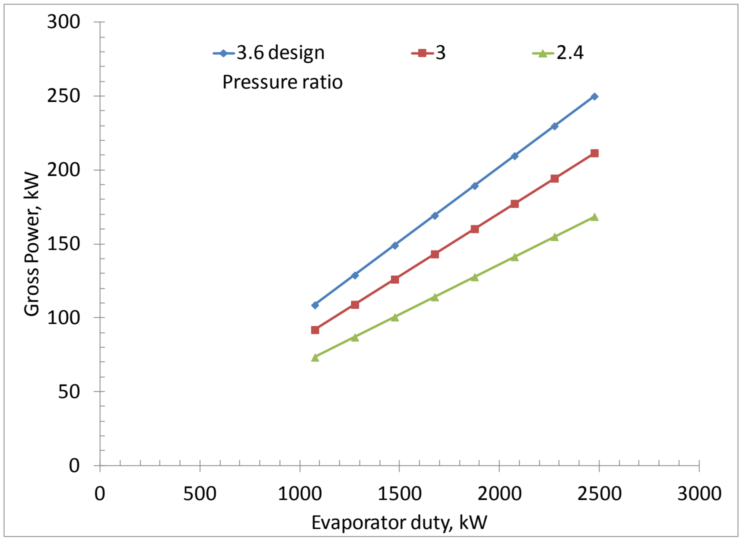

Figure 11 Output power vs. heat input for different pressure ratios

Figure 12 shows the effect of pressure ratio on the cycle efficiency. As expected, increasing the pressure ratio increases the cycle efficiency. As the pressure ratio across the turbine is increased, the power output is increased. Also the power requirement by the pump also increases at the pressure ratio increases. However, the increase in turbine power is significantly higher that the increase in the pump power. Therefore, at higher pressure ratios, more output is generated for the same input energy thereby increasing the cycle efficiency. These results concur with the observations from Figure 11. The maximum pressure ratio obtained for the system is dictated by the resource and the cooling media temperature (saturation pressures for the working fluid sets the boundaries).

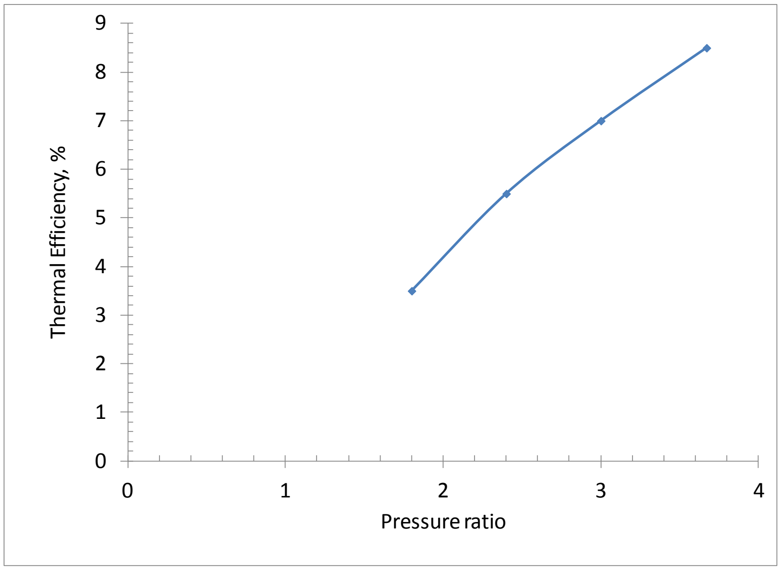

Figure 12 Effect of pressure ratio on the thermal efficiency

Figure 13 shows relation of output power with the inlet temperature of the heat source. As observed, the turbine output increased as the inlet temperature increased. As the inlet temperature is increased, the corresponding saturation pressures are increased. As observed earlier, higher saturation pressures allows for a higher pressure ratio across the turbine increasing the overall efficiency. Also, higher inlet temperatures increase the amount of heat gained by the working fluid which leads to increased output power of the turbine. The Carnot efficiency indicates that higher thermal efficiency can be obtained by increasing evaporating temperature. It can be concluded that for given temperature of resource and cooling media, higher turbine inlet temperatures increases turbine power subsequently increasing the thermal efficiency.

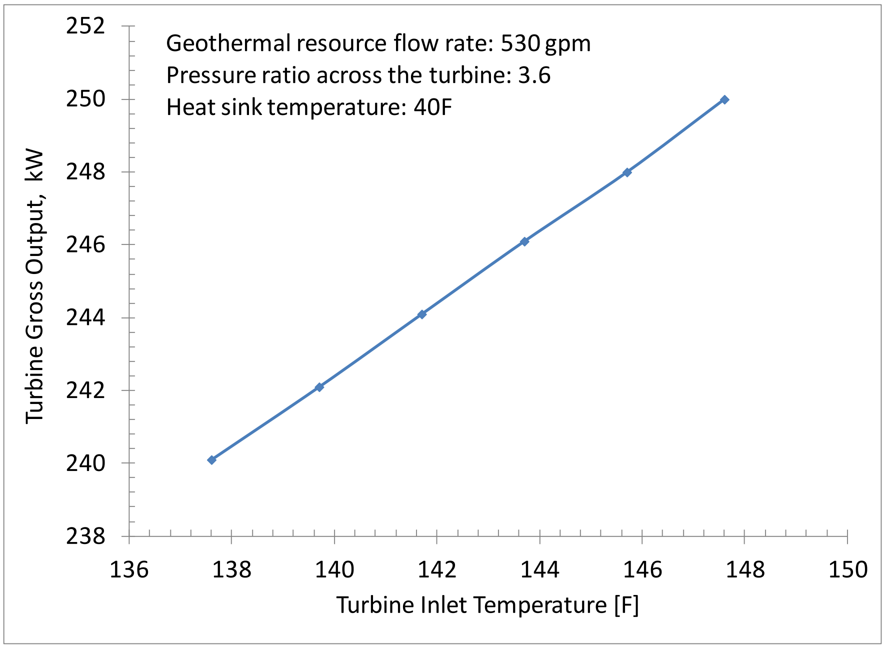

Figure 13 Turbine output power as a function of geothermal water temperature

Next, the effect of the cooling water temperature on the power output of the ORC was observed. The output of ORC is also dependent on the cooling water temperature. As observed in Figure 14, the output power decreases as the temperature of the cooling water increases. The condensation temperature decreases as the temperature of heat sink decreases lowering the condensation pressure. Lower condensation pressure results in higher pressure ratios across the turbine for a same given resource yielding higher turbine power. The condenser pressure is limited by the temperature at which the heat is rejected.

As per Carnot efficiency, the thermal efficiency can be increased by decreasing the condensing temperature.

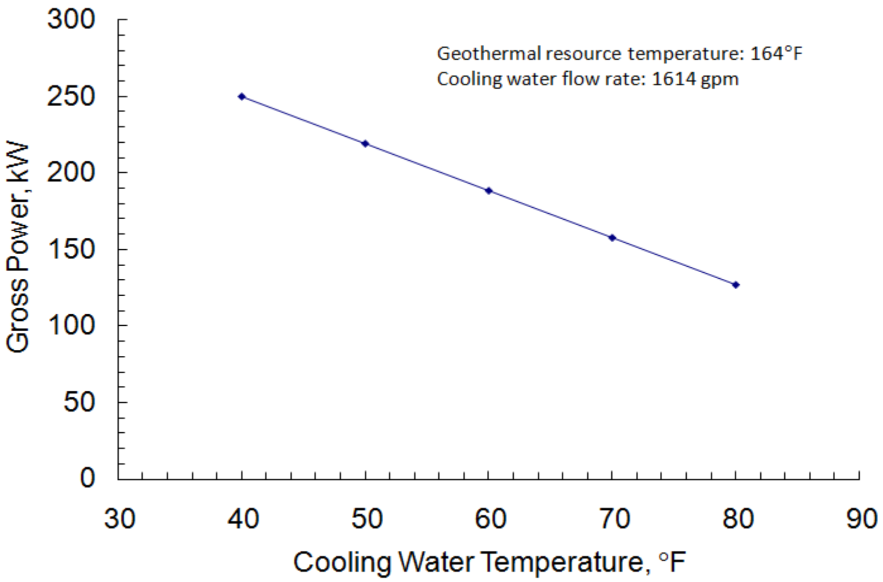

Figure 14 Turbine output power as a function of cooling water temperature

3.3 Energy Analysis – Base Configuration

A simple ORC can be represented as base configuration and is shown in Figure 15. The energy analysis of the constrained base configuration is discussed in this section. The resource temperature and flow rate is 210°F and 875gpm respectively, and the cooling media temperature is assumed 77°F and remains constant for both designs. The equipment sizing is optimized for each working fluid. The maximum values allowed for each equipment sizing are constrained and showed in Table 7. The energy analysis using the first law of thermodynamics was performed for the 12 workings fluids in the base configuration. The gross power for this case is kept constant at 250 kW. The ORC was optimized for each working fluid and the simulation results obtained were compared to the NIST standard database.

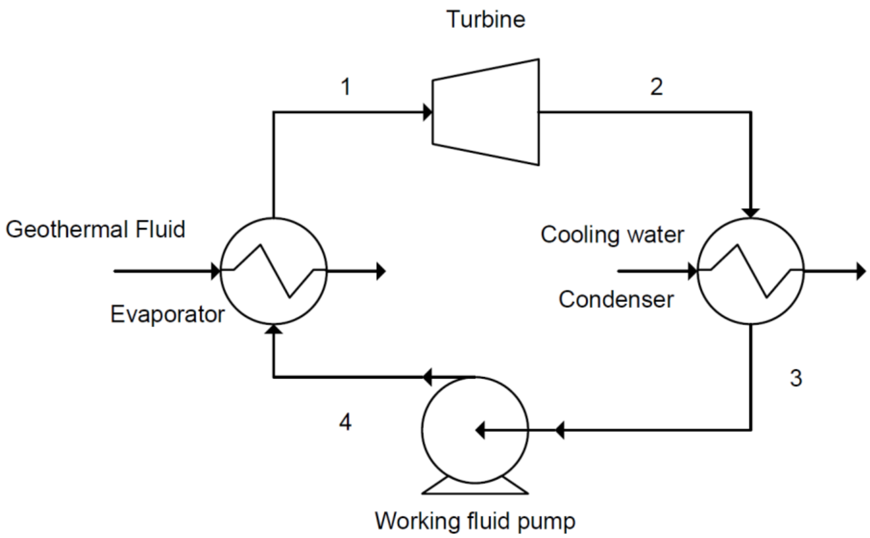

Figure 15 Schematic of base ORC configuration

Table 7 Conditions for the Constrained ORC Design

	Constrained
Geothermal resource temperature(°F)	210
Geothermal resource Flow rate, gpm	875
Cooling water temperature (°F)	77
Maximum gross turbine output, kW	250
Maximum Evaporator UA value (Btu/F-hr)	2.20×10^5
Maximum Condenser UA value (Btu/F-hr)	5.85×10^5
Maximum Turbine Size, m	0.15

First and second law efficiency for power generation depends on the temperature of geothermal source (Heberle & Brüggemann, 2010). First law analysis takes into account the actual energy transferred to the ORC whereas the second law analysis is based on the potentially available energy of geothermal source. First law efficiency represents the fraction of heat transferred that is converted into useful work. Figure 16 shows the thermal efficiencies of the 12 working fluids for the same given gross power output. The net power changed for each working fluid even though the net power was same for all the fluids. The net power is different for each working fluid since the cycle operates at different pressures governed by the working fluid. Net power dictates thermal efficiency and hence, the thermal efficiencies are not the same for the working fluids with the given same gross power output. R245ca and R123 are the fluids that yielded the highest thermal efficiency out of the selected 12 working fluids.

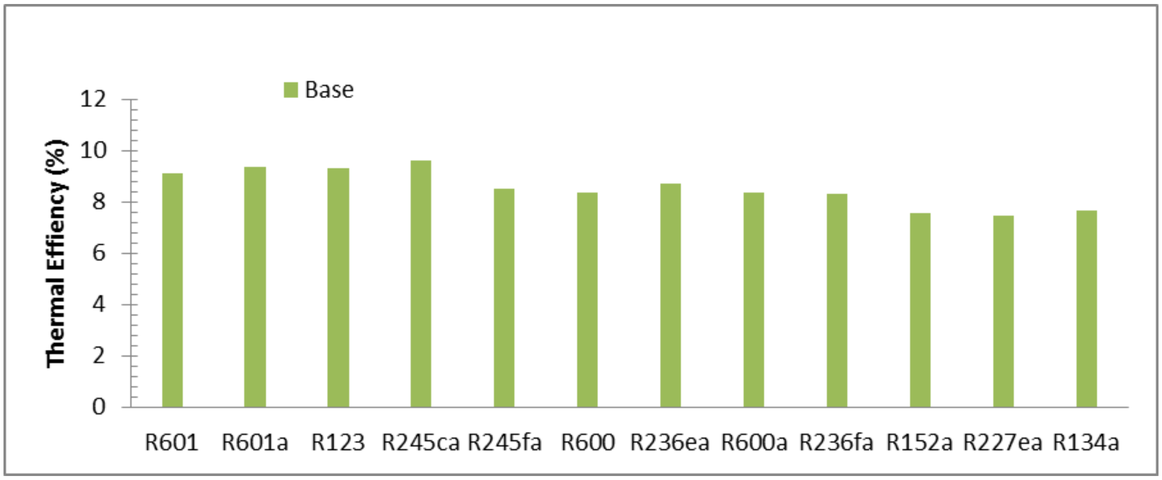

Figure 16 Thermal efficiencies of the working fluids

The second law of thermodynamics dictates that both the higher evaporation temperature and the lower condensation temperature increase the thermal efficiency (Quoilin et al., 2011). However, the evaporation temperature and condensation temperature are restricted by the heat source temperature and the ambient temperature respectively. The Carnot efficiency is estimated to be 19.8%. Since for all working fluid the resource and heat sink temperatures are constant, the Carnot efficiency remained the same for all cases. The difference in efficiency from 7.7% to 9.6% for the best and poorest performing working fluids translates into 18% increase in net power output. The thermal efficiency of R245ca was 25.8% higher than the efficiency of R152a.

3.4 Exergy Analysis – Base Configuration

Exergy analysis is based on the second law of thermodynamics and gives a measure of irreversibilities in the cycle. Exergy analysis reveals the degradation of the system's ability to perform work with respect to the surroundings (Yari, 2010). Figure 17 compares the exergy efficiencies for the working fluids for the same power output. Exergy efficiency is a measure of performance relative to performance under reversible conditions. Similar to thermal efficiency, exergy efficiency is highest for R245ca and lowest for R152a. It can be observed that second law efficiency follows the same trend as the first law efficiency. This is due to the fact that the second law efficiency is the ratio of first law efficiency to the maximum work possible. For given heat source and ambient conditions, the maximum work remains constant. Therefore, second law efficiency is directly proportional to first law efficiency. Exergy efficiency of R245ca was calculated as 48.4% and is 37% higher than that of R152a. DiPippo reported geothermal plants having exergy efficiency of 40% or greater (DiPippo, 2004).

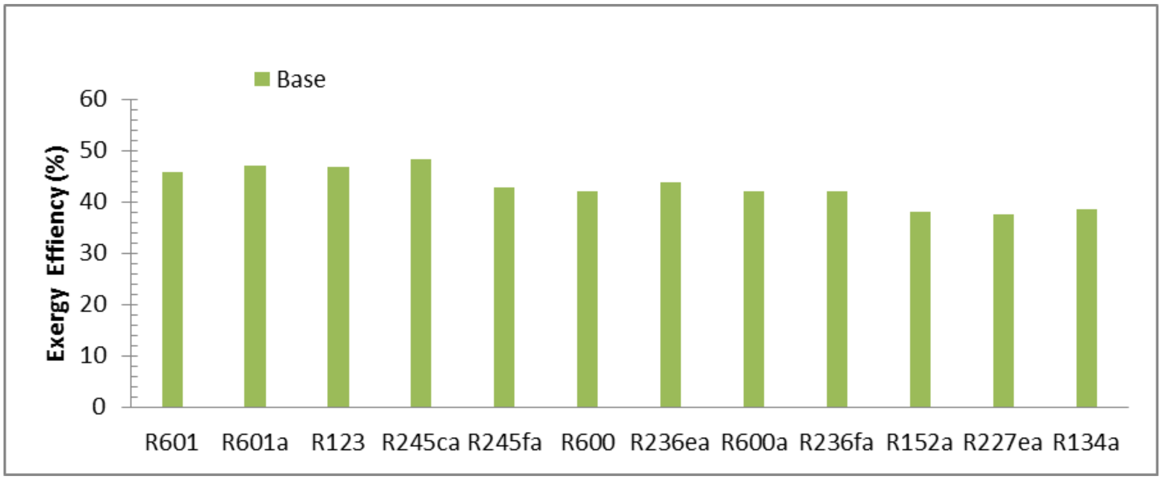

Figure 17 Exergy efficiencies of different working fluids

3.5 Exergy Destruction Factors – Base Configuration

Exergy Destruction Factor (EDF) is ratio of the exergy destruction rate to the net power obtained from the system. EDF values are a good way to compare the performance of different working fluids. EDF is the ratio of irreversibility to the net work of the system. When the EDF value of the system is zero, no exergy is destroyed and the system is free from any irreversibilities. An EDF value of less than one implies more exergy is recovered than destroyed from the system. When the exergy destroyed equals to the net work of the system, the EDF value of the system approaches unity. Higher EDF values indicate system is getting more inefficient. An increase in EDF value from 1 to 1.7 results in 43% increase in total exergy destruction.

Table 8 shows the exergy destruction factor for each component calculated by exergy analysis. The exergy destruction factor indicates the distribution of irreversibility for each component. For all the 12 working fluids, the evaporator has the highest value of EDF and the pump has lowest value. Similar results were observed by Aljundi, 2011, Hung 2001 and DiPippo, 2004 in their studies. R245ca and R152a have the lowest and the highest value of EDF for the total system. A low EDF value indicates less irreversibility in the system and leads to higher efficiency. Therefore, R245ca exhibits the highest value of thermal and exergy efficiency.

Table 8 EDF for each Component for the Working Fluids

Working fluid	EDF_T[1]	EDF_C	EDF_P	EDF_E	EDF_{TOT}
R601	0.23	0.58	0.03	0.47	1.32
R601a	0.24	0.56	0.05	0.40	1.25
R123	0.32	0.50	0.05	0.39	1.26
R245ca	0.24	0.49	0.05	0.41	1.19
R245fa	0.24	0.45	0.06	0.73	1.48
R600	0.25	0.52	0.09	0.65	1.51
R236a	0.25	0.33	0.07	0.77	1.42
R600a	0.26	0.34	0.11	0.80	1.52
R236fa	0.25	0.27	0.09	0.91	1.53
R152a	0.33	0.20	0.13	1.13	1.79
R227ea	0.28	0.33	0.19	1.03	1.82
R134a	0.27	0.25	0.17	1.05	1.75

---

[1] Subscripts: T- Turbine, C- Condenser, P- Pump, E- Evaporator, TOT- Total

Exergy destruction varied as the match degree varied between fluid streams in the evaporator (DiPippo, 2004). Larjola observed that higher power output is obtained when the working fluid matches the heat source (Larjola, 1995). This implies that decreasing the temperature difference between heat source and working fluid results in lower irreversibility thereby showing better performance. It can also be observed that the EDF value for pumps is very low except for fluids R600a, R152a, R227ea and R134a. This could be explained by the higher pressure rise across the pump for these fluids compared to the rest of the working fluids. Higher pressure drop across the turbine resulted in higher EDF value of the turbine. Higher pressure drop across the turbine requires higher pressure across the pump. Hence for a cycle having higher pressure drop across the turbine will have higher EDF values which will subsequently increase the required pressure rise across the pump and EDF value for pump. Hung et al. observed that the total irreversibility of the system decreased as the turbine inlet pressure increased (T. Hung, 2001). As the turbine inlet pressure is increased, the corresponding saturation temperature is increased. This lead to decrease in temperature difference between the heat source and working fluid. Tchanche et al. observed that for basic ORC the highest irreversibility occurs in the evaporator followed by the turbine, condenser and pump (B. F. Tchanche et al., 2009). Aljundi observed that highest and lowest exergy destruction occurs in evaporator and pump respectively (Aljundi, 2011). The results reported here are in agreement with the previous studies conducted by various authors.

Exergy analysis is used to identify process deficiencies and allows to choose system components that represent the most potential for improving the overall efficiency of the entire system. Figure 18 shows the exergy destruction rate across the each component for the ORC. Similar to the EDF values, the rate of exergy destruction is highest in evaporator, followed by condenser, turbine and pump. This is expected as the EDF values are derived from the exergy destruction rate. Overall, exergy analysis suggests that highest work potential is lost in the evaporator and condenser. Similar observations has been made by other authors (El-Emam & Dincer, 2013), (P J; Mago et al., 2008). For R600 shown in the Figure 18, 77% of the exergy destruction occurs in the evaporator and condenser combined. Therefore the heat exchangers represent the components for most potential for improving the overall cycle efficiency. Figure 19 shows the temperature entropy diagram for the R600 in the base configuration. It can be observed that there is some superheating of the working fluid R600 in the evaporator region. Superheating is not desirable since it decreases the overall efficiency of the ORC.

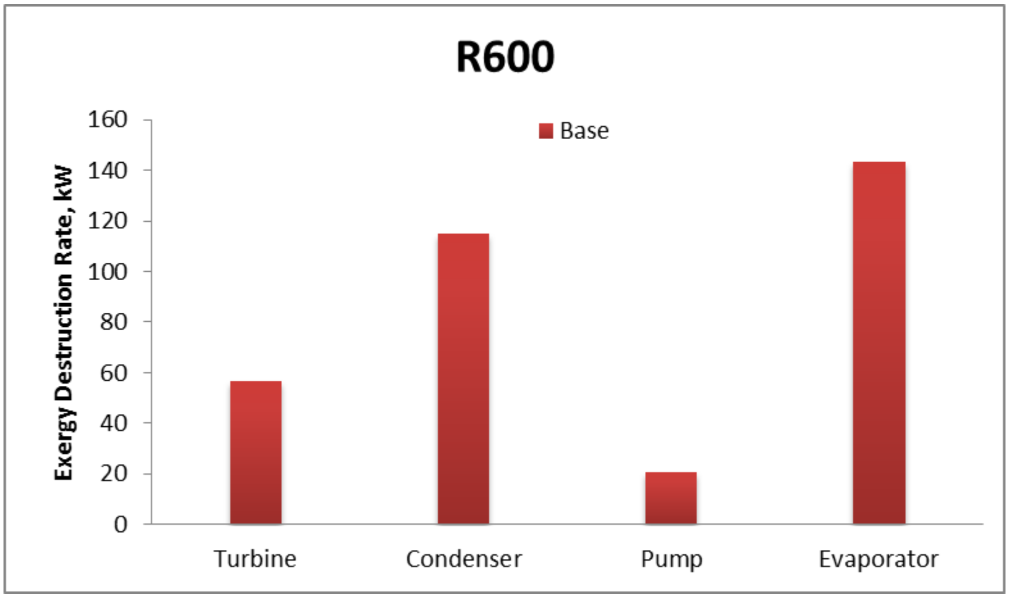

Figure 18 Exergy destruction rate across each component

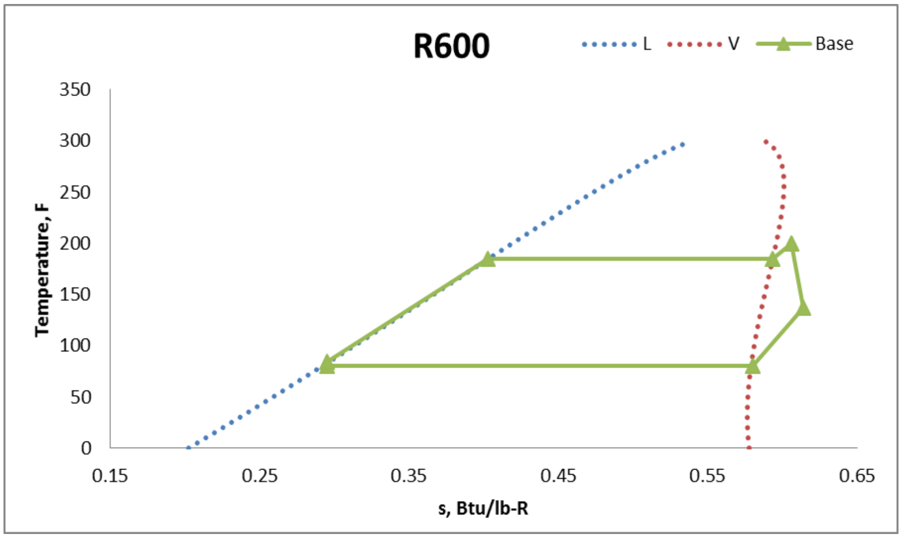

Figure 19 Temperature entropy diagram for R600 in base configuration

Table 9 shows the simulation results obtained for the 12 working fluids. The turbine inlet and outlet pressure is observed to increase as the critical temperature (T_c) of the fluid decreased. As well, an increasing trend is observed in the mass flow rate with decrease in T_c. As the mass flow rate and maximum pressure increases in the cycle, more power is consumed and can also be confirmed from Table 9. The net power of the cycle decreases as the pump power increases. The gross power for the cycle is constant and an increase in pump power would decrease the net power.

Table 9 Results Obtained From the Simulation for the Base Case

Working fluid	P_{in} (psia)	P_{out} (psia)	$\dot{m}_{ORC}$ (lb/hr)	η_I	η_{II}	W_p (kW)	W_{net} (kW)
R601	64	16	4.7E+04	9.1	45.8	11	239
R601a	90	20	4.6E+04	9.3	47.0	16	234
R123	95	20	9.2E+04	9.3	46.9	15	217
R245ca	110	22	8.0E+04	9.6	48.4	16	234
R245fa	116	28	9.0E+04	8.5	42.8	18	232
R600	163	47	4.6E+04	8.4	42.2	29	221
R236a	139	33	1.0E+05	8.7	43.8	23	227
R600a	182	56	4.9E+04	8.4	42.1	34	219
R236fa	156	40	1.1E+05	8.3	42.0	28	222
R152a	250	86	6.2E+04	7.6	38.1	36	200
R227ea	240	66	1.3E+05	7.5	37.7	52	199
R134a	302	98	9.4E+04	7.7	38.6	49	201

Figure 20 plots the critical temperature of the working fluids with the corresponding first law efficiency obtained by simulation. It can be observed that the efficiency increased as the critical temperature of the working fluids increased. Aljundi found similar results demonstrating strong correlation between critical temperature and efficiency. A similar correlation was also observed for the plot of first law efficiency and normal boiling point of fluids from Figure 21. Mago et al. also concluded that dry organic fluids with higher boiling point have better efficiencies (P J; Mago et al., 2008). Liu et al. reported that the thermal efficiency of subcrtical ORCs is a weak funciton of the crtical temepraure of the working fluid (Liu et al., 2004). Lee et al. concluded that the ORC system efficiency is correlated to the working fluid's normal boiling point, critical pressure and molecular weight (Lee, M J; Tien, D L; Shao, 1993). High molecular weight leads to high Van Der Waals force and implies that the fluid would have high evaporating temperature at the same pressure (Gu et al., 2009). High molecular weight also impacts positively on the turbine efficiency (Bao & Zhao, 2013) and reduces turbine nozzle velocity (Nafey & Sharaf, 2010). The density difference between vapor and liquid phase is smaller for high molecular weight organic fluids (Quoilin et al., 2013). Zhai et al., suggested that thermal efficiency is affected by the presence of fluorine and the molecular structure of the working (Zhai, Shi, & An, 2014). The molecular structure and the interactions that occur between the molecules differentiate two working fluids and govern the properties. They also observed that working fluids with double bonds and cyclic structures display higher efficiencies.

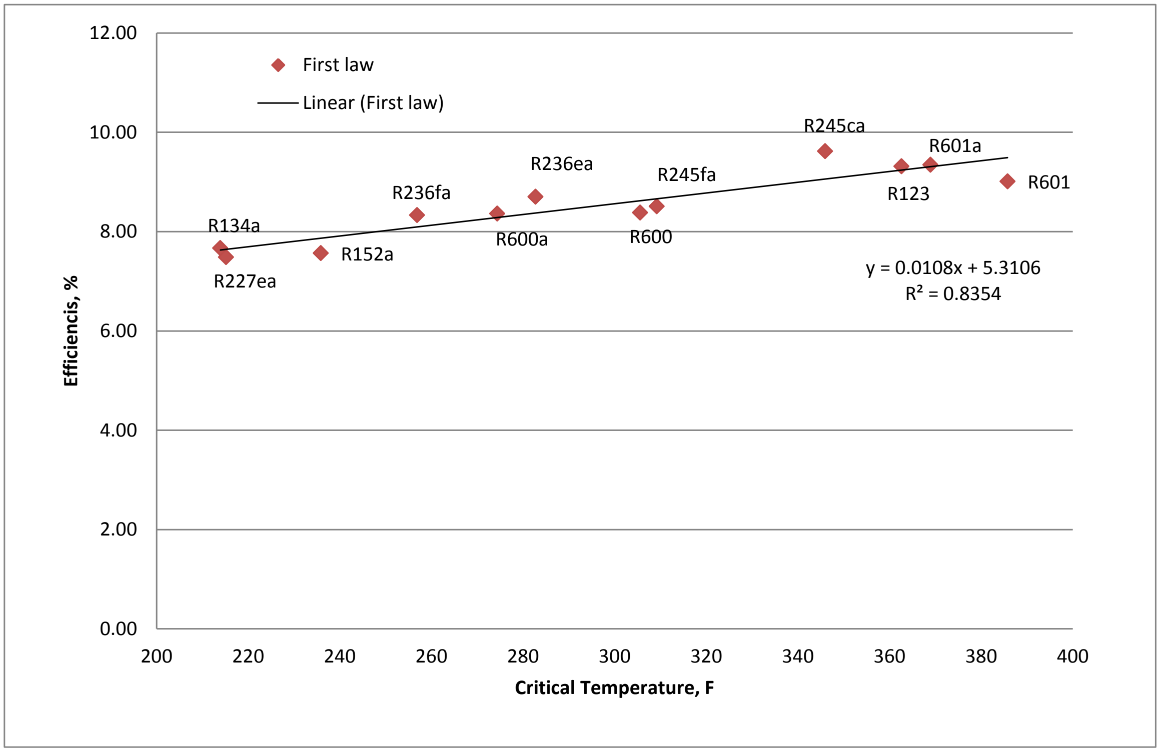

Figure 20 Plot of first law efficiency versus critical temperature of working fluids

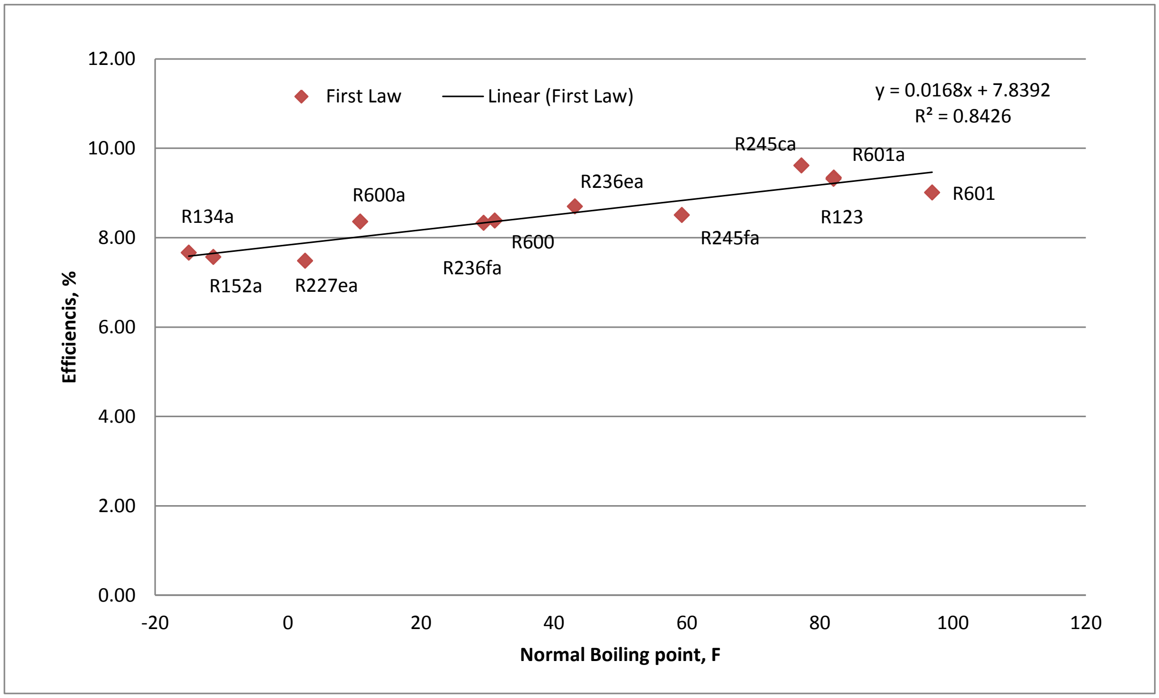

Figure 21 Plot of first law efficiency versus normal boiling point of working fluids

3.6 Internal Heat Exchanger Configuration

The thermal efficiency of an ORC system can be increased by adding an internal heat exchanger (IHX) (E. H. Wang et al., 2011). Internal heat exchanger configuration includes a heat exchanger which preheats the fluid entering the evaporator by using heat from the vapors leaving the turbine. The IHX configuration increases the average temperature of heat added to the system and lowers the average temperature at which the system rejects the heat. This results in increase in the overall efficiency of the ORC (P J; Mago et al., 2008). Figure 22 shows the schematic of ORC with Internal Heat Exchanger configuration.

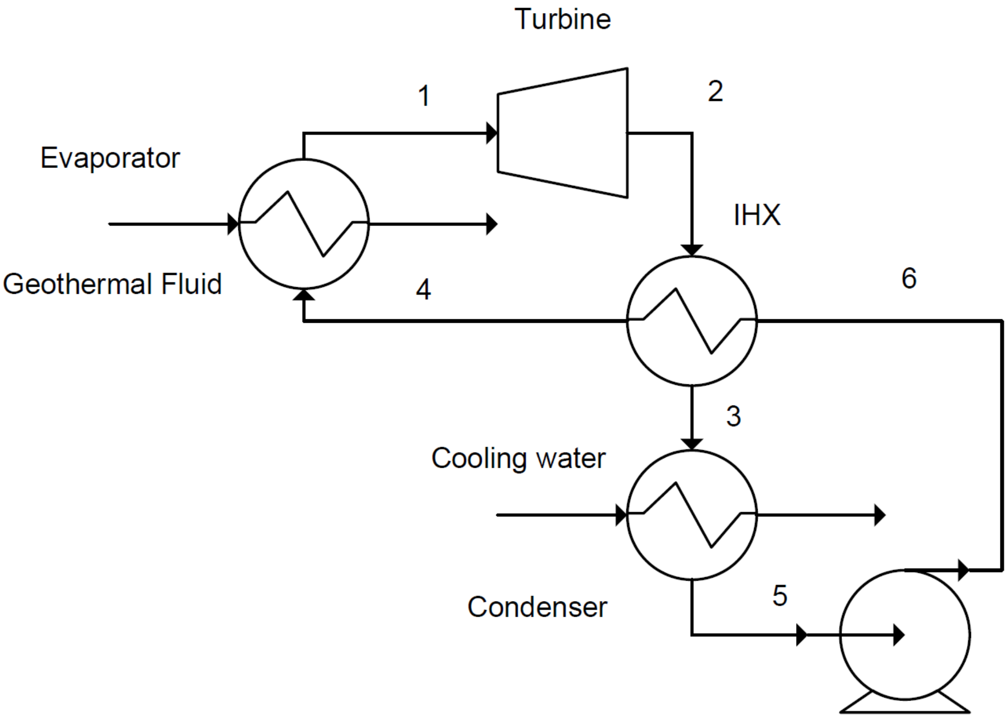

Figure 22 Schematic of Internal Heat Exchanger Configuration

Figure 23 compares the first law efficiency obtained for each working fluid for base and IHX configuration. It can be clearly observed that the first law efficiency increased for the all the working fluids by adding an internal heat exchanger. This is due to the fact that IHX decreases heat input to the cycle while maintaining the same power output. The heat input required is less to the cycle because fluid is preheated in the IHX. Figure 24 shows increase in second law efficiency by addition of internal heat exchanger.

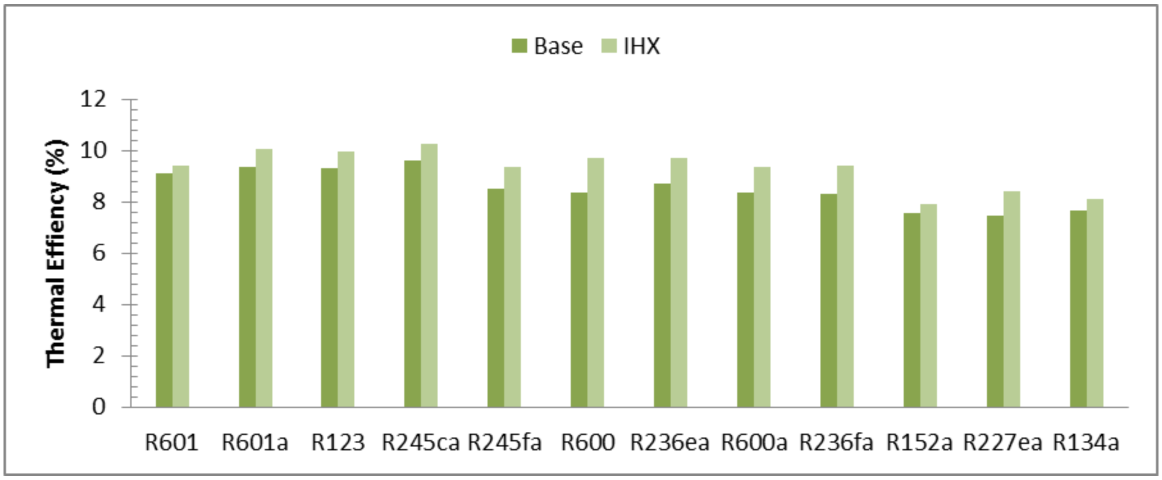

Figure 23 First law efficiencies for IHX configuration

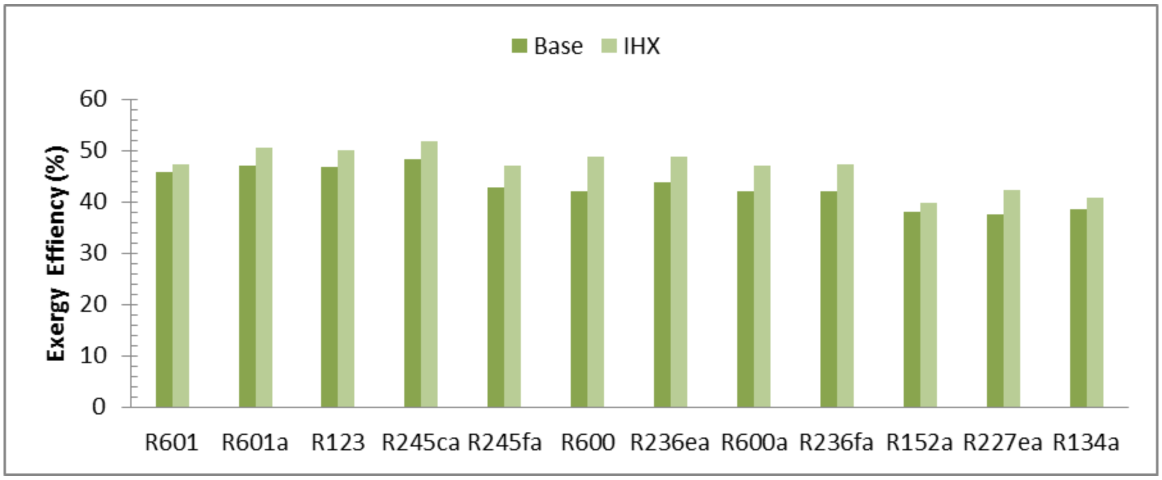

Figure 24 Second law efficiencies for IHX configuration

Table 10 compares the efficiency obtained in IHX to the base configuration. R600 and R601 show the highest and lowest increment in efficiency. It can also be observed that the increase in efficiency is more sensitive towards the working fluid with mid-range critical temperature. Cayer et al. observed that adding IHX to the ORC results in significant increase in heat exchanger areas with a small increments in thermal and exergy efficiencies (Cayer et al., 2009).

Table 10 Comparison of Base Configuration with IHX

	Base		IHX		% Increase	
	First	Second	First	Second	First	Second
R601	9.0	45.4	9.4	47.4	4.6	4.6
R601a	9.3	47.0	10.1	50.6	7.6	7.6
R123	9.3	46.9	10.0	50.1	6.8	6.8
R245ca	9.6	48.4	10.3	51.8	7.0	7.0
R245fa	8.5	42.8	9.3	47.0	9.8	9.8
R600	8.4	42.2	9.7	48.9	15.8	15.8
R236ea	8.7	43.8	9.7	48.8	11.5	11.5
R600a	8.4	42.1	9.4	47.2	12.0	12.0
R236fa	8.3	42.0	9.4	47.4	12.9	12.9
R152a	7.6	38.1	7.9	39.8	4.5	4.5
R227ea	7.5	37.7	8.4	42.4	12.6	12.6
R134a	7.7	38.6	8.1	40.8	5.6	5.6

Figure 25 shows the exergy destruction rate across each component for IHX configuration. The rate of exergy destruction is highest in the evaporator, followed by the condenser, turbine and pump. By adding the IHX, the exergy destruction rate decreased in all components. The decrease in exergy destruction is highest in evaporator. This is due the fact that IHX increases the average temperature of heat addition to the system. The temperature difference on the hot side across the heat exchanger is reduced. Exergy destruction rate is proportional to the temperature difference. A higher temperature difference between the hot and cold side leads to a higher exergy destruction rate. Exergy destruction occurs across the IHX, however, it is much smaller compared to the rest of the components. Part of the decrease in exergy destruction in the evaporator and condenser is achieved at the expense of exergy destruction in IHX. Figure 26 shows the temperature entropy diagram for R600 in the IHX configuration. The effect of adding the IHX to the ORC can be clearly observed by the temperature entropy diagram. The inlet temperature of the working fluid entering the evaporator is increased. This improves the temperature profile match between the streams in the evaporator and subsequently decreases losses. This helps in increasing the overall efficiency of the ORC. As well, the inlet temperature of the working fluid entering the condenser is decreased which leads to decreased losses. The decreased losses in the evaporator and condenser due to better profile match by adding IHX can be confirmed by the decreased exergy destruction observed in Figure 25. Superheating of the working fluid is observed in the evaporator which is known to reduce efficiency for the cycle.

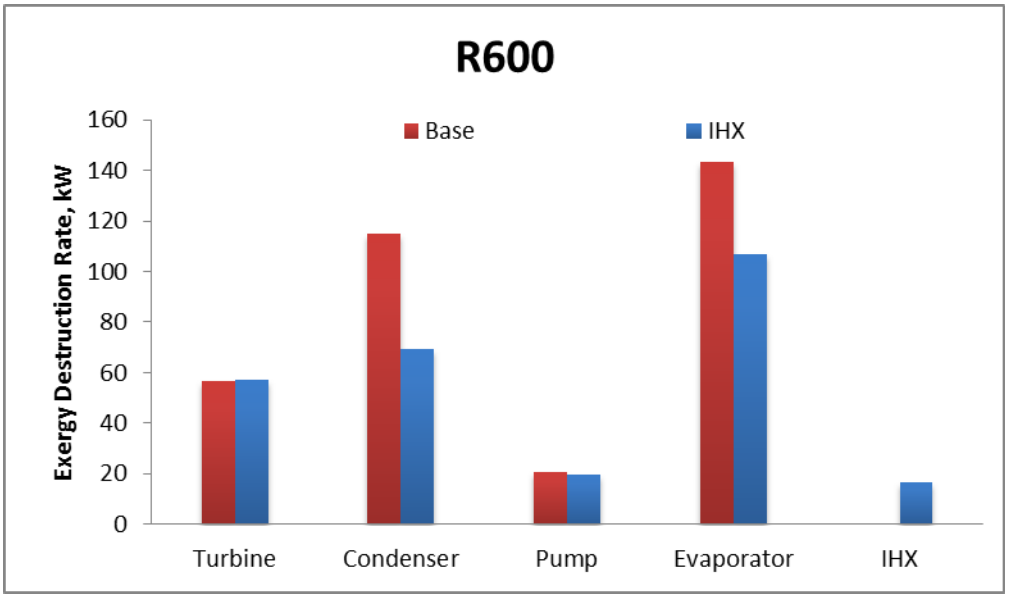

Figure 25 Exergy destruction diagram for IHX configuration

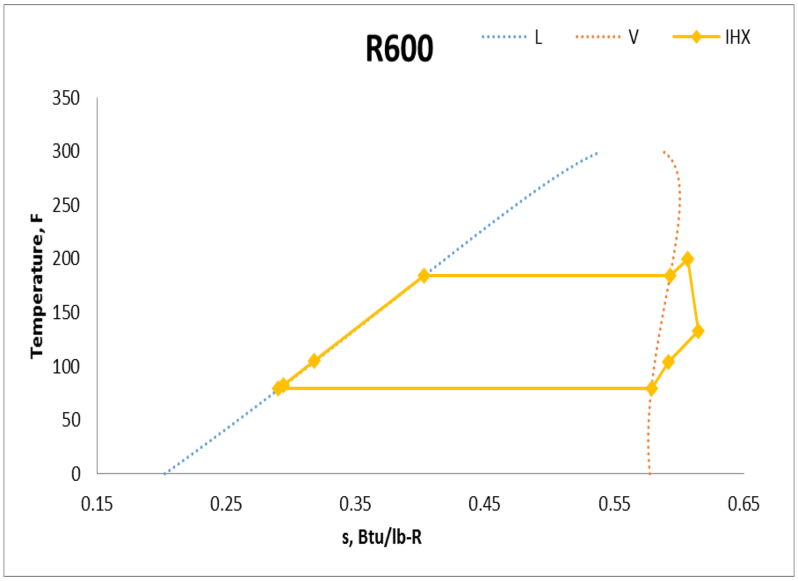

Figure 26 Temperature entropy diagram for R600 in base configuration

Table 11 shows the EDF values obtained for the IHX configuration. The values listed in Table 11 show that the highest exergy is lost is still in evaporator, even with the internal heat exchange. EDF_{TOT} values imply that more potential is lost than actual work produced for all the working fluids. The EDF values for IHX are much smaller compared to the remaining components. It can be concluded from Figure 25 and Table 11 that adding an IHX decreases the exergy destruction across the components and increases the efficiency of the overall system. The last two columns compares the EDF_{TOT} values obtained for IHX case to the base case. The EDF_{TOT} values for IHX case decreased for most of the working fluids except for R601, R245ca and R236ea.

Table 11 EDF Values for the IHX Configuration

Working fluid	EDF_T	EDF_C	EDF_P	EDF_E	EDF_{IHX}	IHX EDF_{TOT}	Base EDF_{TOT}
R601	0.24	0.21	0.04	0.72	0.10	1.32	1.32
R601a	0.24	0.41	0.05	0.44	0.03	1.17	1.25
R123	0.23	0.44	0.03	0.51	0.01	1.22	1.26
R245ca	0.28	0.17	0.19	0.78	0.19	1.61	1.19
R245fa	0.25	0.10	0.07	0.63	0.13	1.17	1.48
R600	0.26	0.31	0.09	0.48	0.07	1.21	1.51
R236ea	0.27	0.17	0.17	0.95	0.01	1.58	1.42
R600a	0.27	0.27	0.13	0.55	0.08	1.29	1.52
R236fa	0.32	0.40	0.05	0.34	0.03	1.13	1.53
R152a	0.24	0.39	0.05	0.35	0.04	1.07	1.79
R227ea	0.26	0.11	0.09	0.71	0.14	1.31	1.82
R134a	0.33	0.12	0.13	1.06	0.09	1.72	1.75

Table 12 shows the results obtained for the IHX configuration. The highest efficiency is observed for R245ca and lowest for R134a. R601 has the lowest working fluid flow rate and turbine inlet pressure. R227ea has the highest working fluid flow rate and one of the highest turbine inlet pressure. A general trend could be observed that working fluids that have higher working fluid flow rates and higher inlet pressures exhibit lower efficiencies. The pump power is proportional to the turbine inlet pressure. Therefore, higher inlet pressures result in increased pumping power and lowering the net power of the cycle.

Table 12 Results Obtained for the IHX Configuration

Working fluid	P_{in} (psia)	P_{out} (psia)	$\dot{m}_{ORC}$ (lb/hr)	η_I	η_{II}	W_p(kW)	W_{net}(kW)
R601	57	14	4.2E+04	9.4	47.4	9	215
R601a	90	19	4.3E+04	10.1	50.6	15	235
R123	92	19	9.0E+04	10.0	50.1	14	218
R245ca	106	21	7.9E+04	10.3	51.8	15	235
R245fa	95	23	8.9E+04	9.3	47.1	15	235
R600	162	42	4.3E+04	9.7	48.8	28	222
R236ea	133	31	10.2E+04	9.7	48.8	23	231
R600a	204	57	4.7E+04	9.4	47.2	38	212
R236fa	156	38	10.4E+04	9.4	47.4	28	221
R152a	245	84	6.2E+04	7.9	39.8	35	201
R227ea	239	66	13.5E+04	8.4	42.4	52	198
R134a	305	97	9.2E+04	8.1	40.8	39	201

3.7 Turbine Bleeding Configuration

Turbine bleeding is a configuration which involves taking part of the stream entering the turbine and mixing it with the stream entering the evaporator. The average temperature of heat addition to the system is increased and increases the efficiency of the system. Figure 27 shows the schematic of ORC in turbine bleeding configuration.

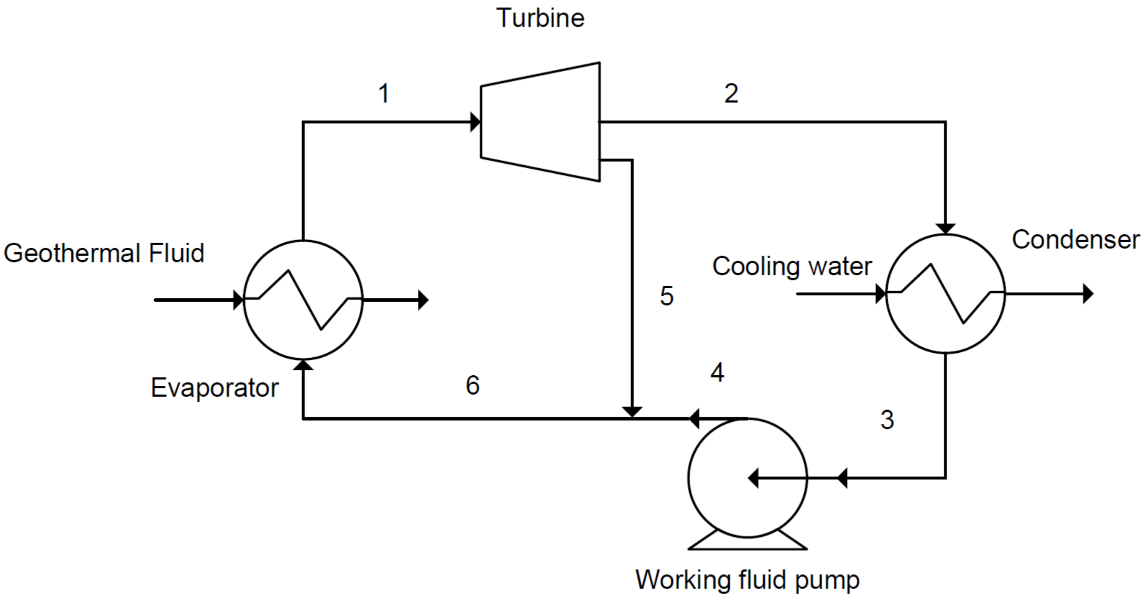

Figure 27 Schematic of Turbine Bleeding Configuration

Figure 28 and Figure 29 show the first and second law efficiency for the turbine bleeding configuration. It can be observed that the efficiency increased compared to the base configuration. The amount of heat input to the cycle is reduced compared to the basic configuration which in translated into increased thermal efficiency. Turbine bleeding decreases required heat input by increasing the mean addition temperature across the evaporator. However, the increased efficiency comes at the expense of added mass flow rates which increases work required by pump. Turbine bleeding only makes sense when the decrease in heat input is significantly higher than the increment in the pump power (Desai & Bandyopadhyay, 2009).

For all the working fluids, the efficiency increased compared to the base configuration. The highest increase in efficiency compared to base configuration is observed for R600 followed by R601. The efficiency increased for R601, R601a, R600, R152a and R277ea compared to the IHX configuration. For remaining working fluids, there was decrease in efficiency with respect to the IHX configuration. The measure of increase or decrease in efficiency is listed in Table 13. The negative sign indicate decrease in efficiency. The decrease in efficiency is observed to the increased power consumption of pump which decreases the net power.

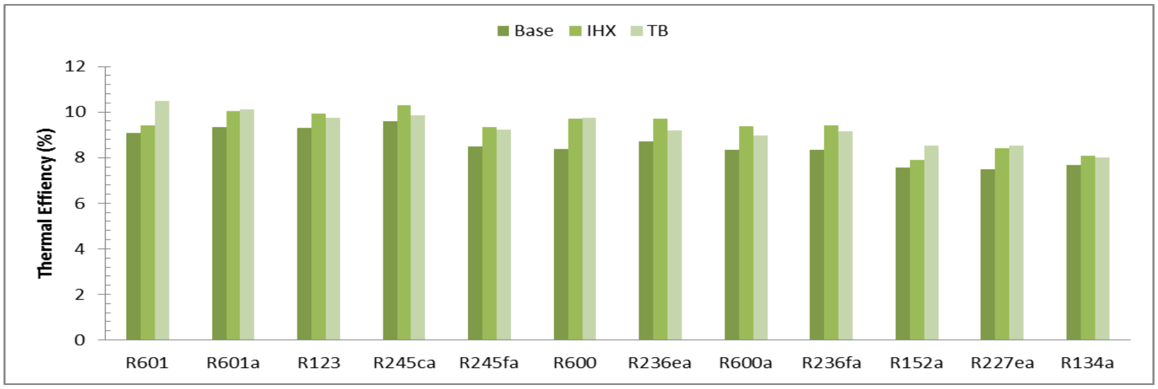

Figure 28 First law efficiencies for TB configuration

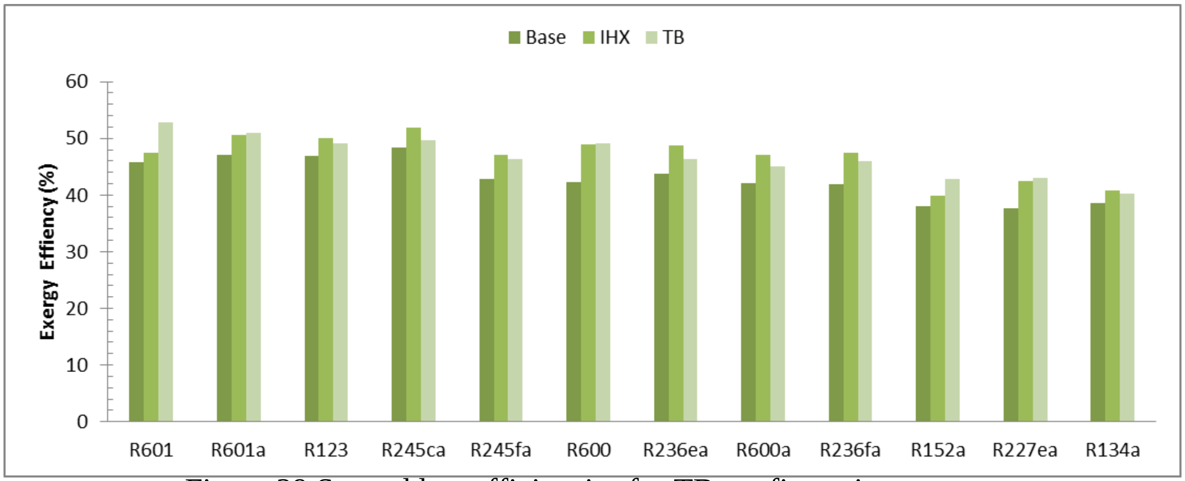

Figure 29 Second law efficiencies for TB configuration

Table 13 Comparison of Turbine Bleeding Configuration Efficiency

	% Increase with respect to base configuration		% Increase with respect to IHX configuration	
	First	Second	First	Second
R601	15.4	15.5	11.5	11.5
R601a	8.5	8.5	0.8	0.8
R123	4.6	4.6	-2.1	-2.1
R245ca	2.7	2.7	-4.0	-4.0
R245fa	8.3	8.3	-1.8	-1.4
R600	16.4	16.4	0.5	0.5
R236ea	5.8	5.8	-5.1	-5.1
R600a	7.2	7.2	-4.3	-4.3
R236fa	9.8	9.8	-2.8	-2.8
R152a	12.6	12.6	7.8	7.8
R227ea	14.2	14.2	1.4	1.4
R134a	4.3	4.4	-1.2	-1.2

Figure 30 shows the exergy destruction rates across the components for the turbine bleeding configuration. It can be observed that the exergy destruction rate is lowest for the turbine bleeding configuration. Among the components, most of the exergy destruction occurs in the evaporator. In the turbine bleeding configuration, the exergy destruction rates decrease for the evaporator and condenser. The exergy destruction rates remain almost unchanged for the turbine and pump. In terms of exergy destruction rates, the turbine bleeding configuration display lowest exergy destruction rate. However, in terms of efficiency, the IHX configuration displays marginal higher efficiency. Figure 31 shows the temperature entropy diagram for R600 in the turbine bleeding configuration. The temperature entropy diagram reveals that better temperature profile is obtained in the evaporator due to the increased evaporator inlet temperature. That explains the decreased exergy loss in the evaporator and increase in efficiency compared to base and IHX configurations.

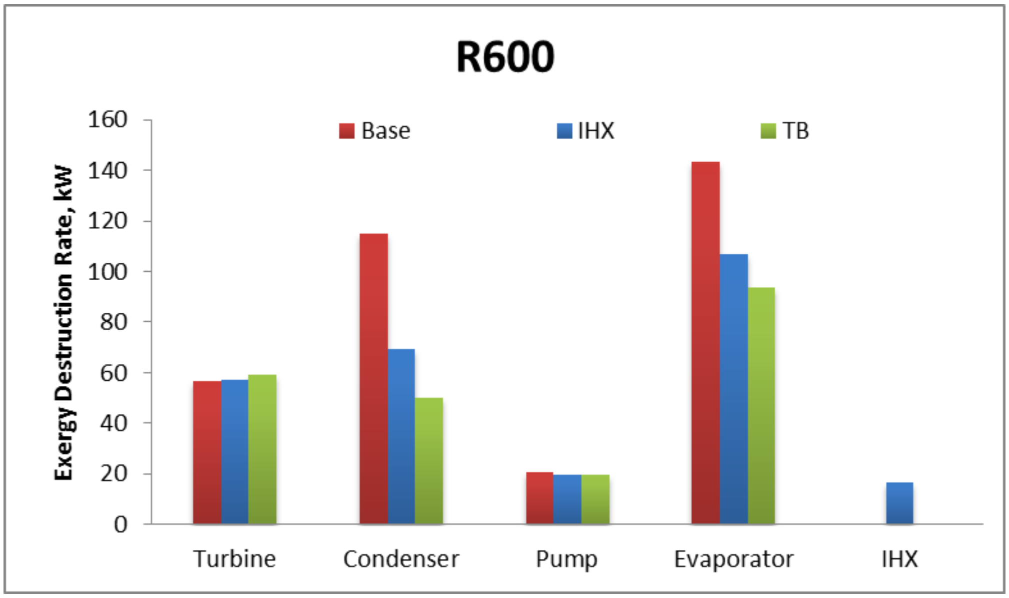

Figure 30 Exergy destruction rates across components

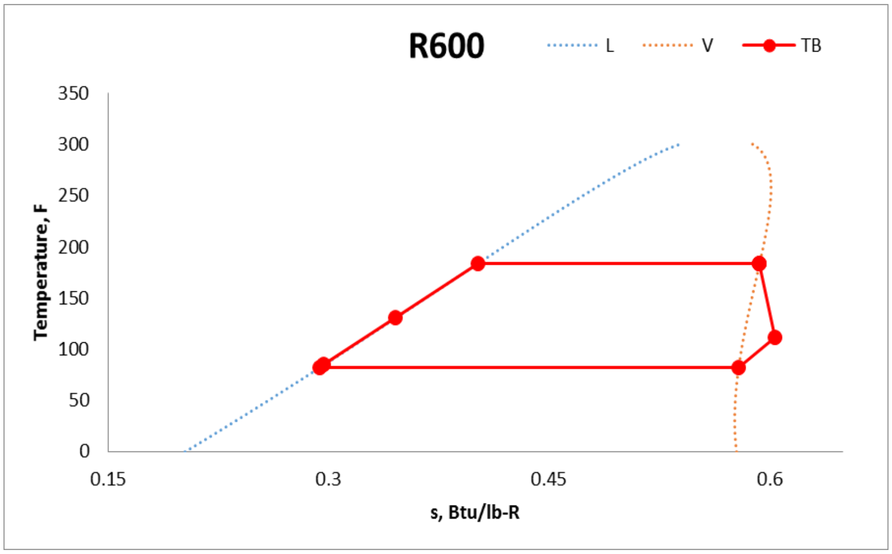

Figure 31 Temperature entropy diagram for R600 in Turbine Bleeding configuration

Table 14 shows the EDF values for the turbine bleeding configuration. It can be observed that EDF values are highest for the evaporator and lowest for the pump. Highest and lowest value of EDF$_{TOT}$ is observed for R134a and R601 respectively. As observed in previous configurations, highest EDF value is displayed by evaporator for all working fluids.

Table 14 EDF Values for Turbine Bleeding Configuration

Working fluid	EDF$_{T}$	EDF$_{C}$	EDF$_{P}$	EDF$_{E}$	TB EDF$_{TOT}$	IHX EDF$_{TOT}$	Base EDF$_{TOT}$
R601	0.24	0.22	0.03	0.43	0.92	1.32	1.32
R601a	0.24	0.43	0.05	0.35	1.07	1.17	1.25
R123	0.32	0.27	0.04	0.63	1.26	1.22	1.26
R245ca	0.25	0.26	0.04	0.46	1.00	1.61	1.19
R245fa	0.26	0.21	0.05	0.57	1.09	1.17	1.48
R600	0.27	0.23	0.09	0.42	1.00	1.21	1.51
R236a	0.26	0.30	0.09	0.43	1.08	1.58	1.42
R600a	0.27	0.21	0.13	0.55	1.15	1.29	1.52
R236fa	0.27	0.06	0.09	0.61	1.03	1.13	1.53
R152a	0.33	0.12	0.18	0.74	1.37	1.07	1.79
R227ea	0.33	0.06	0.28	0.51	1.18	1.31	1.82
R134a	0.27	0.36	0.31	0.63	1.57	1.72	1.75

Table 15 gives the result obtained for the turbine bleeding configuration. The fluids are listed in order of their critical temperature, with the first fluid, R601 having the lowest critical temperature. This order was chosen because critical temperature of the working fluid has correlation with the cycle efficiency. It can be observed that the mass flow rate of the working fluid, turbine inlet pressure, and pump power are generally increasing from the top to the bottom of the column with some exceptions. The exceptions observed could be a result of the way the working fluids are ordered based on the critical temperature. The trend may change based on the order the working fluids are arranged. As well, the working fluids are comprised of wet, dry and isentropic fluids, and do not follow any specific order and may also affect the trend observed in Figure 32. The net power and hence efficiency decreases from the top to the bottom of the column. Highest and lowest net power is observed for R601 and R134a respectively. They also display the highest and lowest efficiency. This is because the efficiency depends on the net power produced by the system. Figure 32 shows the variation of the parameters as the function of critical temperature of fluid.

Table 15 Results Obtained for the Turbine Bleeding Configuration

Working fluid	P_{in} (psia)	P_{out} (psia)	$\dot{m}_{ORC}$ (lb/hr)	η_I	η_{II}	W_p(kW)	W_{net}(kW)
R601	60	11	4.0E+04	10.5	52.9	10	240
R601a	90	18	4.3E+04	10.1	51.0	16	234
R123	79	16	9.0E+04	9.7	49.0	29	222
R245ca	88	17	8.0E+04	9.9	49.7	12	238
R245fa	105	23	9.0E+04	9.2	46.4	17	233
R600	160	38	4.2E+04	9.8	49.1	27	223
R236ea	160	34	1.0E+05	9.2	46.3	28	222
R600a	192	53	4.9E+04	9.0	45.1	36	214
R236fa	163	36	1.1E+05	9.1	46.1	28	222
R152a	311	91	6.4E+04	8.5	42.9	50	200
R227ea	324	60	1.2E+05	8.5	43.0	69	181
R134a	400	107	1.0E+05	8.0	40.3	76	174

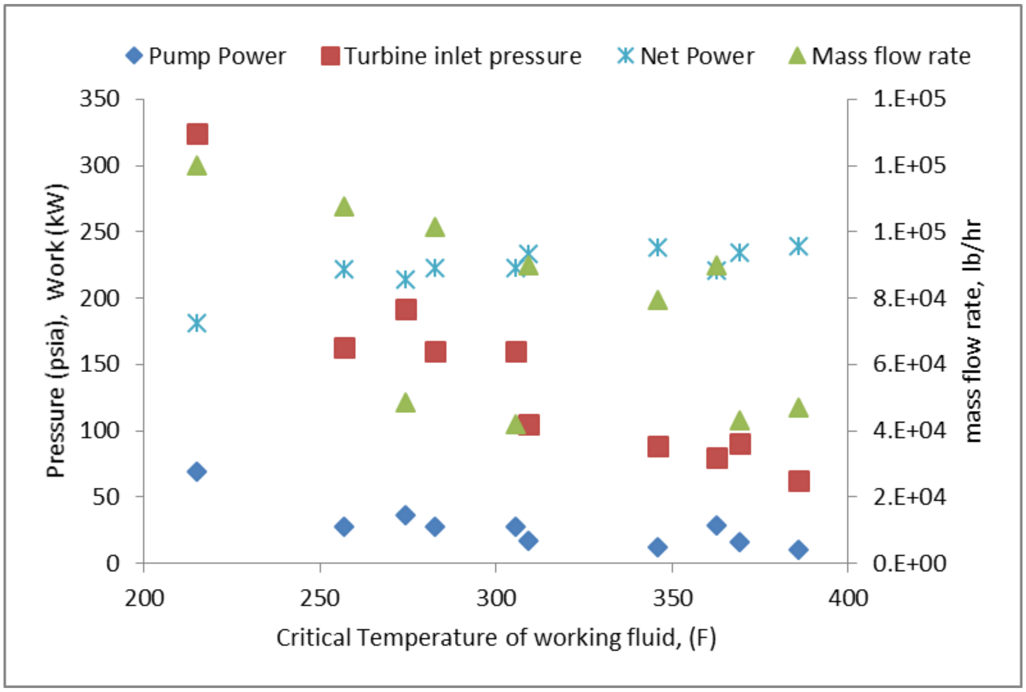

Figure 32 Variation of parameters for the working fluid as a function of T_c

3.8 Non-Constrained Base Configuration

In the previous sections, base, IHX and turbine bleeding configurations were discussed in detail. So far it was observed that IHX configuration displayed better results in terms of efficiency. These configurations were studied with a constraint that the gross output power was kept constant at 250kW. This constraint was removed and the three configurations were studied. The component sizing and gross turbine output was adjusted to optimize the performance for each case. The resource and cooling water conditions for the analysis remained unchanged. Table 16 shows the design conditions for the non-constrained ORC.

Table 16 Conditions for the Constrained ORC Design

	Non-Constrained
Geothermal Resource Temperature(°F)	210
Geothermal Resource Flowrate, gpm	875
Cooling Water Temperature (°F)	77
Maximum Gross Turbine Output, kW	Variable
Maximum Evaporator UA Value (Btu/F-hr)	Variable
Maximum Condenser UA Value (Btu/F-hr)	Variable
Maximum Turbine Size, m	Variable

Figure 33 and Figure 34 show the first and second law efficiency for the non-constrained base configuration. For a majority of the working fluids, the efficiencies increased for the non-constrained configuration. R245ca and R601 have the highest efficiency for this configuration. Wet fluid R152a displays the lowest efficiencies. Table 17 shows the increment in efficiency for the non-constrained base configuration compared to the other configurations. Negative value indicates a decrease in efficiency and indicates that R227ea and R134a have highest efficiency in the TB configuration among the four configurations discussed so far.

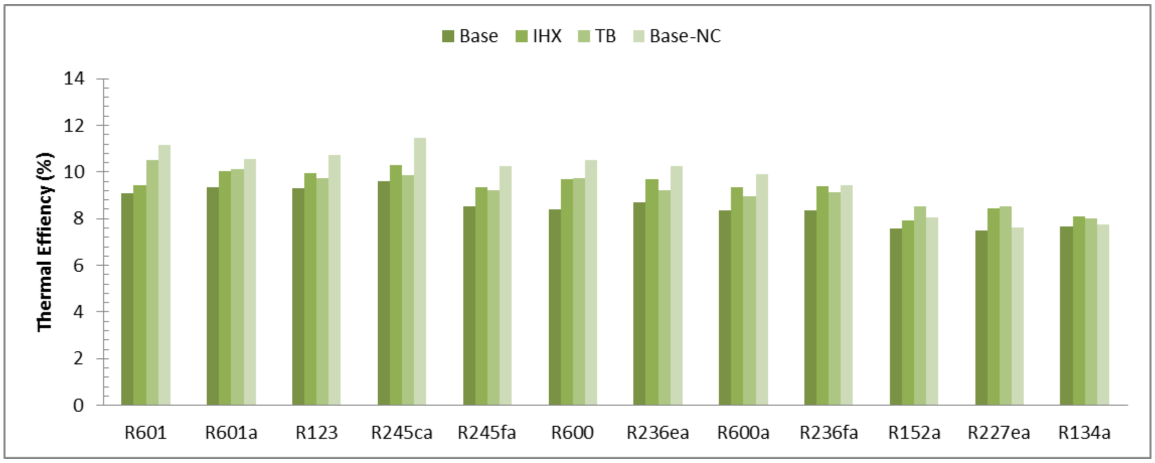

Figure 33 First law efficiency for non- constrained base configuration

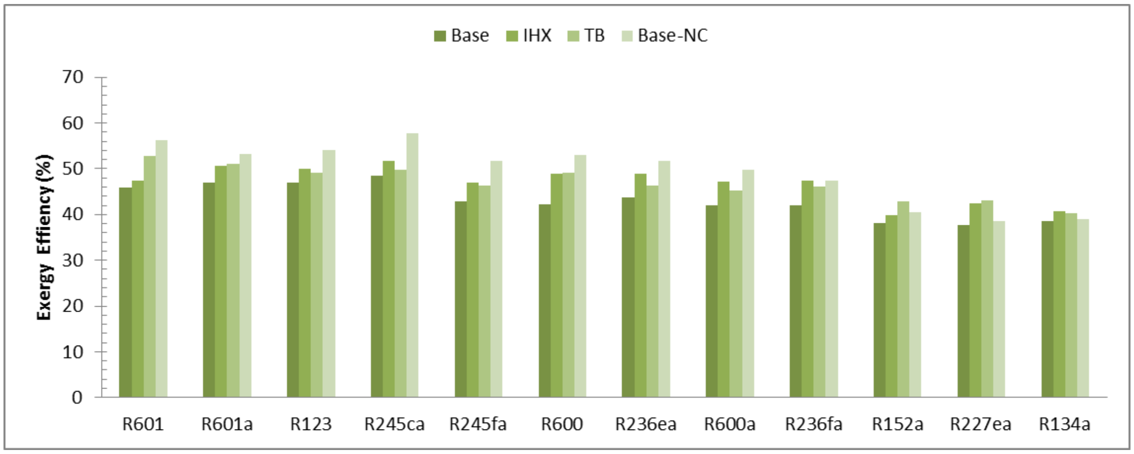

Figure 34 Second law efficiency for non- constrained base configuration

Table 17 Comparison of Non-Constrained Base Configuration Efficiency

	% Increase with respect to base configuration		% Increase with respect to IHX configuration		% Increase with respect to TB configuration	
	First	Second	First	Second	First	Second
R601	22.9	22.9	18.7	18.7	6.5	6.5
R601a	13.2	13.2	5.2	5.2	4.4	4.4
R123	15.3	15.3	7.9	7.9	10.2	10.2
R245ca	19.3	19.3	11.5	11.5	16.2	16.2
R245fa	20.8	20.8	10.0	10.0	11.5	11.5
R600	25.5	25.5	8.3	8.3	7.8	7.8
R236ea	17.8	17.8	5.7	5.7	11.3	11.3
R600a	18.3	18.3	5.6	5.6	10.3	10.3
R236fa	13.1	13.1	0.2	0.2	3.0	3.0
R152a	6.3	6.3	1.8	1.8	-5.6	-5.6
R227ea	2.1	2.1	-9.4	-9.4	-10.6	-10.6
R134a	0.9	0.9	-4.5	-4.5	-3.4	-3.4

Figure 35 shows the exergy destruction rate across the components for the non-constrained base configuration. It can be observed that the highest exergy destruction rate occurs in the evaporator followed by turbine, condenser and pump for the non-constrained base configuration. Compared to the constrained scenario, the non-constrained base configuration has much lower exergy destruction rates. This explains the higher increment in the efficiencies from Table 17. The non-constrained base configuration also display lower exergy destruction rates compared to the IHX and base configuration and is reflected in the increased efficiencies. Figure 36 shows the temperature entropy diagram for the R600 in the non-constrained base configuration. No superheating is observed in the evaporator resulting in better temperature match in the evaporator compared to the base case. This explains the decrease in exergy destruction in the evaporator and increase in efficiency compared to the base case.

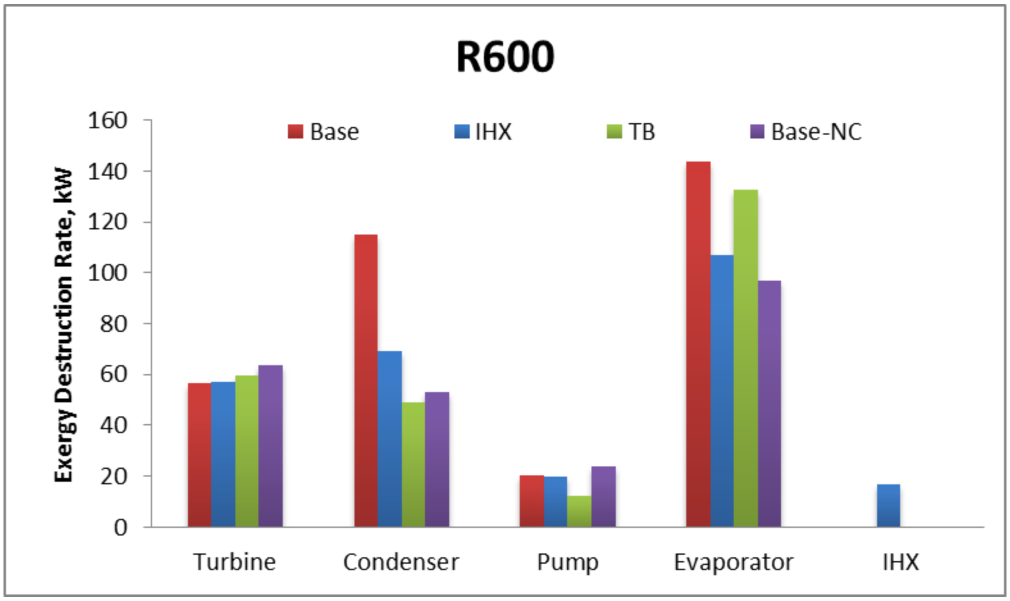

Figure 35 Exergy destruction rates across components

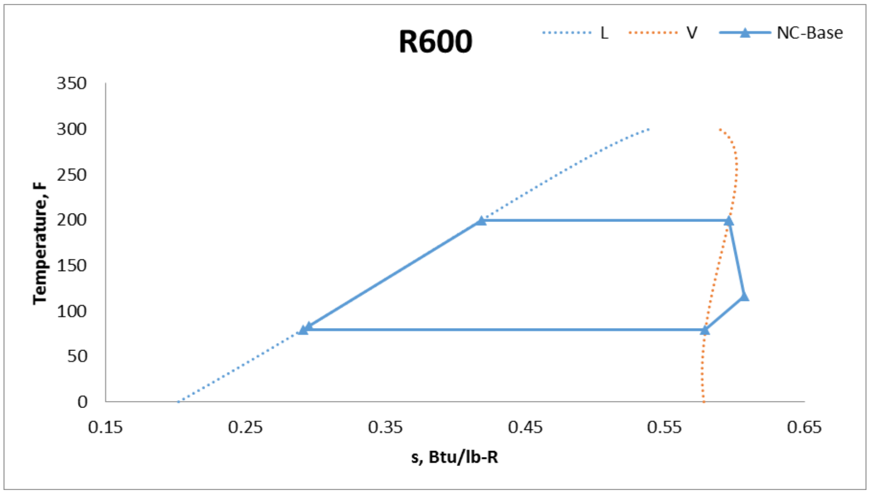

Figure 36 Temperature entropy diagram for R600 in non-constrained base configuration

Two things were accomplished by removing the constraints of the ORC cycle. First, the gross power increased because the turbine power was no longer restricted at 250kW. If the increase in the turbine power is greater than the increase in pump power, then the overall net power for the cycle is increased. Increased net power increases the thermal efficiency. Second, by removing the constraints, the total exergy destruction in the cycle is decreased. This is mostly due to better profile match is obtained in the heat exchangers. Lower EDFTOT values obtained in non-constrained cases compared to the constrained cases implies that exergy destruction decreases in non-constrained cases. EDFTOT values obtained for R601, R601a, R123 and R245ca is less than one suggesting less potential is destroyed than net power generated.

The EDF value for the non-constrained configuration is given in Table 18. The evaporator shows the highest value for EDF among the four components of ORC. R601 and R227ea have the lowest and highest EDF_{TOT} value respectively

Table 18 EDF Values for Non-Constrained Base Configuration

Working fluid	EDF_T	EDF_C	EDF_P	EDF_E	EDF_{TOT}
R601	0.23	0.25	0.03	0.36	0.88
R601a	0.24	0.32	0.04	0.38	0.99
R123	0.33	0.23	0.04	0.36	0.96
R245ca	0.25	0.17	0.04	0.37	0.83
R245fa	0.26	0.28	0.07	0.45	1.05
R600	0.27	0.22	0.10	0.41	1.00
R236a	0.26	0.22	0.10	0.48	1.05
R600a	0.28	0.20	0.15	0.50	1.13
R236fa	0.28	0.24	0.13	0.58	1.23
R152a	0.39	0.30	0.21	0.73	1.62
R227ea	0.30	0.35	0.24	0.87	1.76
R134a	0.27	0.26	0.18	1.02	1.73

Table 19 shows the results obtained for the non-constrained base configuration. R601 shows the highest first and law efficiency of 11.2 and 56.3%. Since the maximum power is not limited to 250 kW in the non-constrained configuration, the net power obtained exceeds 250kW. The net power for R601 is estimated to be 308 kW.

Table 19 Results Obtained for the Non-Constrained Base Configuration

Working fluid	P_{in} (psia)	P_{out} (psia)	$\dot{m}_{ORC}$ (lb/hr)	η_I	η_{II}	W_p (kW)	W_{net} (kW)
R601	72	12	4.7E+04	11.2	56.3	14	308
R601a	90	16	5.5E+04	10.6	53.2	20	324
R123	97	15	9.4E+04	10.7	54.1	16	263
R245ca	115	16	9.5E+04	11.5	57.8	21	343
R245fa	153	26	9.0E+04	10.3	51.7	26	274
R600	193	39	4.0E+04	10.5	53	33	237
R236a	190	32	1.1E+05	10.3	51.6	38	280
R600a	240	53	4.4E+04	9.9	49.8	46	221
R236fa	221	42	1.0E+05	9.4	47.5	41	218
R152a	355	97	6.4E+04	8.0	40.5	56	203
R227ea	283	70	1.3E+05	7.6	38.5	64	192
R134a	311	99	9.5E+04	7.7	38.9	52	204

3.9 Non Constrained Internal Heat Exchanger Configuration

Figure 37 and Figure 38` show the first and second law efficiency for the non-constrained IHX configuration. It can be observed that there was increase in efficiency for all working fluids compared to the non-constrained base configuration except for R601 and R152a. The exceptions are observed since the net power decreased for R601 and R152a compared to the non-constrained base configuration. The highest increase in efficiency compared to the constrained IHX was reported for R601a, R245fa and R600. It can be concluded that for most of the working fluids studied here, non-constrained IHX configurations delivers highest efficiency among the five configurations.

Figure 37 First law efficiency for non- constrained IHX configuration

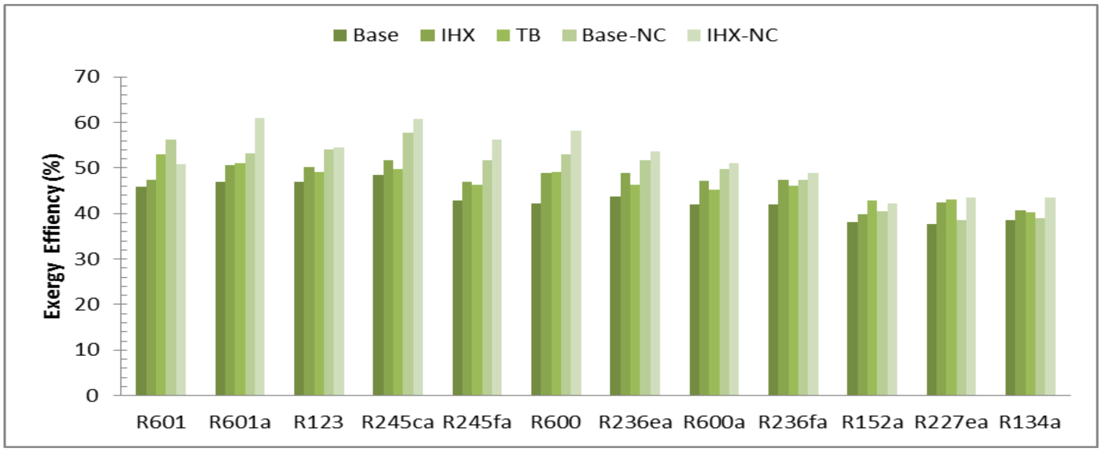

Figure 38 Second law efficiency for non- constrained IHX configuration

Table 20 compares the increase in efficiency for the non-constrained IHX configuration compared to the other configurations. The highest increment in efficiency is observed for R600 between base and non-constrained IHX configuration.

Table 20 Comparison of Non-Constrained IHX Configuration Efficiency

	% Increase with respect to base configuration		% Increase with respect to IHX configuration		% Increase with respect to TB configuration		% Increase with respect to non-constrained base configuration	
	First	Second	First	Second	First	Second	First	Second
R601	10.9	10.9	7.03	7.03	-4.0	-4.0	-9.8	-9.8
R601a	29.8	29.8	20.6	20.6	19.7	19.7	14.7	14.7
R123	16.4	16.4	9.0	9.0	11.3	11.3	1.0	1.0
R245ca	25.5	25.5	17.3	17.3	22.3	22.3	5.2	5.2
R245fa	31.1	31.1	19.3	19.3	21.0	21.0	8.5	8.5
R600	38.0	38.0	19.2	19.2	18.6	18.6	10.0	10.0
R236ea	22.3	22.3	9.7	9.7	15.6	15.6	3.8	3.8
R600a	21.1	21.1	8.1	8.1	12.9	12.9	2.4	2.4
R236fa	16.6	16.6	3.3	3.3	6.2	6.2	3.1	3.1
R152a	10.8	10.8	6.0	6.0	-1.6	-1.6	4.2	4.2
R227ea	15.3	15.3	2.4	2.4	1.0	1.0	12.9	12.9
R134a	12.7	12.7	6.7	6.7	8.0	8.0	11.8	11.8

Figure 39 shows the exergy destruction rate for the non-constrained IHX configuration. The non-IHX configuration shows much lower exergy destruction rates for evaporator and condenser compared to other configurations. Lower destruction rates led to the 38% increase between the base and non-constrained IHX configuration. There was increase in exergy destruction rate in the IHX.

Table 21 displays that lowest exergy destruction occurs for R245ca followed by R601a and hence, have higher efficiencies compared to the remaining fluids. The EDF values for the IHX and pump are much smaller compared to rest of the components. In some cases, the EDF_{TOT} values are higher than that for non-constrained base configuration. This implies in those cases, there is more exergy loss than the gain realized in the evaporator and condenser. Figure 40 shows the temperature entropy diagram for R600 in the non-constrained IHX configuration and reveals a better profile match in the heat exchangers.

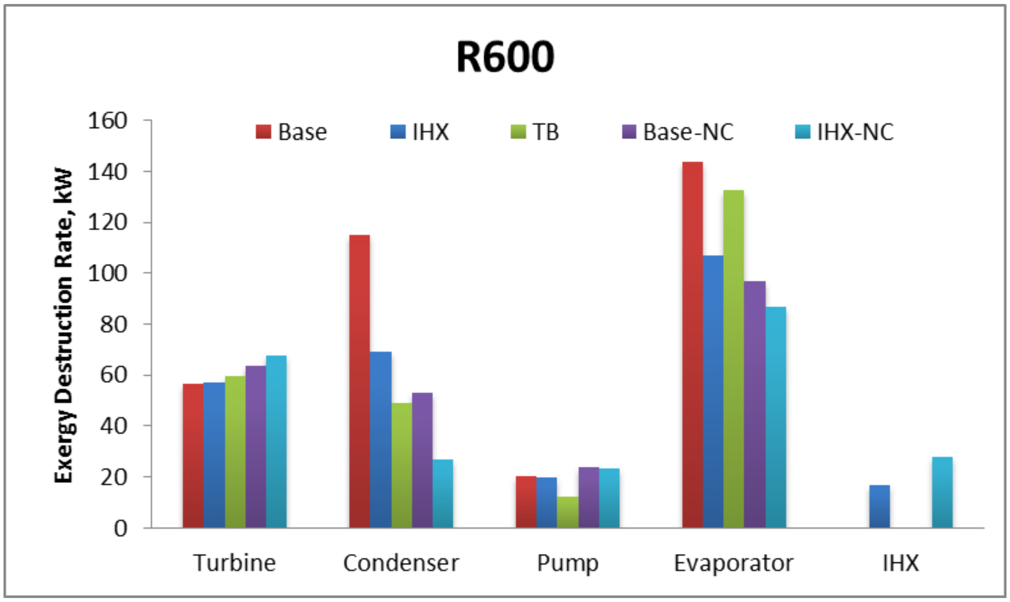

Figure 39 Exergy destruction rates across components

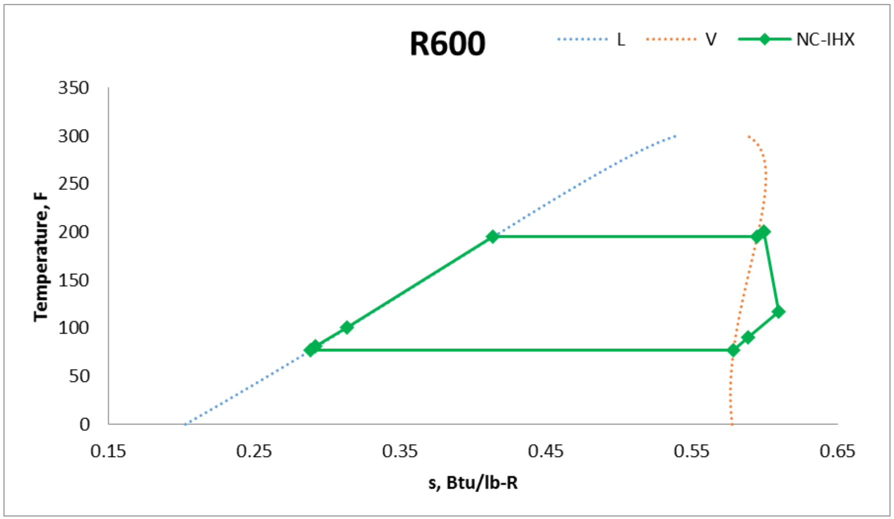

Figure 40 Temperature entropy diagram for R600 in non-constrained IHX configuration

Table 21 EDF Values for Non-Constrained IHX Configuration

Working fluid	EDF_T	EDF_C	EDF_P	EDF_E	EDF_{IHX}	IHX EDF_{TOT}	Base EDF_{TOT}
R601	0.23	0.36	0.03	0.44	0.01	1.07	0.88
R601a	0.24	0.17	0.04	0.37	0.12	0.94	0.99
R123	0.31	0.20	0.04	0.38	0.09	1.02	0.96
R245ca	0.25	0.14	0.04	0.31	0.16	0.89	0.83
R245fa	0.25	0.18	0.06	0.38	0.14	1.01	1.05
R600	0.27	0.11	0.09	0.34	0.11	0.91	1.00
R236a	0.26	0.07	0.10	0.34	0.24	1.02	1.05
R600a	0.28	0.19	0.14	0.45	0.11	1.17	1.13
R236fa	0.26	0.18	0.10	0.60	0.33	1.46	1.23
R152a	0.35	0.19	0.16	0.80	0.13	1.63	1.62
R227ea	0.31	0.23	0.26	0.60	0.39	1.79	1.76
R134a	0.28	0.15	0.20	0.80	0.01	1.44	1.73

Table 22 shows the results for the non-constrained IHX configuration. As previously observed, the thermal efficiency increased in the non-constrained IHX configuration compared to the non-constrained base configuration. However, this increase in efficiency comes at the expense of decreased net power of the cycle. The net power decreases compared to the non-constrained base case. This is due to the fixed temperature and flow rate of the geothermal resource which limits the amount of heat input to the cycle.

Table 22 Results Obtained for the Non-Constrained IHX Configuration

Working fluid	P_{in} (psia)	P_{out} (psia)	$\dot{m}_{ORC}$ (lb/hr)	η_I	η_{II}	W_p(kW)	W_{net}(kW)
R601	60	13	5.0E+04	10.1	50.8	12	278
R601a	90	15	4.3E+04	12.1	61.1	16	269
R123	83	15	9.7E+04	10.8	54.6	15	257
R245ca	104	16	8.3E+04	12.1	60.8	16	290
R245fa	139	24	8.9E+04	11.1	56.1	24	275
R600	183	35	4.1E+04	11.6	58.3	33	253
R236ea	197	36	1.0E+05	10.6	53.6	35	240
R600a	220	54	4.6E+04	10.1	51.0	43	226
R236fa	164	42	1.2E+05	9.7	49.0	33	240
R152a	300	90	6.0E+04	8.4	42.2	44	199
R227ea	300	71	1.4E+05	8.6	43.4	71	199
R134a	340	96	9.0E+04	8.6	43.5	56	205

3.10 Non Constrained Turbine Bleeding Configuration

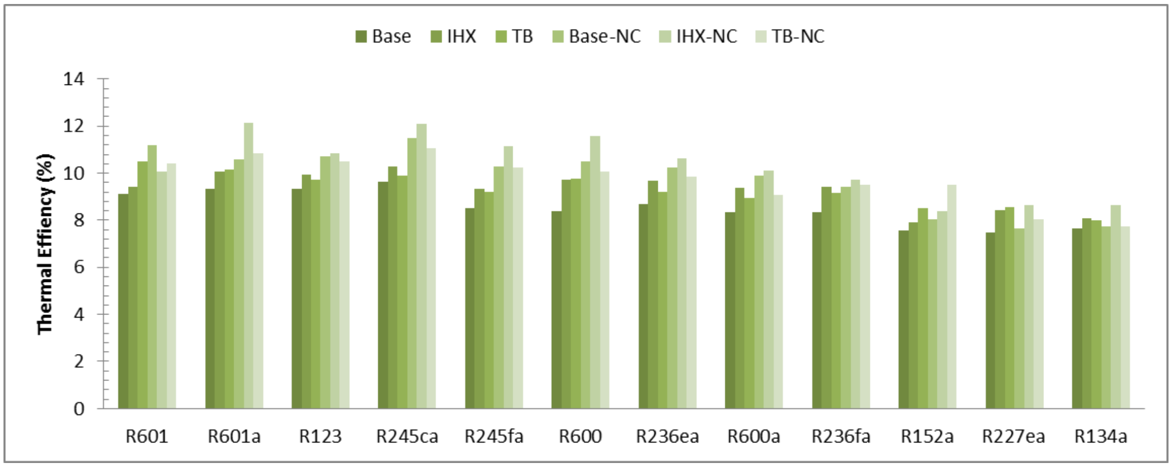

Figure 41 First law efficiency for non- constrained Turbine bleeding configuration

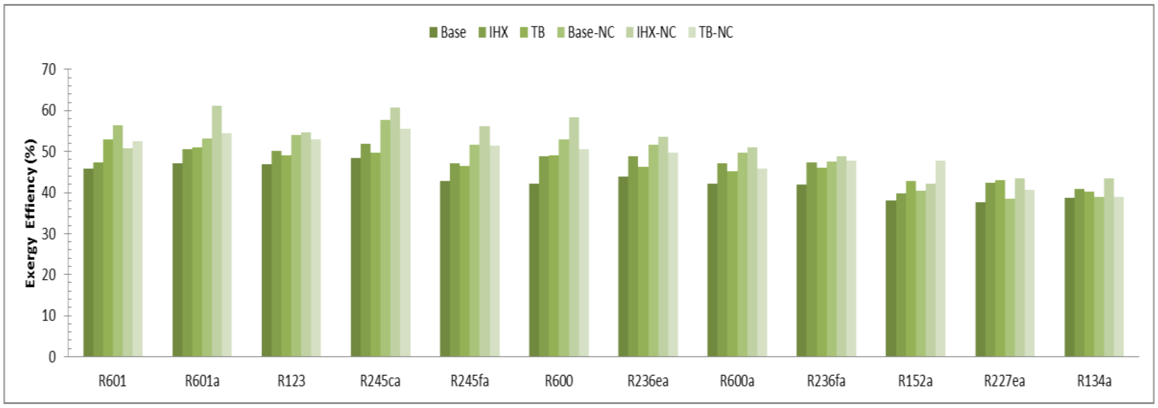

Figure 42 Second law efficiency for non- constrained Turbine bleeding configuration

Table 23 Comparison of Non- Constrained Turbine Bleeding Configuration Efficiency

	% Increase with respect to base configuration		% Increase with respect to IHX configuration		% Increase with respect to TB configuration		% Increase with respect to non-constrained base configuration		% Increase with respect to non -constrained IHX configuration	
	First	Second	First	Second	First	Second	First	Second	First	Second
R601	14.6	14.6	10.6	10.6	-0.7	-0.8	-6.8	-6.8	3.4	3.4
R601a	15.9	15.9	7.7	7.6	6.9	6.9	2.4	2.4	-10.7	-10.7
R123	12.7	12.8	5.5	5.5	7.8	7.8	-2.2	-2.2	-3.1	-3.1
R245ca	14.9	14.9	7.4	7.4	11.9	11.9	-3.7	-3.7	-8.5	-8.5
R245fa	20.1	20.1	9.4	9.4	10.9	10.9	-0.5	-0.5	-8.3	-8.3
R600	20.0	20.0	3.6	3.6	3.1	3.1	-4.3	-4.3	-13.1	-13.1
R236ea	13.4	13.4	1.8	1.8	7.2	7.2	-3.7	-3.7	-7.2	-7.2
R600a	8.8	8.8	-2.9	-2.9	1.4	1.4	-8.0	-8.0	-10.2	-10.2
R236fa	13.8	13.8	0.8	0.8	3.7	3.7	0.6	0.6	-2.4	-2.4
R152a	25.6	25.5	20.2	20.1	11.5	11.4	18.1	18.1	13.4	13.4
R227ea	7.6	7.6	-4.5	-4.5	-5.8	-5.8	5.4	5.4	-6.7	-6.7
R134a	0.7	0.8	-4.7	-4.6	-3.5	-3.4	-0.1	-0.1	-10.7	-10.7

Figure 43 shows the exergy destruction rates for all the configurations including the non-constrained turbine bleeding. The non-constrained turbine bleed has lower destruction rates compared to all the constrained cases. The non-constrained turbine bleed has higher evaporator losses than that in the other non-constrained cases. The condenser losses are lower than non-constrained base but higher than that in the non-constrained

IHX. The turbine and pump has lower destruction rates in non-constrained turbine bleeding than that in other non-constrained cases. Among all the six configurations studied, the non-constrained IHX configurations have the lowest total exergy destruction rates. The base configuration has the highest destruction rates. This validates the fact that by changing configuration, the exergy destruction is lowered thereby increasing efficiency. Most of the exergy destruction occurs in the evaporator for all configurations. The exergy destruction occurs in heat exchangers occur due to the dissimilar temperature profile of the hot and cold fluids. From Figure 43 it can be observed that highest exergy loss occurs in the evaporator and condenser combined indicating highest efficiency gain can be achieved by reducing these values. Switching the configuration from base to IHX and turbine bleeding reduced the combined losses in evaporator and condenser. In addition to this, for the non-constrained cases, condenser losses decreased and were lower than that in the turbine. The reduction in losses in the evaporator and the condenser is caused by better temperature profile in the heat exchangers. The reduction is the evaporator and the condenser in the IHX case comes at an expense of added losses in the IHX. Another key observation can be made here that the turbine losses are slightly increased going from constrained to non-constrained cases. This is due to increase in pressure drop across the turbine from constrained to non-constrained cases. The turbine losses are pretty much fixed and are governed by the shape of the temperature entropy curve. Figure 44 shows the temperature entropy diagram for R600 in the non-constrained turbine bleeding configuration.

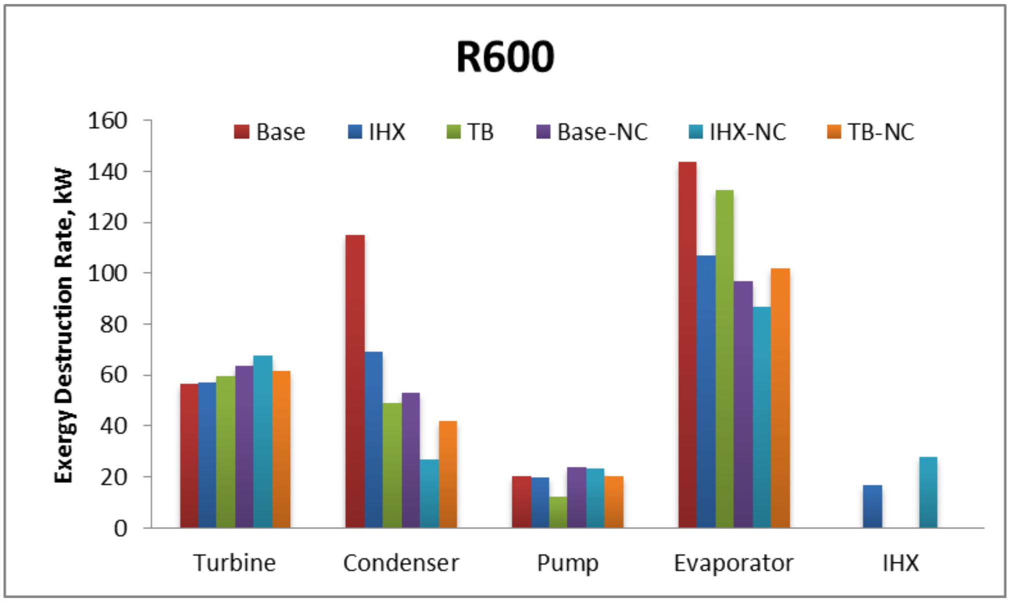

Figure 43 Exergy destruction rates across components

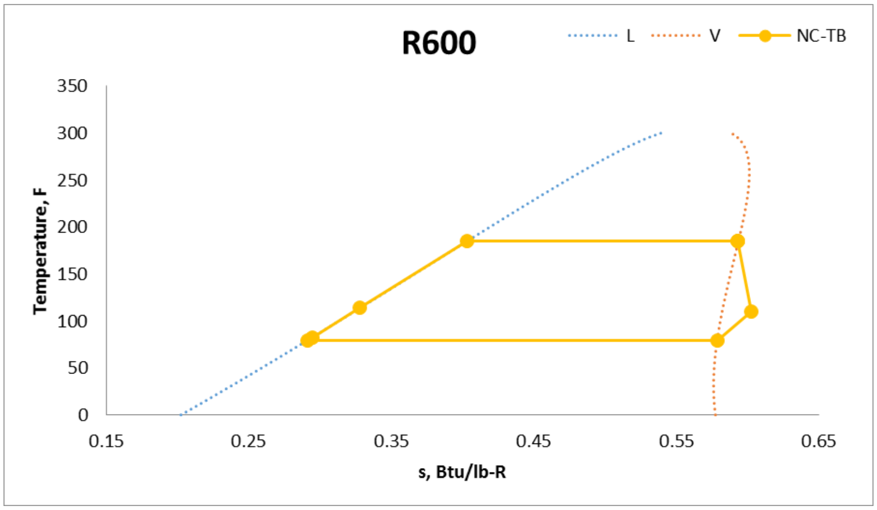

Figure 44 Temperature entropy diagram for R600 in non-constrained TB configuration

Table 24 EDF Values for Non-Constrained Turbine Bleeding Configuration

Working fluid	EDF_t	EDF_c	EDF_p	EDF_e	EDF_{tot}
R601	0.24	0.22	0.03	0.35	0.84
R601a	0.24	0.20	0.04	0.27	0.75
R123	0.31	0.20	0.04	0.55	1.09
R245ca	0.23	0.16	0.04	0.31	0.74
R245fa	0.26	0.19	0.06	0.30	0.81
R600	0.27	0.18	0.09	0.44	0.98
R236a	0.26	0.20	0.09	0.30	0.86
R600a	0.29	0.25	0.14	0.43	1.11
R236fa	0.28	0.20	0.13	0.31	0.92
R152a	0.10	0.34	0.23	0.43	1.10
R227ea	0.35	0.06	0.35	0.32	1.09
R134a	0.12	0.49	0.33	0.59	1.54

Table 25 shows the results obtained for the non-constrained turbine bleeding case. R245ca shows the highest efficiency of 11% and 56%.

Table 25 Results Obtained for Non-Constrained Turbine Bleeding Configuration

Working fluid	P_{in} (psia)	P_{out} (psia)	$\dot{m}_{ORC}$ (lb/hr)	η_I	η_{II}	W_p (kW)	W_{net} (kW)
R601	59	11	4.85E+04	10.4	52.5	12	289
R601a	80	14	4.50E+04	10.8	54.5	15	268
R123	85	14	8.98E+04	10.5	52.9	13	242
R245ca	99	15	8.28E+04	11.1	55.6	15	284
R245fa	130	23	9.00E+04	10.2	51.5	22	265
R600	163	37	4.20E+04	10.1	50.6	29	232
R236ea	170	32	1.12E+05	9.9	49.7	34	268
R600a	211	55	6.00E+04	9.1	45.8	53	267
R236fa	220	41	1.08E+05	9.5	47.8	44	232
R152a	401	92	6.40E+04	9.5	47.8	70	221
R227ea	330	59	1.17E+05	8.1	40.5	79	167
R134a	430	105	1.00E+05	7.7	38.9	94	178

3.11 Cost Analysis

The previous sections demonstrated that the ORC efficiency changes with working fluid and configuration. The change in efficiency occurs due to changes in thermodynamic conditions of the cycle and affects the power generated, equipment sizing and hence economics of the overall plant. A cycle maximizing the efficiency may not be the most cost effective mode of operation. Therefore, it is necessary to study the economics of the cycle and a balance between efficiency and cost must be achieved. The cost analysis of the ORC system was performed using overall efficiency, net power, combined heat exchanger area, size parameter and levelized cost of electricity (LCOE). The assumptions used in this analysis are given in Section 2.3 and an example of LCOE calculation can be found in the Appendix.

Previous sections were focused on discussing the technical performance of the cycle using the 12 working fluids in the six configurations. Findings of previous sections revealed that R601a shows the highest efficiency followed by R245ca and R600 in the non-constrained IHX configuration. The next candidates for highest efficiency are R245ca and R601 in base non-constrained configuration. Figure 45 compares the net power obtained for each working fluid in the six configurations. Highest net power is observed for R245ca followed by R601a and R601 in non-constrained base configuration. This implies that a cycle displaying the highest efficiency does not necessarily exhibit highest net power.

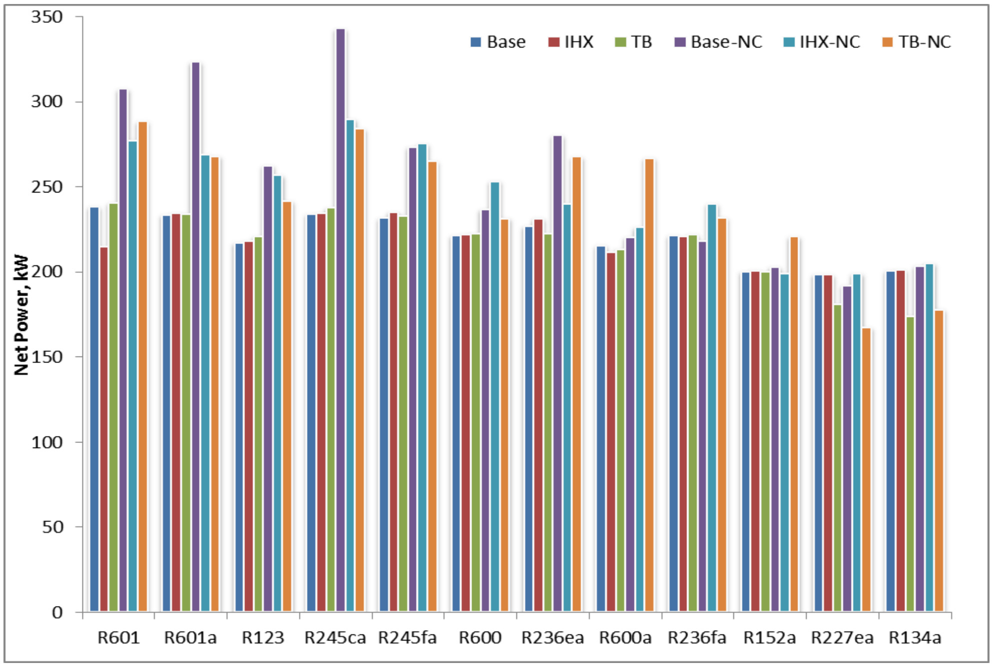

Figure 45 Net power for the working fluids in the configurations

The economics of ORC is governed by the equipment costs. Equipment sizing gives a good measure of the equipment costs. Equipment sizing is based on the total heat exchanger area for the heat exchangers in the cycle. Figure 46 shows the combined heat exchanger areas for the all cases. A general increasing trend in area is observed as we progress from R601 to R134a suggesting that working fluids with lower critical temperature require larger heat exchangers. Based on the results obtained in previous sections, it was observed that working fluids with lower critical temperature required higher mass flow rates. Higher mass flow rates tend to require higher heat exchanger areas. In addition, the efficiency decreases as the critical temperature of working fluid decreases. Lower efficiencies require higher amounts of heat to be exchanged in the heat exchangers which subsequently increases the heat exchanger areas.

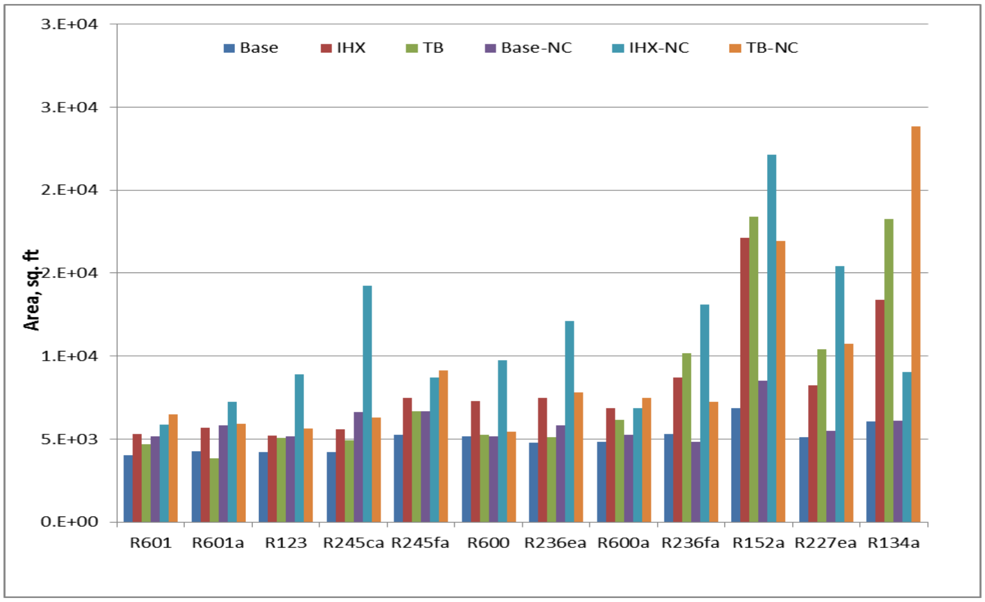

Figure 46 Combined heat exchanger areas for the working fluids

Sizing of the expander is represented by a size parameter and is given in Figure 47. The size parameter is the ratio of square root of volumetric flow across the turbine to the fourth root of the enthalpy drop across the turbine, and allows for a comparison of the different designs. A general increasing trend similar to combined heat exchanger area is observed for size parameter from left to right. However, more variability is observed in the results obtained. The increase in size parameter from R601a to R134a can be attributed to the increase in mass flow rates of working fluid and decreased turbine output. For comparison the size parameter for the Chena power plant was calculated to be 0.16. Size parameters exceed 0.16 in some cases for R236ea, R236fa, R227ea and R134a.

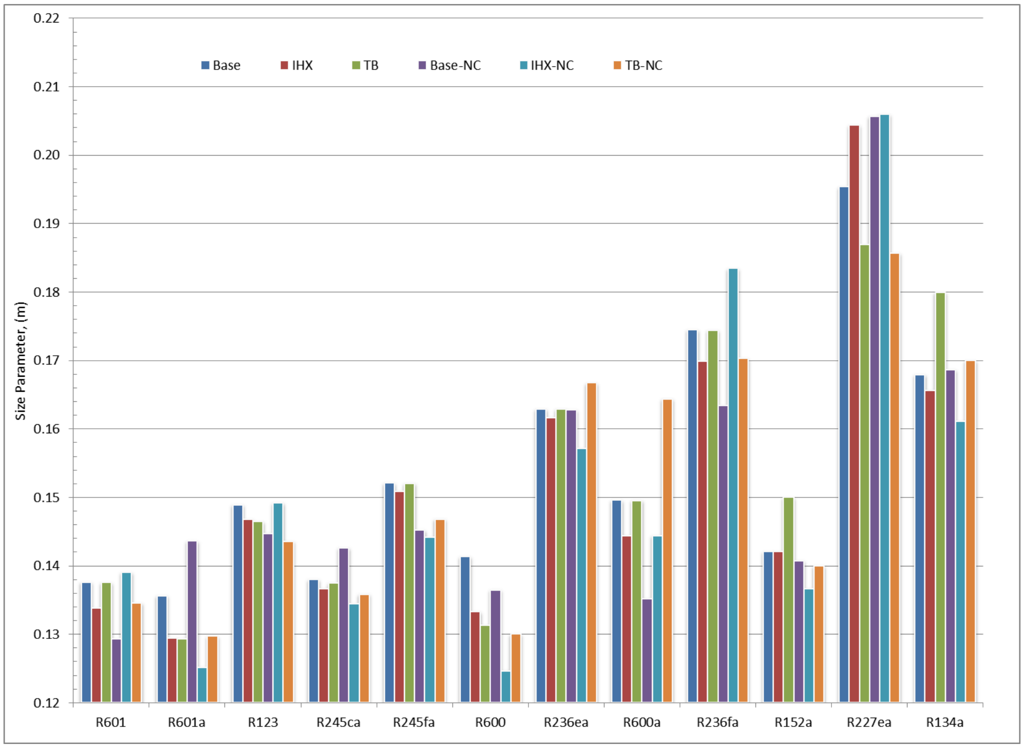

Figure 47 Size parameters for the working fluids

Figure 48 compares the capital cost for the geothermal systems to the corresponding thermal efficiency for the different configurations and working fluids. The value of $/kW was calculated by using the total installed cost calculated by the simulation and the net power for each case. In order to have cost effective performance, it is desired to have higher efficiency while minimizing the capital cost. R245ca in non-constrained base configuration shows the lowest $/kW value while R601a shows the highest efficiency in the non-constrained IHX configurations. Figure 48 is useful to help select the working fluids and configuration that show the best efficiency and cost based on the desired criteria.

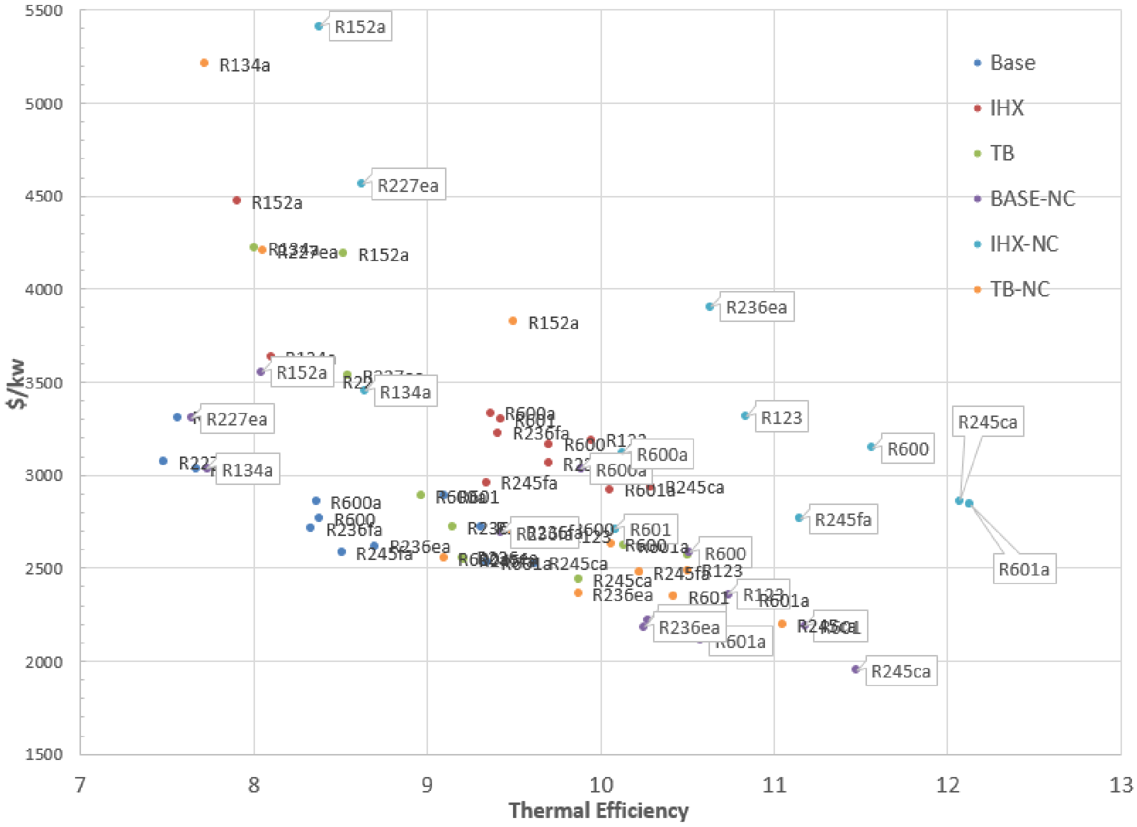

Figure 48 Comparison of efficiency vs. capital cost for the working fluids

Table 26 lists the calculated levelized cost of electricity for all the cases. LCOE was calculated using NREL's simple LCOE calculator. The lowest LCOE, 3.9 cents/kWh, can be observed for R245ca in base non-constrained configuration. R601a and R236ea have the next lowest LCOE 4.1 cents/kWh in the same configuration. R601a, R245ca and R600 show the highest efficiency in the non-constrained IHX configuration and have LCOE of 4.7, 4.7 and 5.0 cents/kWh respectively. R245ca, R601a and R601 displayed the highest net power in non-constrained base configuration. The LCOE was estimated to be 3.9, 4.1 and 4.2 respectively. This reveals that the LCOE is correlated with the net power generated by the cycle and is typically the highest for the base non-constrained case. Based on the overall cost analysis, R245ca, R601a, R601, R245fa and

R236ea show better performance among the 12 selected fluids in non-constrained base configurations and R245ca in non-constrained turbine bleeding configurations.

Table 26 Levelized Cost of Electricity (cents/kWh)

Working Fluid	BASE	IHX	TB	BASE-NC	IHX-NC	TB-NC
R601	4.7	4.9	4.5	4.2	4.6	4.3
R601a	4.4	4.8	4.5	4.1	4.7	4.3
R123	4.6	5.0	4.5	4.3	5.1	4.4
R245ca	4.4	4.8	4.4	3.9	4.7	4.2
R245fa	4.5	4.8	4.5	4.2	4.6	4.4
R600	4.6	5.0	4.6	4.5	5.0	4.5
R236ea	4.5	4.9	4.5	4.1	5.6	4.3
R600a	4.7	5.1	4.7	4.9	4.9	4.5
R236fa	4.6	5.0	4.6	4.6	8.4	4.6
R152a	5.1	6.1	5.8	5.3	6.9	5.5
R227ea	4.9	5.3	5.3	5.1	6.2	5.9
R134a	4.9	5.4	5.9	4.9	5.2	6.7

CHAPTER IV

CONCLUSIONS

An ORC model was successfully developed using Aspen HYSYS® process simulator and validated using the data from the Chena geothermal power plant.

A strong correlation was observed between the critical temperature of the working fluid and the efficiency for the working fluids. The efficiency increased as the critical temperature of working fluid increased. Exergy analysis of the cycle revealed that the highest exergy destruction occurs in evaporator followed by condenser, turbine and working fluid pump for the base case scenarios.

Performance of ORC was studied using 12 dry working fluids in three constrained and non-constrained (base, IHX and turbine bleeding) configurations. R601a, R245ca, R600 showed highest first and second law efficiency in the non-constrained IHX configuration. The highest net power was observed for R245ca, R601a and R601 working fluids in the non-constrained base configuration. Combined heat exchanger area and size parameter of the turbine showed an increasing trend as the critical temperature of the working fluid decreased. The lowest levelized cost of electricity was observed for R245ca followed by R601a, R236ea in non-constrained base configuration. The next best candidates in terms of LCOE were R601a, R245ca and R600 in non-constrained IHX configuration. LCOE is dependent on net power and higher net power favors to lower the cost of electricity.

Overall R245ca, R601, R601a, R600 and R236ea show better performance among the 12 working fluids under consideration. Non constrained configurations display better performance compared to the constrained configurations. Base non-constrained offered the highest net power and lowest LCOE.

CHAPTER V

FUTURE WORK

Any geothermal resource is finite in size and the temperature and flow rate may drop over the life of the project. The decrease in rate is dependent on the rate of resource being utilized. Efforts should be made to characterize predict the life of the resource. The effect of declining temperature and flow-rate on the ORC performance and economics should be studied.

A correlation between working fluid's critical temperature and thermal efficiency was observed in this study. An in-depth study understanding the effect of fluid's properties on the system performance should be conducted. This would help understanding the correlation between fluid properties and ORC performance and will help in choosing working fluids for better performance.

An important observation was made during this study that most of the exergy is lost in the evaporator. The exergy destruction occurs due to the temperature profile match in the evaporator. One of the ways to better match the temperature profile is to design the cycle in supercritical region. However, supercritical cycle usually requires higher pressure which increases working fluid pump consumption and capital costs. An effort should be made to study supercritical cycles for better profile match keeping in mind the higher costs associated with it.

APPENDIX

Below is the example calculation of the LCOE for R601 in the constrained base case. The capital cost ($/kW) does not include drilling and exploration cost, and represents the total installed equipment cost calculated by Aspen Hysys.

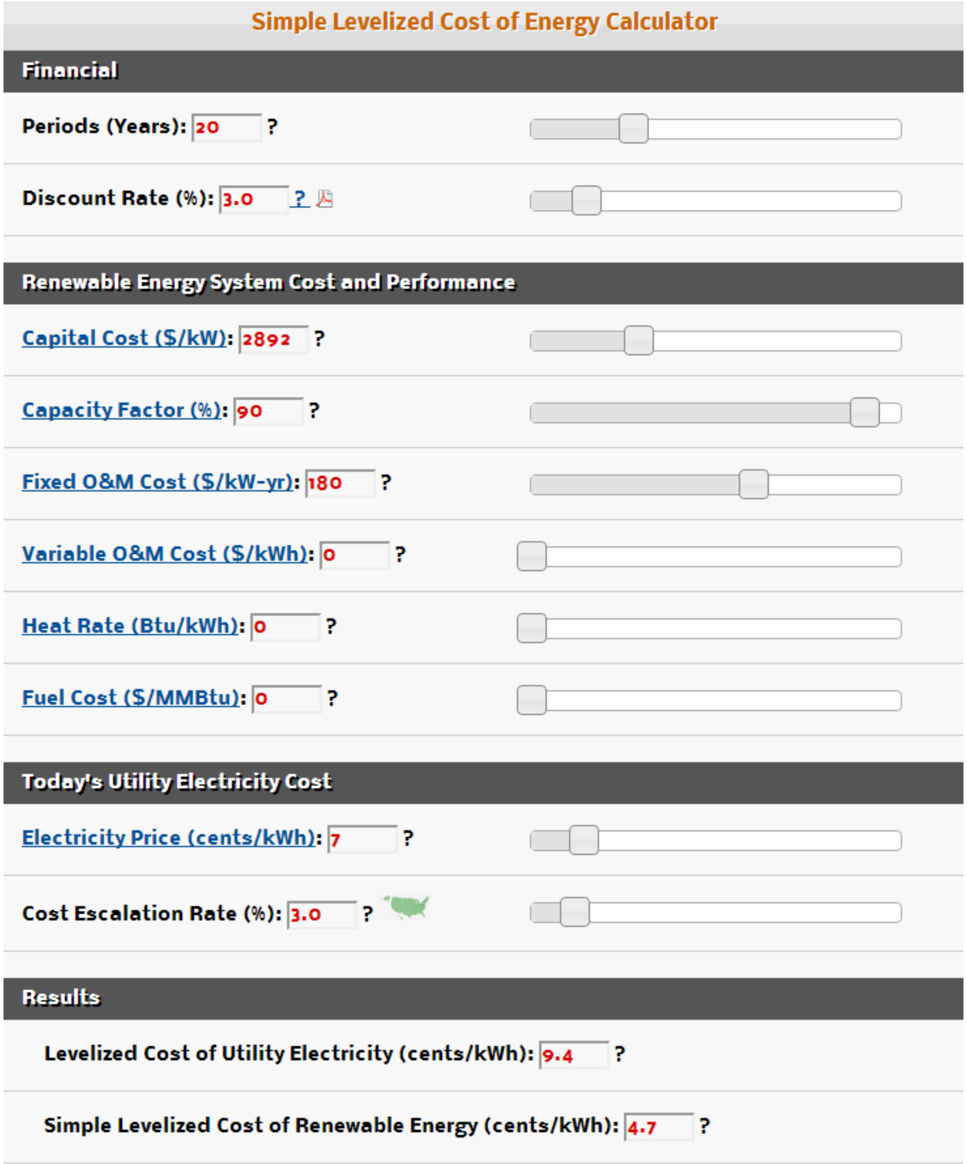

Simple Levelized Cost of Energy Calculator

Financial

Periods (Years): 20 ?

Discount Rate (%): 3.0 ?

Renewable Energy System Cost and Performance

Capital Cost ($/kW): 2892 ?

Capacity Factor (%): 90 ?

Fixed O&M Cost ($/kW-yr): 180 ?

Variable O&M Cost ($/kWh): 0 ?

Heat Rate (Btu/kWh): 0 ?

Fuel Cost ($/MMBtu): 0 ?

Today's Utility Electricity Cost

Electricity Price (cents/kWh): 7 ?

Cost Escalation Rate (%): 3.0 ?

Results

Levelized Cost of Utility Electricity (cents/kWh): 9.4 ?

Simple Levelized Cost of Renewable Energy (cents/kWh): 4.7 ?

Bibliography

Aljundi, I. H. (2011). Effect of dry hydrocarbons and critical point temperature on the efficiencies of organic Rankine cycle. *Renewable Energy*, *36*(4), 1196–1202. doi:10.1016/j.renene.2010.09.022

Aneke, M., Agnew, B., & Underwood, C. (2011). Performance analysis of the Chena binary geothermal power plant. *Applied Thermal Engineering*, *31*(10), 1825–1832. doi:10.1016/j.applthermaleng.2011.02.028

Angelino, G., Colonna, P., & Paliano, D. I. (1998). MULTICOMPONENT WORKING FLUIDS FOR ORGANIC RANKINE CYCLES (ORCs). *Energy*, *23*(6), 449–463.

Arvay, P., Muller, M. R., & Ramdeen, V. (2011). Economic Implementation of the Organic Rankine Cycle in Industry. In *ACEEE Summer Study on Energy Efficiency in Industry* (pp. 12–22).

Bamgbopa, M. O., & Uzgoren, E. (2013). Numerical analysis of an organic Rankine cycle under steady and variable heat input. *Applied Energy*, *107*, 219–228. doi:10.1016/j.apenergy.2013.02.040

Bao, J., & Zhao, L. (2013). A review of working fluid and expander selections for organic Rankine cycle. *Renewable and Sustainable Energy Reviews*, *24*, 325–342. doi:10.1016/j.rser.2013.03.040

Borsukiewicz-gozdur, A., & Nowak, W. (2007). Maximising the working fluid flow as a way of increasing power output of geothermal power plant. *Applied Thermal Engineering*, *27*(11-12), 2074–2078. doi:10.1016/j.applthermaleng.2006.11.013

Bruno, J. C., López-Villada, J., Letelier, E., Romera, S., & Coronas, A. (2008). Modelling and optimisation of solar organic rankine cycle engines for reverse osmosis desalination. *Applied Thermal Engineering*, *28*(17-18), 2212–2226. doi:10.1016/j.applthermaleng.2007.12.022

Calise, F., Capuozzo, C., & Vanoli, L. (2013). Design and Parametric Optimization of an Organic Rankine Cycle Powered By Solar Energy. *American Journal of Engineering and Applied Sciences*, *6*(2), 178–204. doi:10.3844/ajeassp.2013.178.204

Cayer, E., Galanis, N., Desilets, M., Nesreddine, H., & Roy, P. (2009). Analysis of a carbon dioxide transcritical power cycle using a low temperature source. *Applied Energy*, *86*(7-8), 1055–1063. doi:10.1016/j.apenergy.2008.09.018

Cayer, E., Galanis, N., & Nesreddine, H. (2010). Parametric study and optimization of a transcritical power cycle using a low temperature source. *Applied Energy*, *87*(4), 1349–1357. doi:10.1016/j.apenergy.2009.08.031

Cengel, Y., & Boles, M. (2006). *Thermodynamics: An Engineering Apporach* (Fifth Edit.). McGraw Hill.

Chen, H., Goswami, D. Y., & Stefanakos, E. K. (2010). A review of thermodynamic cycles and working fluids for the conversion of low-grade heat. *Renewable and Sustainable Energy Reviews*, *14*(9), 3059–3067. doi:10.1016/j.rser.2010.07.006

Chen, Y., Lundqvist, P., Johansson, a., & Platell, P. (2006). A comparative study of the carbon dioxide transcritical power cycle compared with an organic rankine cycle with R123 as working fluid in waste heat recovery. *Applied Thermal Engineering*, *26*(17-18), 2142–2147. doi:10.1016/j.applthermaleng.2006.04.009

Dai, Y., Wang, J., & Gao, L. (2009). Parametric optimization and comparative study of organic Rankine cycle (ORC) for low grade waste heat recovery. *Energy Conversion and Management*, *50*(3), 576–582. doi:10.1016/j.enconman.2008.10.018

Datla, B. V, & Brasz, J. J. (2012). Organic Rankine Cycle System Analysis for Low GWP Working Fluids. In *International Refrigeration and Air Conditioning Conference* (pp. 1–7).

Delgado-Torres, A. M., & García-Rodríguez, L. (2010). Analysis and optimization of the low-temperature solar organic Rankine cycle (ORC). *Energy Conversion and Management*, *51*(12), 2846–2856. doi:10.1016/j.enconman.2010.06.022

Desai, N. B., & Bandyopadhyay, S. (2009). Process integration of organic Rankine cycle. *Energy*, *34*(10), 1674–1686. doi:10.1016/j.energy.2009.04.037

DiPippo, R. (2004). Second Law assessment of binary plants generating power from low-temperature geothermal fluids. *Geothermics*, *33*(5), 565–586. doi:10.1016/j.geothermics.2003.10.003

Drescher, U., & Brüggemann, D. (2007). Fluid selection for the Organic Rankine Cycle (ORC) in biomass power and heat plants. *Applied Thermal Engineering*, *27*(1), 223–228. doi:10.1016/j.applthermaleng.2006.04.024

El-Emam, R. S., & Dincer, I. (2013). Exergy and exergoeconomic analyses and optimization of geothermal organic Rankine cycle. *Applied Thermal Engineering*, *59*(1-2), 435–444. doi:10.1016/j.applthermaleng.2013.06.005

Gosnold, W. (2006). Geothermal prospects in the north central United States. In *SMU Conference on Geothermal Energy in Oil and Gas Settings*.

Gu, W., Weng, Y., Wang, Y., & Zheng, B. (2009). Theoretical and experimental investigation of an organic Rankine cycle for a waste heat recovery system. *Proceedings of the Institution of Mechanical Engineers, Part A: Journal of Power and Energy*, *223*(5), 523–533. doi:10.1243/09576509JPE725

Guo, J., Xu, M., & Cheng, L. (2010). Thermodynamic analysis of waste heat power generation system. *Energy*, *35*(7), 2824–2835. doi:10.1016/j.energy.2010.03.012

Guo, T., Wang, H., & Zhang, S. (2010). Comparative analysis of CO2-based transcritical Rankine cycle and HFC245fa-based subcritical organic Rankine cycle using low-temperature geothermal source. *Science China Technological Sciences*, *53*(6), 1638–1646. doi:10.1007/s11431-010-3123-4

He, C., Liu, C., Gao, H., Xie, H., Li, Y., Wu, S., & Xu, J. (2012). The optimal evaporation temperature and working fluids for subcritical organic Rankine cycle. *Energy*, *38*(1), 136–143. doi:10.1016/j.energy.2011.12.022

Heberle, F., & Brüggemann, D. (2010). Exergy based fluid selection for a geothermal Organic Rankine Cycle for combined heat and power generation. *Applied Thermal Engineering*, *30*(11-12), 1326–1332. doi:10.1016/j.applthermaleng.2010.02.012

Hettiarachchi, M., Golubovic, M., Worek, W. M., Ikegami, Y., & Madhawa Hettiarachchi, H. D. (2007). Optimum design criteria for an Organic Rankine cycle using low-temperature geothermal heat sources. *Energy*, *32*(9), 1698–1706. doi:10.1016/j.energy.2007.01.005

Holdmann, G. (2007). Renewable baseload energy: Geothermal Heat Pumps to engineered reservoirs. In *Geothermal Resource Council - Annual Meeting of the Geothermal Resource Council* (pp. 515–519).

Hung, T. (2001). Waste heat recovery of organic Rankine cycle using dry fuids. *Energy Conversion and Management*, *42*, 539–553.

Hung, T. C., Shai, T. ., Wang, S. K., & Polytechnic, K. (1997). A REVIEW OF ORGANIC RANKINE CYCLES (ORCs) FOR THE RECOVERY OF LOW-GRADE WASTE HEAT. *Energy*, *22*(7), 661–667.

Hung, T. C., Wang, S. K., Kuo, C. H., Pei, B. S., & Tsai, K. F. (2010). A study of organic working fluids on system efficiency of an ORC using low-grade energy sources. *Energy*, *35*(3), 1403–1411. doi:10.1016/j.energy.2009.11.025

Invernizzi, C., Iora, P., & Silva, P. (2007). Bottoming micro-Rankine cycles for micro-gas turbines. *Applied Thermal Engineering*, *27*(1), 100–110. doi:10.1016/j.applthermaleng.2006.05.003

Jing, L., Gang, P., & Jie, J. (2010). Optimization of low temperature solar thermal electric generation with Organic Rankine Cycle in different areas. *Applied Energy*, *87*(11), 3355–3365. doi:10.1016/j.apenergy.2010.05.013

Kang, S. H. (2012). Design and experimental study of ORC (organic Rankine cycle) and radial turbine using R245fa working fluid. *Energy*, *41*(1), 514–524. doi:10.1016/j.energy.2012.02.035

Kanoglu, M. (2002). Exergy analysis of a dual-level binary geothermal power plant. *Geothermics*, *31*(6), 709–724. doi:10.1016/S0375-6505(02)00032-9

Kanoglu, M., & Bolatturk, A. (2008). Performance and parametric investigation of a binary geothermal power plant by exergy. *Renewable Energy*, *33*(11), 2366–2374. doi:10.1016/j.renene.2008.01.017

Khennich, M., & Galanis, N. (2012). Thermodynamic analysis and optimization of power cycles using a finite low temperature heat source. *Entropy*, *14*(March 2011), 871–885. doi:10.1002/er

Lakew, A. A., & Bolland, O. (2010). Working fluids for low-temperature heat source. *Applied Thermal Engineering*, *30*(10), 1262–1268. doi:10.1016/j.applthermaleng.2010.02.009

Larjola, J. (1995). Electricity from industrial waste heat using high-speed organic Rankine cycle (ORC). *Int. J. Production Economics*, *41*, 227–235.

Lee, M J; Tien, D L; Shao, C. T. (1993). Thermophysical capability of ozone safe working fluids for an organic rankine cycle system. *Heat Recovery Systems & CHP*, *13*(5), 409–418.

Li, M., Wang, J., He, W., Gao, L., Wang, B., Ma, S., & Dai, Y. (2013). Construction and preliminary test of a low-temperature regenerative Organic Rankine Cycle (ORC) using R123. *Renewable Energy*, *57*, 216–222. doi:10.1016/j.renene.2013.01.042

Li, Y.-R., Wang, J.-N., & Du, M.-T. (2012). Influence of coupled pinch point temperature difference and evaporation temperature on performance of organic Rankine cycle. *Energy*, *42*(1), 503–509. doi:10.1016/j.energy.2012.03.018

Liu, B.-T., Chien, K.-H., & Wang, C.-C. (2004). Effect of working fluids on organic Rankine cycle for waste heat recovery. *Energy*, *29*(8), 1207–1217. doi:10.1016/j.energy.2004.01.004

Lund, J. W. (2005). Combined heat and power plant Neustadt-Glewe, Germany. *GHC Bulletin*, 31–34.

Mago, P. J., Chamra, L. M., & Somayaji, C. (2007). Performance analysis of different working fluids for use in organic Rankine cycles. *Proceedings of the Institution of Mechanical Engineers, Part A: Journal of Power and Energy*, *221*(3), 255–265. doi:10.1243/09576509JPE372

Mago, P. J., Chamra, L. M., Srinivasan, K., & Somayaji, C. (2008). An examination of regenerative organic Rankine cycles using dry fluids. *Applied Thermal Engineering*, *28*(8-9), 998–1007. doi:10.1016/j.applthermaleng.2007.06.025

Mago, P. J., Srinivasan, K. K., Chamra, L. M., & Somayaji, C. (2008). An examination of exergy destruction in organic Rankine cycles. *International Journal of Energy Research*, *32*(October 2007), 926–938. doi:10.1002/er

Maizza, V., & Maizza, A. (2001). Unconventional working fluids in organic Rankine-cycles for waste energy recovery systems. *Applied Thermal Engineering*, *21*, 381–390.

Manolakos, D., Kosmadakis, G., Kyritsis, S., & Papadakis, G. (2009). Identification of behaviour and evaluation of performance of small scale, low-temperature Organic Rankine Cycle system coupled with a RO desalination unit. *Energy*, *34*(6), 767–774. doi:10.1016/j.energy.2009.02.008

Nafey, a. S., & Sharaf, M. a. (2010). Combined solar organic Rankine cycle with reverse osmosis desalination process: Energy, exergy, and cost evaluations. *Renewable Energy*, *35*(11), 2571–2580. doi:10.1016/j.renene.2010.03.034

Nguyen, V. M., Doherty, P. S., & Ri, S. B. (2001). Development of a prototype low-temperature Rankine cycle electricity generation system, *21*(x).

NREL. (2013). No Title. Retrieved from http://www.nrel.gov/analysis/tech_lcoe.html

Obernberger, I., Thonhofer, P., & Reisenhofer, E. (2002). Description and evaluation of the new 1 , 000 kW el Organic Rankine Cycle process integrated in the biomass CHP plant in Lienz , Austria. *Euroheat & Power*, *10*, 1–17.

Pan, L., Wang, H., & Shi, W. (2012). Performance analysis in near-critical conditions of organic Rankine cycle. *Energy*, *37*(1), 281–286. doi:10.1016/j.energy.2011.11.033

Papadopoulos, A. I., Stijepovic, M., & Linke, P. (2010). On the systematic design and selection of optimal working fluids for Organic Rankine Cycles. *Applied Thermal Engineering*, *30*(6-7), 760–769. doi:10.1016/j.applthermaleng.2009.12.006

Quoilin, S., Broek, M. Van Den, Declaye, S., Dewallef, P., & Lemort, V. (2013). Techno-economic survey of Organic Rankine Cycle (ORC) systems. *Renewable and Sustainable Energy Reviews*, *22*, 168–186. doi:10.1016/j.rser.2013.01.028

Quoilin, S., Declaye, S., Tchanche, B. F., & Lemort, V. (2011). Thermo-economic optimization of waste heat recovery Organic Rankine Cycles. *Applied Thermal Engineering*, *31*(14-15), 2885–2893. doi:10.1016/j.applthermaleng.2011.05.014

Quoilin, S., Lemort, V., & Lebrun, J. (2010). Experimental study and modeling of an Organic Rankine Cycle using scroll expander. *Applied Energy*, *87*(4), 1260–1268. doi:10.1016/j.apenergy.2009.06.026

Rayegan, R., & Tao, Y. X. (2011). A procedure to select working fluids for Solar Organic Rankine Cycles (ORCs). *Renewable Energy*, *36*(2), 659–670. doi:10.1016/j.renene.2010.07.010

Roy, J. P., Mishra, M. K., & Misra, A. (2011). Performance analysis of an Organic Rankine Cycle with superheating under different heat source temperature conditions. *Applied Energy*, *88*(9), 2995–3004. doi:10.1016/j.apenergy.2011.02.042

Rushing, A. S., Kneifel, J. D., & Lippiatt, B. C. (2013). *Energy Price Indices and Discount Factors for Life-Cycle Cost Analysis – 2013 Annual Supplement to NIST Handbook 135 and NBS Special Publication 709*.

Saleh, B., Koglbauer, G., Wendland, M., & Fischer, J. (2007). Working fluids for low-temperature organic Rankine cycles. *Energy*, *32*(7), 1210–1221. doi:10.1016/j.energy.2006.07.001

Schuster, a., Karellas, S., & Aumann, R. (2010). Efficiency optimization potential in supercritical Organic Rankine Cycles. *Energy*, *35*(2), 1033–1039. doi:10.1016/j.energy.2009.06.019

Schuster, a., Karellas, S., Kakaras, E., & Spliethoff, H. (2009). Energetic and economic investigation of Organic Rankine Cycle applications. *Applied Thermal Engineering*, *29*(8-9), 1809–1817. doi:10.1016/j.applthermaleng.2008.08.016

Shengjun, Z., Huaixin, W., & Tao, G. (2011). Performance comparison and parametric optimization of subcritical Organic Rankine Cycle (ORC) and transcritical power cycle system for low-temperature geothermal power generation. *Applied Energy*, *88*(8), 2740–2754. doi:10.1016/j.apenergy.2011.02.034

Stefánsson, V. (2002). Investment cost for geothermal power plants. *Geothermics*, *31*(2), 263–272. Retrieved from http://linkinghub.elsevier.com/retrieve/pii/S0375650501000189

Tchanche, B. F. F., Lambrinos, G., Frangoudakis, a., & Papadakis, G. (2010). Exergy analysis of micro-organic Rankine power cycles for a small scale solar driven reverse osmosis desalination system. *Applied Energy*, *87*(4), 1295–1306. doi:10.1016/j.apenergy.2009.07.011

Tchanche, B. F., Papadakis, G., Lambrinos, G., & Frangoudakis, A. (2009). Fluid selection for a low-temperature solar organic Rankine cycle. *Applied Thermal Engineering*, *29*(11-12), 2468–2476. doi:10.1016/j.applthermaleng.2008.12.025

Tidball, R., Bluestein, J., Rodriguez, N., & Knoke, S. (2010). *Cost and Performance Assumptions for Modeling Electricity Generation Technologies Cost and Performance Assumptions for Modeling Electricity Generation Technologies*.

Wang, E. H., Zhang, H. G., Fan, B. Y., Ouyang, M. G., Zhao, Y., & Mu, Q. H. (2011). Study of working fluid selection of organic Rankine cycle (ORC) for engine waste heat recovery. *Energy*, *36*(5), 3406–3418. doi:10.1016/j.energy.2011.03.041

Wang, J., Dai, Y., Gao, L., & Ma, S. (2009). A new combined cooling, heating and power system driven by solar energy. *Renewable Energy*, *34*(12), 2780–2788. doi:10.1016/j.renene.2009.06.010

Wang, X. D., Zhao, L., Wang, J. L., Zhang, W. Z., Zhao, X. Z., & Wu, W. (2010). Performance evaluation of a low-temperature solar Rankine cycle system utilizing R245fa. *Solar Energy*, *84*(3), 353–364. doi:10.1016/j.solener.2009.11.004

Wei, D., Lu, X., Lu, Z., & Gu, J. (2007). Performance analysis and optimization of organic Rankine cycle (ORC) for waste heat recovery. *Energy Conversion and Management*, *48*(4), 1113–1119. doi:10.1016/j.enconman.2006.10.020

White, D. Williams, D. (1975). *Assessment of Geothermal Resources of the United States*.

Xi, H., Li, M.-J., Xu, C., & He, Y.-L. (2013). Parametric optimization of regenerative organic Rankine cycle (ORC) for low grade waste heat recovery using genetic algorithm. *Energy*, *58*, 473–482. doi:10.1016/j.energy.2013.06.039

Yamamoto, T., Furuhata, T., Arai, N., & Mori, K. (2001). Design and testing of the Organic Rankine Cycle. *Energy*, *26*(3), 239–251. doi:10.1016/S0360-5442(00)00063-3

Yari, M. (2010). Exergetic analysis of various types of geothermal power plants. *Renewable Energy*, *35*(1), 112–121. doi:10.1016/j.renene.2009.07.023

Zhai, H., Shi, L., & An, Q. (2014). Influence of working fluid properties on system performance and screen evaluation indicators for geothermal ORC (organic Rankine cycle) system. *Energy*. doi:10.1016/j.energy.2013.12.030